Mario Alberto Madrid Pérez

Biomechanical Evaluation of Three New Implants for the First Metatarsophalangean Joint of the Human Foot

Director/es
Bayod López, Javier
Bea Cascarosa, José Antonio

Universidad
Zaragoza
1542

Tesis Doctoral

BIOMECHANICAL EVALUATION OF THREE NEW IMPLANTS FOR THE FIRST METATARSOPHALANGEAN JOINT OF THE HUMAN FOOT

Autor

Mario Alberto Madrid Pérez

Director/es

Bayod López, Javier
Bea Cascarosa, José Antonio

UNIVERSIDAD DE ZARAGOZA
Escuela de Doctorado

Programa de Doctorado en Ingeniería Mecánica

2022

Biomechanical Evaluation of Three New Implants for the First Metatarsophalangean Joint of the Human Foot

Dissertation submitted in Partial Fulfillment of the Requirements for the Doctoral Degree in

Mechanical Engineering at University of Zaragoza

by

Mario Alberto Madrid Pérez

Faculty Advisors

PhD Javier Bayod López
University of Zaragoza

&

PhD José Antonio Bea Cascarosa
University of Zaragoza

September 2021

ACKNOWLEDGEMENTS

To my Family

RESUMEN

Hallux valgus y hallux rigidus son las dos patologías más comunes en el primer radio del pie. Los tratamientos para estas patologías han tenido un avance considerable en los últimos años. Entre las técnicas quirúrgicas destructivas están la artrodesis, artroplastia y quilectomia mientras que entre las técnicas quirúrgicas no destructivas se incluyen varios tipos de osteotomías. La artroplastia de la primera articulación metatarsofalángica es un procedimiento que conserva la dorsiflexión de la articulación, además de aliviar el dolor causado por las patologías mencionadas. Por otro lado, realizar un análisis estructural del pie mediante métodos análiticos es sumamente difícil por lo que los métodos numéricos son una buena herramienta para comprender la biomecánica del pie, en particular los análisis de elementos finitos. El objetivo de esta investigación es realizar una evaluación biomecánica del pie tras de haberse desarrollado los diferentes tipos de artroplastia en la primera articulación metatarsofalángica. Cinco modelos de elementos finitos son comparados y tres diferentes implantes son investigados. Los resultados en los modelos de elementos finitos arrojan consecuencias en la biomecánica del pie tras haberse desarrollado los distintos procesos de artroplastia. Para los implantes investigados se realiza un estudio a fatiga partiendo de los resultados de las simulaciones computacionales, basándose en un enfoque de deformación y realizando aproximaciones con series de Taylor de primer orden, utilizando las expresiones de Ramberg-Osgood y Coffin-Basquin-Manson para la construcción de un modelo B de salto de unidad.

ABSTRACT

Hallux valgus and hallux rigidus are the two most common pathologies in the first ray of the foot. The treatments against these pathologies have had considerable advances in recent years. The destructive surgical techniques include arthrodesis, arthroplasty, and cheilectomy, while the nondestructive surgical techniques include many kinds of osteotomies. Arthroplasty of the first metatarsophalangeal joint is a procedure that preserves the dorsiflexion of the joint, in addition to relieving pain caused by the aforementioned pathologies. On the other hand, performing a structural analysis of the foot using analytical methods is extremely difficult, so numerical methods are a good tool to understand the biomechanics of the foot, particularly finite element analysis. The objective of this research is to develop a biomechanical evaluation of the foot after having developed the different types of arthroplasty in the first metatarsophalangeal joint. Five finite element models are compared and three different implants are investigated. The results in the finite element models show consequences in the biomechanics of the foot after the different arthroplasty processes have been developed. For the implants investigated, a fatigue study is developed from the results of the computational simulations, based on a strain approach and making approximations with first-order Taylor series, using the Ramberg-Osgood and Coffin-Basquin-Manson expressions for building a one step B model.

CONTENTS

LIST OF FIGURES

LIST OF TABLES

1. INTRODUCCIÓN.

1.1 *Ingeniería y Medicina: Ingeniería biomédica; biomecánica.*

Después de la segunda guerra mundial, surgió la necesidad de implementar tecnologías para el área de la salud. Desde entonces el campo de las tecnologías médicas ha ido avanzando notablemente día a día. Este hecho ha ido limitando a los profesionales médicos en su necesidad de estar al ritmo en estos cambios. Debido a la carencia de conocimientos y comprensión de problemas biológicos y médicos de esos ingenieros se tuvo la necesidad de formar profesionales, que pudieran aplicar los principios y el método de la ingeniería a los problemas médicos y biológicos [19].

La bioingeniería abarca todas las posibles interacciones entre las ciencias naturales y la ingeniería derivándose de ésta la ingeniería biomédica la cual se centra en el ser humano y en el cuidado de la salud. Según Giovanni Gismondi [20] la ingeniería biomédica es la rama de la ingeniería que implementa los principios de las tecnologías al campo de la medicina. Se dedica fundamentalmente al diseño y construcción de equipos médicos, prótesis, dispositivos médicos, dispositivos de diagnóstico y de terapia, también está encargada de unir los mundos de la ingeniería con la medicina y fisiología para lograr avances en el conocimiento científico y desarrollo de la tecnología en medicina y biología.

El Committes of Engineer's Joint Council de los Estados Unidos de Norteamérica definió en 1972 a la Bioingeniería como la aplicación de los conocimientos recopilados de la unión fértil entre la ciencia ingenieril y la médica para su aplicación en beneficio del hombre. Otra definición bastante aceptada es la realizada por Heinz Wolff en 1970 que dice: la bioingeniería consiste en la aplicación de técnicas y las ideas de la ingeniería a la biología, y concretamente a la biología humana. El gran sector de la bioingeniería que se refiere especialmente a la medicina, puede llamarse más adecuadamente ingeniería biomédica [21].

La sociedad de Ingeniería en Medicina y Biología (EMB, por sus siglas en inglés) del instituto de Ingeniería Eléctrica y Electrónica (IEEE por sus siglas en inglés) en un artículo denominado "Designing a career in Biomedical Engineering" publicado en el 2003 [22], definió como áreas de la ingeniería biomédica a la bioinformática, a los sistemas bio-microelectromecánicos, a los biomateriales, a la biomecánica, al procesamiento de bioseñales, a la biotecnología, a la ingeniería clínica, a la genómica, a las imágenes médicas y su procesamiento, a las tecnologías de la información, a la instrumentación, los sensores y las medidas, a la micro y nanotecnología, al sistema nervioso y la ingeniería, a la modelación de los sistemas fisiológicos, a la proteómica, a la radiología, a la ingeniería de rehabilitación, a la robótica en cirugía y a la telemedicina[19].

La aplicación de fuerzas en un organismo viviente y la investigación de los efectos de esas fuerzas en el cuerpo humano o en un sistema humano, incluyendo las fuerzas que surgen desde dentro y fuera del cuerpo, es llamada biomecánica. La biomecánica también incluye el estudio de las estructuras y funciones de un sistema biológico mediante las leyes de la mecánica aplicadas a la actividad muscular [23].

Una buena definición de biomecánica nos dice que es el conjunto de conocimientos interdisciplinarios generados a partir de utilizar, con el apoyo de otras ciencias biomédicas, los aportes de la mecánica y distintas tecnologías en, primero, el estudio del comportamiento de los sistemas biológicos, en particular el cuerpo humano, y segundo, en resolver los problemas que le provocan

las distintas condiciones a las que puede verse sometido [21].

Existen hallazgos de la ingeniería biomédica desde la época del antiguo Egipto. Andreas G. Nerlich en su artículo [1] comenta sobre una momia encontrada en una cámara que data aproximadamente de 1065-740 A.C. La investigación antropológica indicó que la momia era una mujer de 50 a 55 años. Su estatura era 1.69 m aproximadamente. La examinación paleontológica demostró que el primer dedo del pie derecho había sido amputado durante la vida de la persona debido a que en el lugar de la amputación se mostraba el tejido blando intacto como se puede ver en la figura 1.1A. El dedo extraído se había reemplazado por una prótesis de madera, la cual se muestra en la figura 1.1B. Los componentes de la prótesis eran tres piezas de madera, una pieza longitudinal de 12x3.5x3.5 cm atada a dos pequeñas placas de madera de 4x2.5x0.3 cm. Estas placas fueron fijadas mediante cuerdas de cuero. Todas las partes de madera fueron delicadamente talladas imitando de manera asombrosa la forma del primer dedo, incluyendo la uña. Un cordón de cuero fue fijado a las pequeñas placas y al cuerpo prostético, el cual fue atado al antepié. Una inspección cuidadosa reveló el uso del cuerpo prostético como se aprecia en la figura 1.1C. Un examen de radiología y tomografías computarizadas mostraron que el primer metatarsiano estaba poco desmineralizado lo cual se puede ver en la figura 1.1D.

Fig. 1.1: Vistas de la prótesis y del pie derecho de una momia [1].

Un ciudadano romano llamado Galeno de Pérgamo (131-201 D.C.) fue considerado el primer médico de los gladiadores. Galeno escribió un ensayo titulado De Motu Musculorum en el cual describe diferencias entre nervios sensoriales y motores. Él describió el tono muscular e introdujo los términos diartrosis y sinartrosis el cual es usado hasta estos días como la terminología correcta artrología [23]. Otros autores dicen que los primeros desarrollos de la bioingeniería datan de la época de Leonardo Da Vinci (1452-1519) con sus dibujos anatómicos y aproximaciones a brazos de palanca (Glave, n.d.). Isaac Newton (1642-1727) estableció la biomecánica moderna y sus leyes de la inercia, la aceleración y la acción y reacción son las leyes mejor validadas en la biomecánica moderna [23]. Otros pioneros de la biomecánica son Luigi Galvani (1737-1798) y Lord Kelvin (1824-1907) como reflejan en sus trabajos sobre la conducción eléctrica en seres vivos [20]. Podríamos mencionar a muchos más pero, éstos son sólo algunos de los primeros en investigar la anatomía humana y la mecánica.

El primer programa oficial de estudio en ingeniería biomédica comenzó en 1959, como Maestría en la universidad norteamericana de Drexel y en ese mismo año se realizó en París la primera

conferencia internacional sobre ingeniería biomédica. No fue hasta 35 años después en 1994 cuando se celebró la decimoquinta conferencia mundial, en una sede latinoamericana (Rio de Janeiro) [20].

La ingeniería biomédica es una de las profesiones con mayor futuro en el mundo, debido a que cada año los gobiernos de distintos países invierten millones de dólares en el desarrollo de nuevas tecnologías con el fin de elevar la calidad de vida de las personas, teniendo la necesidad de expertos en el diseño y desarrollo en dicha área.

Esta tesis se encuentra en el área de la biomecánica y desarrolla un análisis biomecánico utilizando elementos finitos para conocer las consecuencias de un procedimiento quirúrgico contra el hallux valgus y hallux rigidus llamado artroplastia. En este procedimiento quirúrgico se estudia el efecto de tres implantes diferentes en el primer radio del pie. En el caso de algunos implantes, las tensiones cíclicas pueden producir posibles fallos por fatiga [24]. Esta tesis desarrolla un análisis de fatiga de tres implantes diferentes de los cuales no hay estudios en la actualidad. En las siguientes líneas haremos una descripción de las patologías a estudiar y haremos un recuento histórico del método de elementos finitos para finalmente incluir estos temas en los objetivos, metodología y alcance de la tesis. Para comprender mejor la siguiente lectura de esta tesis, recomendamos que el lector lea primero los anexos I y II. Si el lector tiene antecedentes médicos y tiene buenas bases anatómicas, puede omitir esa lectura sin ningún problema.

1.2 Hallux valgus.

1.2.1 Definición de la patología.

El hallux valgus es una enfermedad que fue descrita por primera vez por Carl Hueter (1838-1882) en 1871 quien describe esta deformidad como una contractura en abducción en la que el primer dedo, desviado lateralmente se aleja del plano medio del cuerpo [25], [26]. Esta patología es una de las deformidades más frecuentes del pie. El término hallux valgus se refiere a la angulación del primer dedo hacia afuera, desviando con frecuencia los otros dos dedos. Es característica la prominencia que forma la cabeza del metatarsiano a la cual se le conoce vulgarmente como juanete. En la mayoría de los casos, la deformidad del primer radio se asocia con una desviación simétrica del quinto radio: Quinto metatarsiano en valgo y quinto dedo en varo junto con deformidades en martillo o luxaciones de los dedos centrales [27].

El hallux valgus es un trastorno de alineación del primer radio del pie, que altera su función estática y dinámica, en cuanto al soporte y transmisión de cargas, y mecanismo de despegue del pie durante la marcha. Esta alteración de la posición del primer metatarsiano repercute distalmente, ocasionando una pérdida de la posición de la cabeza del metatarsiano respecto a su alojamiento en el aparato glenosesamoideo que, manteniéndose en una situación normal, origina un desequilibrio de las fuerzas musculares que actúan sobre el radio, favoreciendo la posición en valgo del dedo y su rotación progresiva en pronación. El desarrollo de la deformidad hallux valgus, en niños mayores y adolescentes, es poco frecuente. Algunos autores sugieren que esta deformidad rara vez se encuentra antes de los 10 años de edad, lo que significa que se produce habitualmente durante el desarrollo. Las siguientes alteraciones caracterizan el hallux valgus. No siempre tienen la misma intensidad ni proporcionalidad entre sí [27].

- Desviación del primer dedo. Un discreto valgo es fisiológico; se considera que es patológico cuando la desviación es superior a los 15 grados. Algunas veces llega a formar casi un ángulo recto con el primer metatarsiano.

- Aumento del ángulo entre el primer y segundo metatarsianos. Normalmente es de unos 10 grados, pero en el hallux valgus aumenta y llega a formar desviaciones en varo de hasta 30 grados.

- Juanete. Es la prominencia que forma el primer metatarsiano junto con la desviación del dedo constituyendo una pequeña exostosis separada por un surco vertical muy claro de la cara articular del metatarsiano.

- Luxación de los sesamoideos. Como consecuencia de la desviación del metatarsiano, los sesamoideos se desvían hacia fuera, no estando simétricos en relación con el primer metatarsiano, sino subluxándose parcial o totalmente en el primer espacio intermetatarsiano.

- Disfunción muscular. El aductor del dedo se convierte en flexor, mientras que los flexores se convierten en abductores. La fuerza que desvía el dedo hacia fuera no se halla neutralizada por el aductor; por ello, la deformidad es progresiva.

- Alteraciones de la articulación metatarsofalángica. La congruencia articular no perfectamente esférica dificulta la corrección pasiva. En personas mayores aparece artrosis que estructura la deformidad y hace dolorosa la articulación.

- Alteraciones en la articulación cuneometatarsiana. Dicha articulación condiciona la dirección del primer metatarsiano. cuando las interlíneas son curvas la desviación es fácilmente corregible, pero cuando son rectas, esta desviación es más difícil de corregir y puede quedar fijada y, posteriormente, aparecer artrosis.

- Síndrome de insuficiencia del primer radio. Estas alteraciones del primer radio suelen ir acompañadas de sus consecuencias que aparecen en los radios vecinos.

- El Origen del dolor en el hallux valgus es producido por las siguientes causas.

  - Dolor por sobrecarga en los metatarsianos centrales. La metatarsalgia suele ser más precoz y más intensa que el dolor en el juanete.

  - Dolor por el roce de la exostosis con el calzado. Aparece hiperqueratosis e higroma, en ocasiones muy doloroso.

  - Dolor en la articulación cuando surge artrosis metatarsofalángica, más frecuente en personas mayores.

Existen varios tipos clínicos de hallux valgus, entre ellos está el hallux valgus congénito el cual tiene una aparición temprana, es decir, antes de los 15 años incluyendo la desaparición de la cresta intersesamoidea con displasia en la articulación metatarsolfalángica y atrofia del sesamoideo lateral. Otro tipo es el hallux valgus por prominencia de la cabeza metatarsiana en el cual la desviación de la falange proximal es pequeña y aparece un engrosamiento de la cabeza metatarsiana. Un tercer tipo es el hallux valgus en antepié triangular apareciendo una gran eminencia del metatarsiano junto a la zona articular medial, una relajación de la cápsula articular medial junto con un desplazamiento de la cabeza metatarsiana de los sesamoideos. El segundo dedo puede quedar por encima o por debajo de hallux con un posible desplazamiento en la articulación por estiramiento de los tejidos blandos o una dislocación de la articulación metatarsofalángica, en la figura 1.2 se puede ver un ejemplo de un paciente el cual ha desarrollado la enfermedad a manera que el hallux está situado por debajo del segundo dedo. Por último, tenemos al hallux valgus severo en el cual hay una deformidad intrínseca ósea en la falange proximal que determina un abultamiento sobre la articulación interfalángica y a veces genera un callo doloroso en la cara media del hallux [3]. El hallux valgus reduce el soporte del peso en el pie por lo que la evaluación de la deformidad debe llevarse a cabo en posición de carga bilateral y debe valorarse el rango de movilidad de la articulación subastragalina, del tobillo, de articulaciones metatarsofalángicas y articulaciones tarsianas en ambos pies y compararlas. Para la evaluación del hallux valgus también debe desarrollarse un examen radiológico en tres posiciones [3].
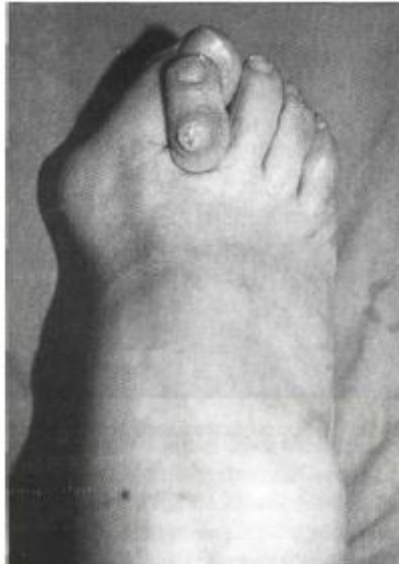
Fig. 1.2: Hallux valgus desarrollado de tal forma que el segundo dedo queda por encima del hallux [2].

1. Proyección dorsoplantar en carga: Se hace para poder medir 4 ángulos. El primero está formado por el eje longitudinal del hueso metatarsiano con el eje longitudinal de la primera falange proximal, este ángulo se conoce como ángulo del hallux valgus y se considera normal si es inferior a 15 grados. El segundo es el ángulo intermetatarsiano, que mide la apertura entre el primer y segundo hueso metatarsiano, y se considera normal si no supera los 9 grados. El tercero es el ángulo del conjunto articular distal, que se forma con la superficie de la articulación y el eje del primer metatarsiano y, por lo general, no es mayor que 10 grados, y el cuarto está formado por los ejes longitudinales de las falanges del primer dedo, también conocido como ángulo interfalángico, que se considera normal cuando es inferior a 10 grados [28], [3], [29]. En la figura 1.3 se muestran los ángulos que se utilizan para medir el agravio del hallux valgus.
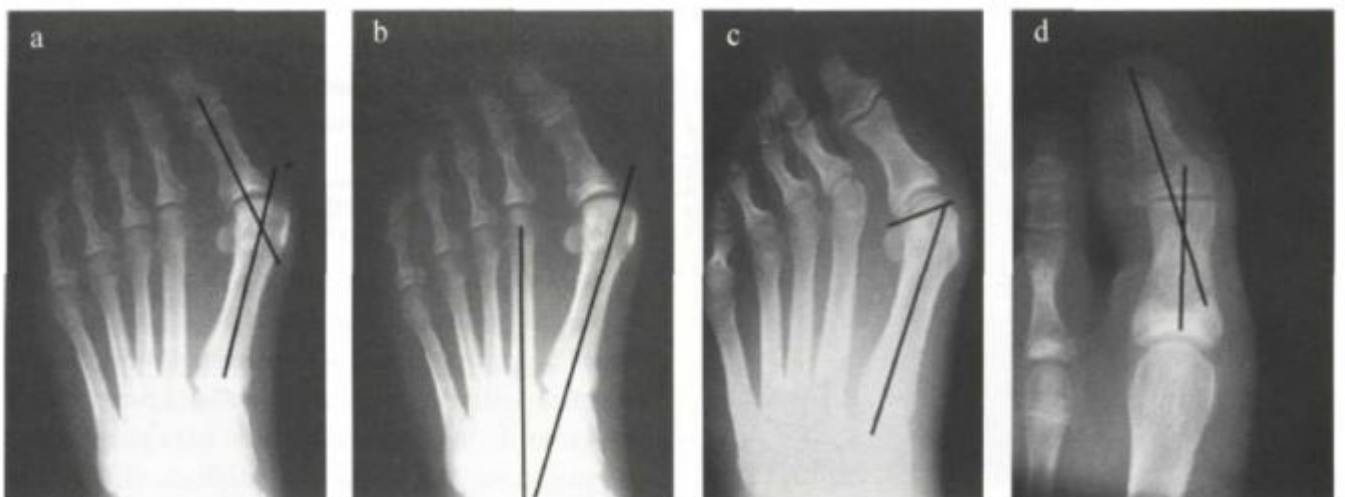
Fig. 1.3: Ángulo de hallux valgus (a). Ángulo intermetatarsiano (b). Ángulo articular distal metatarsiano (c). Ángulo interfalángico [3].

2. Proyección lateral en carga: Indica la información que hay sobre cómo se encuentran las articulaciones metatarsofalángicas y cuneo-metatarsiana.

3. Proyección de Walter-Müller: Esta proyección da la oportunidad de medir la relación entre los sesamoideos con el primer metatarsiano [3].

En el año 2001 Garow et al. describen en el Journal of the American Podiatric Medical Association una nueva técnica no invasiva, mediante el desarrollo y la validación de una serie de fotografías en descarga, diseñada para clasificar el grado de la deformidad del hallux valgus, esta escala es conocida como la escala de Manchester. Algunas limitaciones de esta escala es que se basa en un método cualitativo mediante fotografías, sin mediciones cuantitativas, con lo que el grado de deformidad puede variar según el criterio del explorador. Esta escala se basa principalmente en el grado de abducción y no se consideran otros parámetros como la posición de los sesamoideos, la congruencia articular, el rango de movimiento y el nivel de osteoporosis de la articulación entre otros [25]. En la figura 1.4 se puede apreciar la escala de Manchester donde la parte A corresponde al grado 1 en el cual no hay deformidad, la parte B corresponde al grado 2 en el cual la deformidad es considerada como leve, la parte C corresponde al grado 3 donde la deformidad se considera moderada y la parte D corresponde al grado 4 que es una deformidad severa.

Fig. 1.4: Clasificación de Manchester [4].

Para hacer una correcta evaluación de hallux valgus también se debe realizar un estudio baropodométrico, este tipo de estudio es también conocido como estudio de la pisada, es decir, se estudia la biomecánica estática y dinámica del apoyo del pie. Gracias a estas mediciones se puede clasificar el hallux valgus en tres tipos [3].

1. Hallux valgus mediano. Este tipo es caracterizado por tener un ángulo intermetatarsal menor a 11 grados, un ángulo de hallux valgus menor de 30 grados y un desplazamiento de articulaciones laterales del sesamoideos menor de 50 %.

2. Hallux valgus moderado. Este tipo se caracteriza por tener un ángulo intermetatarsal mayor a 11 grados, pero menor a 16 grados, el ángulo del hallux valgus está entre 30 y 40 grados y desplazamientos de las articulaciones laterales de sesamoideos entre 50 y 75 %.

3. Hallux Valgus severo. Este tipo de deformidad tiene un ángulo intermetatarsal mayor a 16 grados, el ángulo del hallux valgus es mayor a 40 grados y los desplazamientos de las articulaciones laterales de sesamoideos son superiores al 75 %.

En la figura 1.5 se muestran los grados de deformidad del hallux donde las flechas indican la dirección de la subluxación, y las puntas de la flecha la magnitud de la superficie articular. La figura 1.5-A muestra un hallux valgus leve con subluxación primera metatarsofalángica, un ángulo de hallux valgus de 19 grados, un ángulo intermetatarsal 1-2 de 10 grados y una subluxación de sesamoideos menor del 50 %. La figura 1.5-B se puede apreciar un hallux valgus moderado con subluxación primera metatarsofalángica, un ángulo del hallux valgus de 30 grados, un ángulo intermetatarsal 1-2 de 14 grados y subluxación de sesamoideos de 50 al 75 %. Por último, en la figura 1.5-C aparece un hallux valgus severo con subluxación primera metatarsofalángica severa, un ángulo del hallux valgus de 50 grados, un ángulo intermetatarsal 1-2 de 17 grados, una subluxación de sesamoideos mayor al 75 % y la segunda articulación aparece luxada.

Fig. 1.5: Grados de deformidad del hallux valgus [5].

1.2.2   *Etiología y etiopatogenia.*

Existen varios factores estructurales que se relacionan con el desarrollo y la progresión del hallux valgus. Los más aceptados son la laxitud ligamentosa y los pies planos. La longitud del primer metatarsiano se ha considerado longitud de riesgo para la aparición del hallux. La utilización de calzado inadecuado se reconoce como factor desencadenante. En las mujeres el calzado es probablemente más importante como progresión que como factor causante [26], [27].
La existencia de determinadas variaciones anatómicas en el antepié puede producir, en algunas

personas, riesgo de desarrollo de la patología. La forma y orientación de las articulaciones metatarsofalángicas y metatarso cuneiformes pueden ser la clave del desarrollo del hallux valgus, así como la de su corrección. Hasta la fecha no se ha establecido ninguna liga clara entre el hallux valgus y la obesidad ni con otros factores que afecten la carga del pie como el ángulo de progresión del pie [27], [30]. Existen múltiples teorías que explican el origen del hallux valgus, mayoritariamente referidas a la fisiología de dicha deformidad y algunas formas posturales relacionadas con el calzado o con determinadas actividades como el ballet, más que a su etiología. El hallux valgus es sólo un aspecto, el más visible, del síndrome de insuficiencia del primer radio. Por ello se considera que en el hallux valgus existen [27].

1. Factores congénitos predisponentes: Un antepié con un dedo largo, tipo egipcio y un primer metatarsiano corto, desviado en varo. A ello se une una musculatura débil del primer radio con la función alterada.

2. Factores desencadenantes, fundamentalmente el calzado y la artritis reumatoidea.

3. Estructuración de la deformidad, debida a la artritis o la artrosis.

Hay una débil evidencia de una diferencia racial debido a que la prevalencia del hallux valgus en personas blancas ha sido reportada como el doble de las personas africanas de color [26]. Hasta la fecha no se conoce la causa que origina esta patología. En la actualidad el hallux valgus afecta mayormente a las mujeres que a los hombres, aunque no hay una clara evidencia de esto, hay estudios que demuestran que en poblaciones estudiadas en Francia la influencia del hallux valgus era mayor en los hombres durante los siglos XVI y XVII [31]. En la anatomía ósea del hombre y mujer existen diferencias, por ejemplo, la superficie de la cabeza articular de pacientes femeninos es mucho más redondeada y pequeña dando una menor estabilidad a la unión. También hay una tendencia mayor en mujeres a tener más aducción en el primer metatarso que a su vez pueden ser las diferencias en la unión metatarsiana. También hay otras diferencias como el tamaño de la articulación distal y proximal del primer dedo, su forma y ángulo [26]. Existe una nota escrita en 1845 por la reina Victoria de Inglaterra que dice: Una de las causas más ciertas de los juanetes es el uso de zapatos hechos demasiados pequeños con suela muy estrecha [32].

1.2.3   Tratamiento.

Los tratamientos contra el hallux valgus han tenido avances considerables en los últimos años. Las osteotomías son operaciones en las cuales se practican cortes en un hueso de manera que se puedan hacer cambios en su posición como corregir las curvaturas o angulaciones de los metatarsianos y es un procedimiento que se realiza bajo anestesia general. Las osteotomías a nivel del primer metatarsiano, de la primera cuña, las osteotomías y acortamientos de la primera falange, complementadas en la mayor parte de los casos con cirugía sobre partes blandas constituyen los gestos quirúrgicos utilizados con mayor frecuencia para la corrección del hallux valgus y hallux rigidus [3]. Por otro lado, la osteodesis usa estructuras de cerclaje entre el primer y segundo metatarsiano para realinear el primer metatarso y corregir la deformación del ángulo intermetatarsiano. La primera técnica de osteodesis fue reportada en 1961 [33]. La artrodesis es otro procedimiento quirúrgico en el cual se fijan dos piezas óseas, anclando una articulación. Esta es una corrección con alto potencial para el tratamiento contra el hallux valgus [34]. La artroplastia es un procedimiento quirúrgico que consiste en reemplazar la superficie articular enferma o dañada (hueso y cartílago) con otro material (metal, cerámica, polímero, etc.). Este procedimiento se usa en pacientes con patologías de grados avanzados como hallux valgus y hallux rigidus [35]. Otro método quirúrgico es la cirugía percutánea la cual permite hacer incisiones mínimas sin exposición directa de los planos quirúrgicos, esta técnica incluye varios

gestos quirúrgicos debido a que no existe una técnica quirúrgica que por sí sola pueda corregir todos los elementos patológicos de las deformidades por hallux valgus y hallux rigidus [2].

El tratamiento conservador suele ser poco eficaz. El empleo de separadores de dedos o juaneteras es inútil. Pueden recomendarse las mismas medidas indicadas en el tratamiento incruento del síndrome de insuficiencia del primer radio. En cuanto al tratamiento quirúrgico, todavía no existe consenso sobre la cirugía del hallux valgus. Están descritas más de 100 intervenciones; entre ellas, las que alteran la biomecánica del pie suelen dar pésimos resultados, aun consiguiendo una estética relativamente buena. También interesa destacar que, entre las múltiples intervenciones que respetan la biomecánica, los resultados subjetivos son buenos en más del 80 % de los casos. El porcentaje disminuye en la valoración objetiva y la radiología, con frecuencia, es bastante deficiente. Sobre la base de estos hechos son preferibles las técnicas más simples y con el post operatorio más corto. Se puede afirmar que en el caso de hallux valgus, la complejidad de la cirugía no es proporcional a la bondad de sus resultados [27].

Hasta la fecha no hay alguna técnica que pueda ser aplicable a los diferentes tipos de hallux valgus y hallux rigidus. El hallux valgus es una patología muy antigua, debido a ello existen muchos tratamientos conservadores que no son necesariamente efectivos para curar la patología, entre ellos es recomendar al paciente usar calzado suficientemente ancho que no comprima los dedos y usar tacones bajos, alrededor de 5 cm como máximo. También se recomienda aplicar antiinflamatorios y analgésicos en las etapas iniciales del hallux valgus con el fin de mejorar el proceso del caminar. Algunos doctores recomiendan el uso de hielo local durante 20 minutos tres veces al día [4]. También existen ejercicios y masajes para el fortalecimiento y estiramiento del primer dedo del pie. Otra alternativa es el tratamiento quirúrgico del cual hay muchas técnicas las cuales se pueden clasificar en: Procedimientos sobre tejidos blandos, osteotomías, artrodesis, artroplastias y procedimientos combinados [3].

El tratamiento quirúrgico es una alternativa cuando el tratamiento conservador no ha dado buenos resultados y por lo cual la técnica quirúrgica a ser usada debe ser ajustada a las necesidades de cada paciente. A pesar de la etiología, biomecánica y el uso de elementos finitos este problema permanece con un pobre entendimiento [36].

1.3 *Hallux rigidus.*

1.3.1 *Definición de la patología.*

El hallux rigidus es la segunda patología más frecuente de la primera articulación metatarsofalángica después del hallux valgus [6]. Esta patología es una entidad caracterizada por presentar un dolor permanente con sensación de crujidos articulares al realizar la movilización del primer dedo, que aumenta con el apoyo y la marcha y se asocia, habitualmente, con una disminución de la función articular, así como la aparición de un bulto o excrecencia en la región dorsal metatarsofalángica del primer radio [27]. Los sesamoideos son más largos y la distancia con la base de la falange proximal disminuye a medida que la afectación articular progresa [6]. Esta patología generalmente es asociada a una limitación del movimiento del primer radio del pie, especialmente en dorsiflexión, médicamente llamada osteoartritis de la unión metatarsofalángica del primer dedo [8]. La descripción original de esta condición ha sido atribuida a Davies-Colley, quien lo llamó hallux flexus en un artículo publicado en 1887. El nombre hallux rigidus fue propuesto cuatro meses después por Cotterill, y este permanece como la designación más común a pesar de la defensa de varios autores por otros términos como: hallux limitus, hallux dolorosus, metatarsus non extensus, dorsal bunion, (juanete dorsal), winkle-picker disease (enfermedad del zapato puntiagudo o de la bota puntiaguda) y metatarsus primus elevatus. La historia de la terminología fue bien resumida por Kelikian [37], [6].

El arco de movilidad de la primera articulación metatarsofalángica es de 110 grados, con una

flexión plantar de 35 grados y una flexión dorsal de 75 grados. En el hallux rigidus disminuye el rango de movilidad y una disminución de la flexión dorsal, ocasionada tanto por los osteofitos dorsales como por la retracción de los tejidos blandos plantares [6].

Es raro que el hallux rigidus aparezca en pacientes jóvenes, siendo más normal en varones de entre 40 y 60 años. Su síntoma principal es el dolor en el pulpejo del dedo, con sensación de crujidos articulares, a la vez que la movilidad articular se ve disminuida en su curso evolutivo. Es muy frecuente también la aparición de dolor en la cabeza del quinto metatarsiano. La existencia de un bulto en la región dorsal de la primera articulación metatarsofalángica es un signo relativamente frecuente, sobre todo en casos muy avanzados [27].

Una de las razones por las cuales se produce el hallux rigidus es por un desequilibrio de las partes blandas que alteran la biomecánica normal de la primera articulación metatarsofalángica. La falange proximal se va situando progresivamente en una posición plantar respecto a la cabeza metatarsiana causando un gradual desplazamiento del centro de rotación de la articulación pinzando la articulación dorsalmente durante el movimiento en flexión dorsal. La repetida concentración de elevadas solicitaciones a compresión, en la porción dorsal de la cabeza del primer metatarsiano, provoca la aparición de lesiones cartilaginosas y el progresivo desarrollo de osteofitos dorsales evolucionan hacia una degeneración gradual articular pudiendo llegar a la total anquilosis [6]. El hallux rigidus es una enfermedad degenerativa la cual evoluciona con el tiempo. Existen varias clasificaciones para el grado que adquiere la enfermedad. Núñez-Samper [27] en su libro biomecánica, medicina y cirugía del pie dice que el hallux rigidus es un proceso que evoluciona fundamentalmente en tres fases, cada una de los cuales va a presentar una sintomatología y una semiología radiológica diferente, que condicionarán, consecuentemente, el tratamiento.

- Fase I. Es el inicio del proceso, presenta en el paciente un dolor agudo o subagudo de forma esporádica en la etapa de despegue del pie, o cuando hace movimientos libres de flexoextensión del primer dedo. Hay cierta limitación de la movilidad articular. Radiográficamente aparece una ligera condensación periarticular y una disminución del espacio articular, que representa el inicio de una esclerosis subcondral con un mínimo grado de osteofitosis, principalmente en la cara lateral, en forma de tejadillo, que da un aspecto muy típico a la cabeza metatarsiana.

- Fase II. Es la fase de artrosis o degeneración articular propiamente dicha. El paciente refiere que camina con el pie en supinación, puesto que el dolor es constante, aunque de expresión variable, oscilando desde intermitente hasta vivo, cuando se produce la movilización de la articulación. Esta se encuentra limitada casi en su totalidad, a la vez que aparecen hiperqueratosis en las zonas de apoyo plantar de la articulación metatarsofalángica primera y quinta. Radiográficamente hay desaparición de la interlínea articular, con condensación periférica de osteofitosis marginal de aspecto ebúrneo, tanto en la base de la falange como en la cabeza del metatarsiano. Asimismo, hay una irregularidad de los bordes del rodete sesamoideo.

- Fase III. Corresponde a la fase de anquilosis o rigidez completa de la articulación que se transforma en un bloque; los dolores son permanentes por la hipertrofia articular y por compresión del nervio colateral por un osteofito. Al apoyar el pie, el dolor también es patente en la hiperqueratosis plantar. Es frecuente observar en esta fase una retracción del tendón flexor, propio del primer dedo, que produce una entidad llamada hallux rigidus flexus. El estudio radiográfico es manifiesto: desaparición completa de la articulación, hipertrofia anárquica osteofitaria con un puente sesamoideofalángico y con hiper condensación ósea periférica articular, a la vez que la base de la primera falange adopta una forma acampanada típica, que se corresponde proporcionalmente con la cabeza metatarsiana.

Algunos otros autores prefieren considerar para sus estudios la clasificación de Coughlin et al. [38], [8]. Estos autores basan su clasificación en encontrar radiografías y datos clínicos subjetivos y objetivos. Esta clasificación se resume en la tabla 1.1 la cual es mostrada a continuación. Para la tabla 1.1 se usan las radiografías anteroposteriores, laterales y de soporte de peso.

Tab. 1.1: **Sistema clínico y radiológico para la evaluación del hallux rigidus.**

Grado	Dorsiflexión	Hallazgos radiológicos	Hallazgos clínicos
0	40-60 grados y/o 10 % a 20 % de pérdida en comparación con el lado normal	Normal	No hay dolor, solamente rigidez y pérdida de movimiento en la examinación
1	30-40 grados y/o 20 % a 50 % de pérdida en comparación con el lado normal	El principal hallazgo son osteofitos dorsales, un mínimo estrechamiento del espacio articular, una mínima esclerosis periarticular, mínimo aplanamiento de la cabeza del metatarsiano	Dolor medio u ocasional y rigidez, dolor en los extremos de la dorsiflexión y/o flexión plantar en la examinación
2	10-30 grados y/o 50 % a 75 % de pérdida en comparación con el lado normal	Osteofitos dorsales, laterales y posiblemente medios dando la apariencia de aplanado a la cabeza del metatarsiano, no más de 1/4 de espacio articular dorsal se involucra en la radiografía lateral, de leve a moderado el estrechamiento articular y esclerosis, los sesamoideos no suelen participar	Dolor de moderado a severo y rigidez que puede ser constante; el dolor ocurre solo antes de la máxima dorsiflexión y máxima flexión plantar en la examinación
3	$\leq$ 10 grados y/o 75 % a 100 % de pérdida en comparación con el lado normal. Hay una notable pérdida de dorsiflexión plantar metatarsofalángica	Igual que en el grado 2 pero, con un estrechamiento substancial, cambios quísticos posiblemente periarticulares, más de 1/4 del espacio articular dorsal se involucra en la radiografía lateral, los sesamoideos se agrandan	Dolor casi constante y rigidez substancial en extremos del rango del movimiento pero no con el rango medio
4	Igual que en el caso 3	Igual que en el caso 3	Igual que en el caso 3, pero en este el dolor es definitivo en el rango medio del movimiento pasivo

En la figura 1.6 que se muestra a continuación aparecen radiografías del hallux rigidus. En la parte 'a' podemos ver una radiografía posterior, anterior en carga de los pies, con pérdida completa del espacio articular de la primera metatarsofalángica de los dos pies. La parte 'b' muestra una radiografía de perfil en carga observándose el osteofito dorsal en forma de lágrima característica del hallux rigidus y en la parte 'c' se aprecia una radiografía oblicua donde podemos ver el espacio articular real por ausencia de interposición de los osteofitos.
Otra clasificación que se basa en análisis de radiografías es la de Regnauld la cual menciona tres grados de hallux rigidus [39].

- Grado I: Condensación de hueso alrededor de la articulación. Ligero estrechamiento del espacio articular. Los sesamoideos son regulares pero ligeramente agrandados.

- Grado II: Aparición moderada de osteofitos. Estrechamiento del espacio de la unión metatarsofalángica. Subcondral esclerosis o quistes. Hipertrofia e irregularidad de los sesamoideos.

- Grado III: Aparición severa de osteofitos. Completa desaparición del espacio de la unión metatarsofalángica. Articulación degenerativa del hallux y los sesamoideos metatarsianos.

Por otro lado, Hattrup y Johnson realizan otra clasificación también basada en la apariencia radiográfica que también contiene tres grados [39].

- Grado 1: Cambios degenerativos con exostosis media dorsal y una buena preservación de la unión metatarsofalángica.
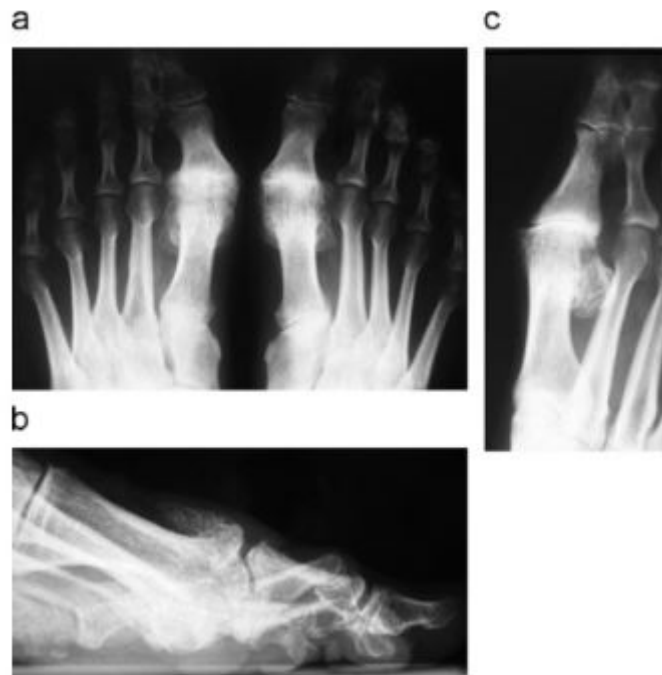
Fig. 1.6: Radiografías del hallux rigidus [6].

- Grado 2: artritis degenerativa con un estrechamiento definido en la unión metatarso-falángica acompañado de osteofitos dorsales y esclerosis Subcondral.

- Grado 3: Osteoartritis marcada con pérdida del espacio de la unión metatarsofalángica y posibles quistes subcondriales.

Como se puede observar la clasificación que menciona Núñez-Samper, la clasificación de Regnauld y la de Hattrup y Johnson son similares, pero aun así hay autores que prefieren citar una en lugar de la otra en sus estudios.

La sociedad americana ortopédica del pie y el tobillo (AOFAS por sus siglas en inglés) introdujo en 1994 una escala para medir el dolor de los pacientes en la unión metatarsofalángica del primer dedo [38]. En el artículo titulado Clinical Rating Systems for the Ankle-Hindfoot, Midfoot, Hallux and Lesser Toes (sistemas de clasificación clínica para el tobillo y el antepié, parte media del pie, hallux, y dedos menores del pie) [40], la AOFAS propone cuatro escalas para tener una mejor comprensión con una manera simple de describir la condición del pie y el tobillo. En dicho artículo mencionan que las escalas deben ser aplicables para diferentes situaciones clínicas como evaluación de pacientes después de una artrodesis, artroplastias con implantes y reconstrucción de ligamentos. En las escalas se pueden alcanzar puntuaciones de hasta 100 puntos donde no se incluyen datos radiológicos para que los datos sean estrictamente clínicos, tampoco asignan valores numéricos, prefieren asignar resultados como: excelente, bueno, regular y malo. Los factores clínicos que constituyen cada escala son subjetivos y objetivos. Las cuatro escalas que presenta el artículo son: la escala del tobillo y antepié, la escala de la parte media del pie, la escala metatarsofalángica-interfalángica del hallux y la escala metatarsofalángica-interfalángica de los dedos menores. La sección de la escala metatarsofalángica-interfalángica del hallux es descrita como una escala para medir el grado del primer metatarsiano, la unión metatarsofalángica, la falange proximal, la falange distal y la unión interfalángica del primer dedo y puede ser aplicada para el hallux valgus, hallux varus, hallux, rigidus, osteoartrosis, artrosis traumáticas o inflamatorias, hallux valgus interfalángico, dedo en garra, dedo en martillo, artrodesis metatarsofalángica, queilectomía, artroplastia con implantes metatarsofalángicos, artroplastia con resección metatarsofalángica, inestabilidad o dislocación metatarsofalángica, fracturas in-

terarticulares y extraarticulares del primer metatarso y las falanges del primer dedo. En la escala se pueden obtener 100 puntos si el paciente no tiene dolor, tiene un rango de movimiento metatarsofalángico e interfalángico completo, no existe inestabilidad metatarsofalángica e interfalángica, una buena alineación del primer radio del pie, no existe limitación alguna en actividades diarias o recreativas y no existe limitación alguna en cuanto al calzado. En la escala fueron asignados 40 puntos según el dolor que pueda tener el paciente, 45 puntos a la funcionalidad del primer radio del pie y 15 puntos a la alineación del primer radio del pie. En el apéndice III se presentan las cuatro escalas propuestas por la AOFAS en su artículo publicado en 1994.

1.3.2 Etiología y etiopatogenia.

El hallux rigidus es una forma común de osteoartritis en el pie. Los signos radiológicos de la enfermedad pueden ser reconocidos en 10 % de la gente de 20 a 34 años y en un 44 % de la gente mayor de 80 años. La causa exacta de la enfermedad es controvertida. Coughlin et al (2003) demostraron que el 80 % de todos los pacientes que padecen de bilateral hallux rigidus tienen un historial familiar. Además, en su estudio pudieron demostrar que la mayoría de los pacientes desarrolla un hallux rigidus bilateral a lo largo del tiempo. Algunos autores culpan al calzado, a un estrecho tendón de Aquiles, un primer dedo largo, un pie plano particularmente cuando la persona usa botas rígidas, un aplanamiento congénito de la cabeza del primer metatarsiano, una osteocondritis disecante en la cabeza del primer metatarsiano o la creencia de un comienzo espontáneo [37], [8]. Otro concepto popular es que un primer radio elevado al cual le llaman metatarsus primus elevatus, da como consecuencia un hallux rigidus, mientras algunos autores están a favor de esta teoría otros se oponen. Coughlin et al dicen que la elevación normal es considerada a ser ≤ 8 mm, y la inclinación normal de primer metatarsiano ha sido reportada a ser entre 19 y 25 grados y proponen que el metatarsus primus elevatus puede ser un cambio secundario debido al hallux rigidus, dejando que permanezca controversial la causa exacta del hallux rigidus [38], [6]. De cualquier forma, es bien sabido que en la actualidad las mujeres desarrollan una incidencia más alta que los hombres y esto ocurre principalmente después de la edad de 40 años [41], [6]. La causa más común para el hallux rigidus unilateral es la creencia de ser un trauma por una lesión aislada o por un microtrauma repetitivo, esta puede ser una lesión condral y dar como resultado un cambio progresivo en artritis [8]. De los estudios realizados por Rochera podemos decir que el aumento anómalo de carga en la cabeza metatarsiana es la causa más fundamental en el desarrollo de esta patología y que aparece en los primeros metatarsianos largos y potentes, con una forma metatarsal índex plus. Serían metatarsianos que durante su desarrollo presentaron una fisis proximal y distal, correspondiendo la mayoría de ellos a varones. Autores como Viladot defienden una etiología por microtraumatismos que, producidos por el uso del zapato, actuarían por choque del primer dedo contra éste, paralelo al segundo y con buen equilibrio muscular. En cambio, De Donker y Kowalski, afirman que la causa de la producción sería un desequilibrio muscular entre flexor largo y corto del dedo gordo con los extensores, lo que produciría una descompensación y una sobrecarga articular, condicionando una alteración metabólica del cartílago con su consecuente degeneración y artrosis. Por último, sitúa la causa de producción en alteraciones metabólicas y osteoporosis, más o menos discretas, producidas en el curso de un traumatismo o microtraumatismos, procesos infecciosos o inflamatorios, o secundario a inmovilizaciones. De cualquier forma, la mayoría de estos conceptos son teóricos y carecen de evidencia científica [27].

1.3.3 Tratamiento.

El tratamiento conservador médico, en principio, es paliativo. El higroma puede ser tratado con pomadas queratolíticas, evitando fundamentalmente la infección. Las ortesis retrocapitales, so-

brealzando y descargando la articulación, pueden ser utilizadas en la fase I. También puede ser útil la utilización de un tacón anterior semicilíndrico en el zapato [27]. En ausencia de dolor, las fases iniciales de la enfermedad o en pacientes con contraindicaciones quirúrgicas se suele indicar el tratamiento conservador. La colocación de una plantilla que produzca una elevación de la cabeza metatarsal aumentando artificialmente la amplitud de la flexión dorsal, puede mejorar la sintomatología del paciente [6]. El tratamiento quirúrgico y el tipo de técnica que se ha de utilizar dependen de la fase en que se encuentre y el tipo morfológico del antepié. No obstante, todos los métodos deben ir encaminados a suplir la función de la primera falange durante el momento del despegue en el paso [27]. Algunas técnicas quirúrgicas han sido brevemente descritas en el apartado que habla del tratamiento contra el hallux valgus, esto es, porque algunas técnicas quirúrgicas son comunes para ambas enfermedades. Dentro de las técnicas quirúrgicas destructivas tenemos la artrodesis, la artroplastia y la queilectomía mientras que como técnicas quirúrgicas no destructivas tenemos la osteotomía de la falange proximal u osteotomía de Moberg, la osteotomía de cierre de cuña dorsal u osteotomía de Watermann, el procedimiento de Youngswick, la osteotomía de Reverdin Green, la osteotomía oblicua distal deslizante, la osteotomía sagital Z, la osteotomía doble de Drago entre otras [8].

Por último, para cerrar esta sección podemos decir que en el grado 0 y 1 de Coughlin y Shurnas, el tratamiento de elección es el conservador. El grado 2 es la indicación ideal para las osteotomías metatarsales, que al descender y acortar el metatarsiano evitan la metatarsalgia de transferencia y descomprimen la articulación metatarsofalángica. También en el grado 2 la queilectomía puede mejorar la dorsiflexión de la articulación metatarsofalángica y la sintomatología dolorosa. En el grado 3 está indicada la queilectomía. También está indicada la hemiartroplastia implantada en la falange asociada con una limpieza articular. En pacientes de edad avanzada la intervención de Keller o la artroplastia metatarsofalángica se utiliza con resultados aceptables, En el grado 4, la técnica de elección es la artrodesis metatarsofalángica. En los pacientes de edad avanzada y con poca demanda funcional tienen su indicación las artroplastias metatarsofalángicas: así mismo, en pacientes con una afectación en el tobillo hemos de evitar, en lo posible, la artrodesis de la articulación metatarsofalángica [6].

1.4 *Historia del método de los elementos finitos.*

A continuación, se presenta un breve recuento histórico del método de los elementos finitos [42]. La idea de los elementos finitos tiene más de un siglo. La idea vino de dos aspectos, uno es ingenieril, el otro es matemático. Los ingenieros fueron inspirados por las estructuras de los problemas de ingeniería y usaron una aproximación intuitiva para construir las funciones de prueba. Por otro lado, los matemáticos introdujeron los elementos finitos para resolver ecuaciones diferenciales y controlar el error de las funciones de prueba.

El clásico método variacional en ingeniería fue desarrollado por Rayleigh hace más de 140 años el cual es llamado método de Rayleigh (John William Strutt, tercer barón de Rayleigh 1842-1919). Otro método variacional fue desarrollado por Walter Ritz (1878-1909) hace 105 años. A estos dos métodos juntos ahora los llamamos método de Rayleigh-Ritz, el cual es comúnmente usado en la mecánica de cuerpos deformables. Después John Hadji Argyris (1913-2004) en 1955 desarrolló la guía de los elementos continuos el cual es un método matricial usado en la mecánica. Richard Courant (1888-1972) especializado en matemáticas aplicadas combinó la ingeniería y las matemáticas, en 1943 estudió sistemáticamente las funciones de prueba continuas. Olgierd Cecil Zienkiewicz (1921-2009) un matemático e ingeniero desarrolló en 1964 una función de prueba de series continuas la cual es uno de los fundamentos modernos de los elementos finitos. El matemático Carl Friedrich Gauss (1777-1855) desarrolló en 1795 el método residual ponderado. Boris Galerkin (1871-1945) contribuyó en gran medida al método de elementos finitos en 1915. Las siguientes personas son pioneros en el campo de los elementos finitos. Courant,

un matemático nacido en Alemania y que después emigró a los Estados Unidos de Norteamérica construyó un instituto para matemáticas aplicadas en 1928. En 1964 el instituto fue llamado Courant Institute for Mathematics Science, el cual su línea principal de investigación es la de elementos finitos. El principio mínimo de Courant es un importante teorema que fue llamado así después de él. Argyris es un griego que emigró a Alemania y es un experto ampliamente distinguido y reconocido en la ciencia computacional. Él es aclamado como uno de los inventores del método de los elementos finitos. Su contribución fue la idea de la matriz de desplazamiento en los análisis mecánicos, lo cual es un predecesor del método de elementos finitos. En 1950 se convirtió en el director del instituto de computación aplicada en la universidad de Stuttgart y trabajó como director por casi 40 años. Zienkiewicz, un inglés, fue profesor del departamento de ingeniería civil en la universidad de Swansea. Él fundó una revista para métodos numéricos en el análisis de elementos finitos y recibió muchos honores. En 1967 publicó su primera monografía en el campo del análisis de elementos finitos y es considerado un clásico. Los tres pioneros del análisis de elementos finitos vivieron considerablemente: Courant vivió 84 años, Argyris vivió 91 años y Zienkiewicz vivió 88 años.

El análisis de elementos finitos está muy cercanamente relacionado al desarrollo de las computadoras. En la década de los 50's y 60's hubo un gran desarrollo en la ciencia computacional, lo cual es un aspecto muy importante en el campo del análisis por elementos finitos.

En 1965 el software ASKA fue desarrollado. El bien conocido MSC.NASTRAN fue desarrollado en 1966 y desde entonces se convirtió en un programa oficial para la NASA. Todos los objetos que vuelan en el sector aeroespacial tienen que ser analizados con NASTRAN antes de su primer vuelo. MARC es un excelente programa para análisis no lineales y fue desarrollado en 1969. El software ANSYS el cual es ampliamente usado en los campos de estructuras y transferencia de calor fue creado en 1970. ADINA el cual tiene amplias ventajas en soluciones de problemas no lineales como problemas de contacto o colisión fue creado en 1975. DYNA2D y DINA3D el cual es comúnmente usado en problemas dinámicos y colisión entre otros fue desarrollado en 1978. Para investigación y solución de problemas no lineales ABAQUS es un excelente programa, este es ampliamente usado por investigadores y universidades, este fue desarrollado en 1979. COSMOS es una buena extensión para todas las formas de CAD software, así como también lo es PRO/E. También hay muchos programas desarrollados para computadoras con menos requerimientos de hardware, por ejemplo, ALGOR el cual fue creado en 1984. También hay cientos de paquetes de software de elementos finitos usados en ingeniería. Los mencionados anteriormente son los más bien conocidos.

Las primeras aplicaciones del método se dieron en ingeniería aeronáutica, poco tiempo después se comenzó a aplicar en ingeniería mecánica, civil, naval entre otras. Una de las ventajas de las simulaciones es que se puede estudiar un tema si tener que estar haciendo prueba y error experimentalmente, lo cual sería muy costoso como es el caso de la aeronáutica y la biomecánica donde los experimentos de prueba y error pueden costar una gran pérdida material y un gran número de vidas, a pesar de esto para realizar una buena investigación y tener más certeza en los resultados se recomienda correlacionar los resultados computacionales con resultados experimentales. En 1981 Sachio Nakamura presenta lo que puede ser el primer artículo del pie haciendo un modelo bidimensional y comienza a asignar propiedades mecánicas a los componentes del pie [12]. Los primeros modelos fueron realizados en 2D, sólo simulaban el tejido óseo y no diferenciaban el hueso cortical y el hueso esponjoso. Con el paso del tiempo, comenzaron a surgir más estudios sobre el pie; comenzaron a considerar diferentes propiedades mecánicas para el hueso cortical el cual es menos poroso y tiene mayor resistencia, y el hueso esponjoso que tiene un módulo de elasticidad bajo y una porosidad mayor [43]. La marcha humana es un problema dinámico, pero algunos autores para su estudio la han dividido en varios problemas estáticos, algunos autores han usado 3 fases para el caminar y otros autores han utilizado 6 fases para la marcha humana, así el problema dinámico se podía simplificar a

3 o 6 problemas estáticos lo cual reduce bastante el costo computacional. Otros autores han realizado simulaciones donde la marcha humana es resuelta como un problema dinámico. Poco a poco se han refinado las simulaciones del pie añadiendo ligamentos, cartílagos, tendones y la planta del pie. Estos materiales han sido caracterizados en laboratorios de pruebas mecánicas y dichas pruebas se llevan a cabo con cadáveres lo cual hace que las simulaciones se alejen de la realidad. En sí, simular una estructura tan compleja como el cuerpo humano es una gran tarea en la cual queda mucho trabajo por hacer, uno de los trabajos más recientes y completos sobre el pie es la tesis de doctorado de Enrique Morales Orcajo donde desarrolla un modelo de elementos finitos del pie completo y detallado en tres dimensiones. Este modelo es creado a partir de geometría real diferenciando hueso cortical y esponjoso, tendón, músculo, cartílago y grasa. En este trabajo también se realizaron ensayos mecánicos de tendones del pie y de la suela plantar para determinar sus propiedades mecánicas y caracterizar computacionalmente su comportamiento no lineal [44]. Por otro lado, también se han realizado estudios de elementos finitos analizando el pie con patologías como es el caso del trabajo de fin de máster del autor mencionado anteriormente donde hace simulaciones mediante un modelo en tres dimensiones para el estudio de la influencia de la geometría de la falange proximal del primer dedo en la formación de juanetes. En este estudio se hace una descripción cualitativa y cuantitativa de las falanges del primer dedo proporcionada mediante la disección de cadáveres [45].

1.5 Objetivos y alcance de la tesis.

La tesis que se presenta realiza una evaluación biomédica de tres implantes para corregir las patologías mencionadas anteriormente, así como dolor al caminar en el primer radio del pie, dichos implantes son nuevos tratamientos quirúrgicos de los cuales se tienen pocos estudios a la fecha.

El objetivo general de esta tesis es hacer una evaluación biomecánica de tres implantes los cuales pueden ser usados en un procedimiento quirúrgico en el primer radio del pie para corregir patologías como el hallux valgus, hallux rigidus y dolor en la articulación metatarsofalángica del primer dedo del pie. La evaluación biomecánica se hace por medio de una simulación en tres dimensiones del pie considerando el hueso cortical, el hueso esponjoso, ligamentos, músculos y tendones. Los demás elementos del pie no son considerados debido a que los huesos del primer radio son los elementos más afectados con el implante y hacer una simulación más compleja aumenta en gran medida el costo computacional. Como la patología es corregida por medio de un tratamiento quirúrgico, la simulación tiene la geometría de un pie corregido, es decir, el ángulo del hallux, así como el ángulo intermetatarsal están dentro de los valores normales. La evaluación biomecánica que se realiza comprende también un estudio a fatiga de los implantes ya que en la actualidad no se tiene información acerca del tema.

Los objetivos particulares de la tesis se pueden enlistar en la siguiente forma.

1. Dar una explicación de las patologías hallux valgus y hallux rigidus, de manera que la solución del problema sea fácil de comprender.

2. Hacer un estudio amplio de las correcciones que realizan los implantes investigados y su análisis estructural.

3. Investigar el problema de fatiga en metales usando un enfoque basado en deformaciones.

4. Realizar una evaluación biomecánica del pie recibiendo a cada implante.

5. Obtener un análisis de fatiga para los implantes biomecánicos.

1.6 **Descripción de la tesis.**

Esta tesis está formada por 5 capítulos y un apéndice como se muestra.

En primer lugar, se expone el primer capítulo de introducción, con el cual se ha dado una visión general del trabajo de tesis, una breve definición e historia de la ingeniería médica, una descripción de las patologías hallux valgus y hallux rigidus, un recuento histórico del método de los elementos finitos hasta nuestros tiempos y su aplicación en la biomecánica especialmente en el pie, así como los objetivos y alcance de tesis.

En el capítulo dos se elabora un estado del arte de las correcciones quirúrgicas más usadas en la aplicación de los implantes estudiados como tratamiento para el hallux valgus y hallux rigidus, en las cuales elegimos la queilectomía, la artroplastia con implante y a pesar de ser un procedimiento quirúrgico sin implante estudiaremos la artroplastia de resección de Keller. También se estudian los modelos de elementos finitos del pie y su evolución en los últimos años.

En el capítulo tres se realiza una evaluación biomecánica de los diferentes tipos de artroplastia en la primera articulación metatarsofalángica. Para esto se desarrollan varios modelos de elementos finitos del pie, en total se presentan cinco modelos: el primero estudia un pie sano libre de patología, el segundo realiza una hemiartroplastia en la primera falange proximal, el tercero analiza una hemiartroplastia en el primer metatarsiano, el cuarto estudia una artroplastia completa en la primera articulación metatarsofalángica y el quinto realiza una artroplastia de resección de Keller.

En el capítulo cuatro se presenta el desarrollo para obtener las curvas, deformación versus vida a fatiga, $\varepsilon - N_f$ para los implantes de la primera articulación metatarsofalángica estudiados en esta tesis. Esto se hace a partir de los resultados deterministas de los modelos de elementos finitos presentados en el capítulo anterior. Se hace una breve explicación de la formulación del método de los elementos finitos probabilistas así cómo el desarrollo de las expresiones de Ramberg Osgood y Coffin-Basquin-Manson para la construcción de modelos B de salto de unidad.

El capítulo cinco hace una recopilación de las conclusiones y aportaciones originales de este trabajo de tesis. También se comenta acerca de las líneas futuras de investigación que se abren tras el desarrollo de esta tesis.

Por último el apéndice A muestra una breve explicación de la validación del modelo no determinista desarrollado en el capítulo cuatro comparando los resultados obtenidos con una simulación de Montecarlo.

1. INTRODUCTION.

1.1 *Engineering and Medicine: Biomedical Engineering; Biomechanics.*

After Second World War the need arose to implement technologies for the health area. Since then the field of medical technologies has been advancing remarkably day by day, this fact has been limiting medical professionals in their need to keep pace with these changes. Due to the lack of knowledge and understanding of biological and medical problems of these first engineers, there was a need to train professionals, who could apply the principles and methods of engineering to medical and biological problems [19].

Bioengineering encompasses all possible interactions between natural sciences and engineering, deriving in biomedical engineering, which focuses on human beings and health care. According to Giovanni Gismondi [20] biomedical engineering is the branch of engineering that implements the principles of technologies to medical field. It is mainly dedicated to the design and construction of medical equipment, prostheses, medical devices, diagnostic and therapy devices, it is also responsible for linking the world of engineering with medicine and physiology to achieve advances in scientific knowledge and technology development in medicine and biology.

The Committes of Engineer's Joint Council of the United States of America defined Bioengineering in 1972 as the application of the knowledge gathered from the fertile union between engineering and medical science for its application for the benefit of man. Another quite accepted definition is that made by Heinz Wolff in 1970 that says: bioengineering consists in the application of engineering techniques and ideas to biology, and specifically to human biology. The large sector of bioengineering that refers especially to medicine, can be more appropriately called biomedical engineering [21].

The Society of Engineering in Medicine and Biology (EMB) of the Institute of Electrical and Electronic Engineering (IEEE) in an article called "Designing a career in Biomedical Engineering" published in 2003 [22], defined as areas of biomedical engineering to bioinformatics, biomicroelectromechanical systems, biomaterials, biomechanics, biosignal processing, biotechnology, clinical engineering, genomics, medical images and their processing, information technology, instrumentation, sensors and measurements, micro and nanotechnology, nervous system and engineering, modeling of physiological systems, proteomics, radiology, rehabilitation engineering, robotics in surgery and telemedicine [19].

The application of forces in a living organism and the investigation of the effects of these forces on the human body or on a human system, including the forces that arise from inside and outside the body, is called biomechanics. Biomechanics also includes the study of the structures and functions of a biological system through the laws of mechanics applied to muscular activity [23].

A good definition of biomechanics tells us that it is the set of interdisciplinary knowledge generated from using, with the support of other biomedical sciences, the contributions of mechanics and different technologies in, first, the study of the behavior of biological systems, in particular the human body, and second, in solving the problems caused by the different conditions to which it can be subjected [21].

There have found biomedical engineering practices since the time of ancient Egypt, Andreas G.

Nerlich in his article [1] comments on a mummy found in a chamber dating from approximately 1065-740 BC. Anthropological research indicated that the mummy was a woman aged 50 to 55 years. Her height was approximately 1.69 m . The paleontological examination showed that the great toe of the right foot had been amputated during the life of the person because in the place of amputation the soft tissue was shown intact as can be seen in Figure 1.1A. The extracted Toe had been replaced by a wooden prosthesis, which is shown in Figure 1.1B. The components of the prosthesis were three pieces of wood, a longitudinal piece of 12x3.5x3.5 cm attached to two small wood plates of 4x2.5x0.3 cm . These plates were fixed by leather ropes. All the wooden parts were delicately carved, amazingly imitating the shape of the great toe, including the nail. A leather cord was attached to the small plates and the prosthetic body, which was tied to the forefoot. A careful inspection revealed the use of the prosthetic body as seen in Figure 1.1C. A radiology and CT scan showed that the first metatarsal was poorly demineralized, which can be seen in Figure 1.1D. A Roman citizen named Galen of Pergamum

Fig. 1.1: Views of the prosthesis and the right foot of a mummy [1].

(131-201 AD) was considered the first doctor of the gladiators. Galen wrote an essay entitled De Motu Musculorum in which he describes differences between sensory and motor nerves. He described the muscle tone and introduced the terms diarthrosis and synarthrosis which are used until these days as the correct arthrology terminology [23]. Other authors say that the first developments in bioengineering date from the time of Leonardo Da Vinci (1452-1519) with his anatomical drawings and approaches to lever arms [20]. Isaac Newton (1642-1727) established modern biomechanics and its laws of inertia, acceleration and action and reaction are the best validated laws in modern biomechanics [23]. Other pioneers of biomechanics are Luigi Galvani (1737-1798) and Lord Kelvin (1824-1907) as they reflect in their work on electrical conduction in living beings [20]. We could mention many more but these are just some of the first to investigate human anatomy and mechanics.

The first official program of study in biomedical engineering began in 1959, as a Master's degree at the American University of Drexel and in that same year the first international conference on biomedical engineering was held in Paris. It was not until 35 years later in 1994 that the fifteenth world conference was held at a Latin American headquarters (Rio de Janeiro) [20].

Biomedical engineering is one of the professions with the greatest future in the world, because every year the governments of different countries invest millions of dollars in the development

of new technologies in order to raise the quality of life of people, having the need for experts in the design and development in that area.

This thesis is in the area of biomechanics and develops a biomechanical analysis using finite elements for a surgical procedure against hallux valgus and hallux rigidus called arthroplasty. In this surgical procedure the effect of three different implants in the first ray of the foot is studied. In the case of some implants, cyclic stresses can produce possible fatigue failure [24]. This thesis develops a fatigue analysis of three different implants of which there are no studies at present. In the following lines we will make a description of the pathologies to study and we will make a historical account of the finite element method to finally include these topics in the objectives, methodology and scope of the thesis. To better understand the following reading of this thesis, we recommend that the reader first read Annexes I and II. If the reader has a medical history and has good anatomical bases, he can skip that reading without any problem.

1.2   *Hallux valgus.*

1.2.1   *Pathology.*

Hallux valgus is a disease that was first described by Carl Hueter (1838-1882) in 1871 who describes this deformity as an abduction contracture in which the first toe, deviated laterally, moves away from the middle plane of the body [25], [26]. This pathology is one of the most frequent deformities of the foot. The term hallux valgus refers to the angulation of the great toe outward, often diverting the other two toes. It is characteristic the prominence that forms the head of the metatarsal which is commonly known as bunion. In most cases, the deformity of the first ray is associated with a symmetric deviation of the fifth ray: Fifth metatarsal in valgus and fifth toe in varus along with hammer deformities or dislocations of the central toes [27].

Hallux valgus is a disorder of alignment of the first ray of the foot, which alters its static and dynamic function, in terms of support and load's transmission, and mechanism of toe-off of during gait. This alteration of the position of the first metatarsal affects distally, causing a loss of the position of the head of the metatarsal with respect to its accommodation in the glenosesamoid apparatus that, keeping in a normal situation, causes an imbalance of the muscular forces acting on the ray , favoring the valgus position of the toe and its progressive rotation in pronation.The development of hallux valgus in older children and adolescents is rare. Some authors suggest that this deformity is rarely found before the age of 10, which means that it usually occurs during development.The following alterations characterize hallux valgus. They do not always have the same intensity or proportionality with each other [27].

- Deviation of the great toe. A discreet valgus is physiological; it is considered pathological when the deviation is greater than 15 degrees. Sometimes it almost forms a right angle with the first metatarsal.

- Increased angle between the first and second metatarsals. Normally it is about 10 degrees, but in the hallux valgus it increases and forms varus deviations of up to 30 degrees.

- Bunion. It is the prominence that forms the first metatarsal together with the deviation of the toe constituting a small exostosis separated by a very clear vertical groove on the articular face of the metatarsal.

- Sesamoid dislocation. As a consequence of the metatarsal deviation, the sesamoids deviate outward, not being symmetrical in relation to the first metatarsal, but subluxing partially or totally in the first intermetatarsal space.

- Muscular dysfunction. The great toe adductor becomes a flexor, while the flexors become abductors. The force that deflects the toe outward is not neutralized by the adductor; therefore, the deformity is progressive.

- Alterations of the metatarsophalangeal joint. Not perfectly spherical joint congruence makes passive correction difficult. In older people, osteoarthritis appears, structuring the deformity and making the joint painful.

- Alterations in the cuneometatarsal joint. This joint determines the direction of the first metatarsal. when the interlines are curved, the deviation is easily corrected, but when they are straight, this deviation is more difficult to correct and may become fixed and, later, osteoarthritis may appear.

- First ray insufficiency syndrome. These alterations of the first ray are usually accompanied by their consequences that appear on neighboring rays.

- Origin of pain in hallux valgus is produced by the following causes.

    - Pain from overload in the central metatarsals. Metatarsalgia is usually earlier and more intense than bunion pain.

    - Pain from rubbing exostosis with footwear. Hyperkeratosis and hygroma appear, sometimes very painful.

    - Joint pain when metatarsophalangeal osteoarthritis arises, more frequent in older people.

There are several clinical types of hallux valgus, among them is congenital hallux valgus which has an early appearance, that is, before the age of 15 years, including the disappearance of the intersesamoid crest with dysplasia in the metatarsophalangeal joint and atrophy of the lateral sesamoid. Another type is hallux valgus due to the prominence of the metatarsal head in which the deviation of the proximal phalanx is small and a thickening of the metatarsal head appears. A third type is the hallux valgus in the triangular forefoot, with a large eminence of the metatarsal appearing next to the medial articular zone, a relaxation of the medial articular capsule together with a displacement of the metatarsal head of the sesamoids. The second toe may be above or below the hallux with a possible displacement in the joint due to stretching of the soft tissues or a dislocation of the metatarsophalangeal joint, in figure 1.2 can be seen an example of a patient who has the disease developed so that the hallux is located below the second toe. Finally we have severe hallux valgus in which there is an intrinsic bone deformity in the proximal phalanx that determines a bulge on the interphalangeal joint and sometimes generates a painful callus on the middle face of the hallux [3].
Hallux valgus reduces weight bearing on the foot, so the evaluation of the deformity should be carried out in a bilateral load position and the range of motion of the subtalar joint, ankle, metatarsophalangeal joints and tarsal joints in both feet and compare them. For the evaluation of hallux valgus, a radiological examination in three positions must also be carried out [3].

1. Dorsoplantar projection under load: It is made to measure 4 angles. The first one is formed by the longitudinal axis of the metatarsal bone with the longitudinal axis of the first proximal phalanx, this angle is known as the hallux valgus angle and is considered normal if deflection is less than 15 degrees. The second one is the intermetatarsal angle, which measures the opening between the first and second metatarsal bone, and it is considered normal if deflection does not exceed 9 degrees. The third one is the distal articular set angle, which is formed with the joint surface and the axis of the first metatarsal and usually deflection is not greater than 10 degrees, and the fourth one is formed by the
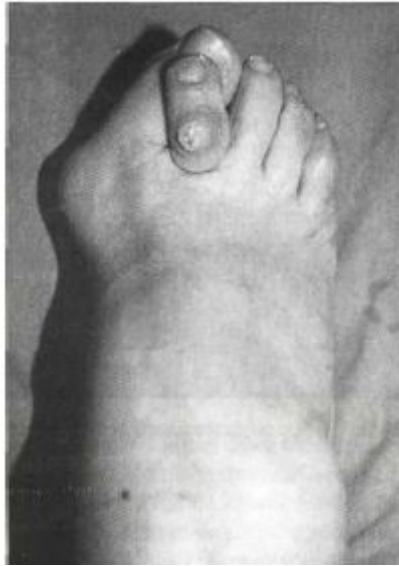
Fig. 1.2: Hallux valgus developed in such a way that the second toe is above the hallux [2].

longitudinal axes of the phalanges of the great toe, also known as interphalangeal angle, which is considered normal when deflection is less than 10 degrees [3], [28] [29]. Figure 1.3 shows the angles used to measure hallux valgus grade.
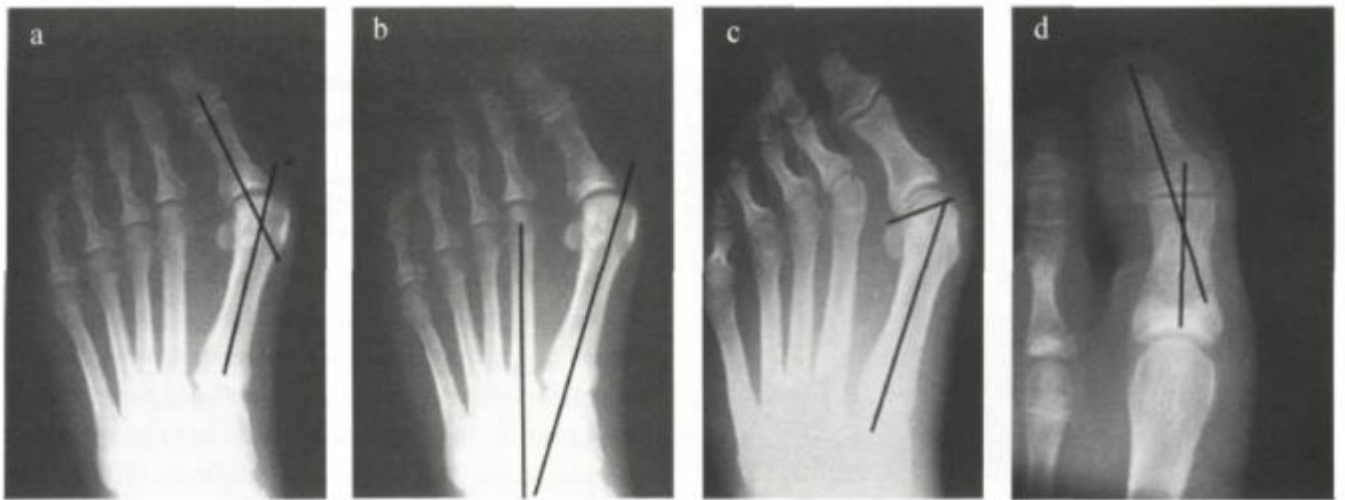
Fig. 1.3: Angle of hallux valgus (a). Intermetatarsal angle (b). Distal metatarsal joint angle (c). Interphalangeal angle [3].

2. Lateral projection under load: Indicates the information on how the metatarsal-phalangeal and cuneo-metatarsal joints are located.

3. Walter-Müller projection: This projection gives us the opportunity to measure the relationship between the sesamoids with the first metatarsal.

In 2001 Garow et al described in the Journal of the American Podiatric Medical Association a new non-invasive technique, through the development and validation of a series of discharged photographs, designed to classify the degree of hallux valgus deformity, this scale is known as the Manchester scale. Some limitations of this scale is that it is based on a qualitative

method using photographs, without quantitative measurements, so the degree of deformity can vary according to the criteria of the explorer. This scale is mainly based on the degree of abduction and other parameters such as the position of the sesamoids, joint congruence, range of movement and the level of osteoporosis of the joint, among others, are not considered [25]. Figure 1.4 shows the Manchester scale where part A corresponds to grade 1 in which there is no deformity, part B corresponds to grade 2 in which the deformity is considered mild, part C corresponds to grade 3 where the deformity is considered moderate and part D corresponds to grade 4 which is a severe deformity.

Fig. 1.4: Manchester Classification [4].

To make a correct evaluation of hallux valgus, a baropodometric study must also be carried out, this type of study is also known as a tread study, that is, the static and dynamic biomechanics of the foot support are studied. Thanks to these measurements, hallux valgus can be classified into three types [3].

1. Hallux valgus medium. This type is characterized by having an intermetatarsal angle of deflection less than 11 degrees, a hallux valgus angle of deflection less than 30 degrees, and a displacement of lateral joints of the sesamoids of less than 50%.

2. Hallux valgus moderate. This type is characterized by having an intermetatarsal angle of deflection greater than 11 degrees, but less than 16 degrees, the deflection in the angle of the hallux valgus is between 30 and 40 degrees and displacement of the lateral joints of sesamoids between 50 and 75%.

3. Hallux Valgus severe. This type of deformity has an intermetatarsal angle of deflection greater than 16 degrees, the angle of the hallux valgus deflection is greater than 40 degrees, and the displacements of the lateral seamoid joints are greater than 75%.

Figure 1.5 shows the degrees of hallux deformity where the arrows indicate the direction of the subluxation, and the tips of the arrows indicate the magnitude of the articular surface.

Figure 1.5-A shows a mild hallux valgus with a first metatarsophalangeal subluxation, a hallux valgus angle of deflection of 19 degrees, an intermetatarsal angle 1-2 of 10 degrees, and a sesamoid subluxation of less than 50%. Figure 1.5-B shows a moderate hallux valgus with first metatarsophalangeal subluxation, a hallux valgus angle of deflection of 30 degrees, an intermetatarsal angle 1-2 of 14 degrees, and sesamoid subluxation of 50 to 75%. Finally, figure 1.5-C shows a severe hallux valgus with drastic first metatarsophalangeal subluxation, a hallux valgus angle of deflection of 50 degrees, an intermetatarsal angle 1-2 of 17 degrees, a sesamoid subluxation greater than 75% and the second joint appears dislocated.

Fig. 1.5: Degrees of deformity of hallux valgus [5].

1.2.2   *Etiology and etiopathogenesis.*

There are several structural factors that are related to the development and progression of hallux valgus. The most widely accepted are ligament laxity and flat feet. The length of the first metatarsal has been considered a risk length for the appearance of hallux. The use of inappropriate footwear is recognized as a trigger factor, in women footwear is probably more important as a progression than as a causative factor [27], [26]. The existence of certain anatomical variations in the forefoot may produce, in some people, the risk of developing the pathology. The shape and orientation of the metatarsophalangeal and metatarsal cuneiform joints may be the key to the development of hallux valgus, as well as its correction. To date, no clear link has been established between hallux valgus and obesity or with other factors that affect foot load such as the angle of progression of the foot [27], [30].
There are multiple theories that explain the origin of hallux valgus, mostly referring to the physiology of said deformity, rather than its etiology. For us, apart from some postural forms related to footwear or certain activities such as ballet, hallux valgus is only one aspect, the

most visible, of the syndrome of insufficiency of the first ray. For this reason we consider that in hallux valgus there are [27].

1. Predisposing congenital factors: An forefoot with a long, Egyptian type toe and a short first metatarsal, deviated in varus. To this is added a weak musculature of the first ray with impaired function.

2. Triggers, mainly footwear and rheumatoid arthritis.

3. Structuring of the deformity, due to arthritis or arthrosis.

There is weak evidence of a racial difference. The prevalence of hallux valgus in whites is reported to be twice that of black Africans [26].

To date, the cause of this pathology is unknown. Currently hallux valgus affects women more than men although there is no clear evidence of this, there are studies that show that in populations studied in France the influence of hallux valgus was greater in men during the 16th and 17th centuries [31]. There are differences in the bone anatomy of men and women, for example, the surface of the articular head of female patients is much more rounded and smaller, giving less stability to the joint. There is also a greater tendency in women to have more adduction in the first metatarsal, which in turn may be the differences in the metatarsal junction. There are also other differences such as the size of the distal and proximal joint of the first toe, its shape and angle [26] There is a note written in 1845 by Queen Victoria of England that says: 'One of the most certain causes of a bunion is the wearing of shoes made too short and with a narrow sole' [32].

1.2.3 **Treatment.**

Treatments against hallux valgus have made considerable progress in recent years. Osteotomies are operations in which cuts are made in a bone so that changes can be made in its position, such as correcting curvatures or angulations of the metatarsals and it is a procedure that is performed under general anesthesia. Osteotomies at the level of the first metatarsal, first wedge, osteotomies and shortening of the first phalanx, supplemented in most cases with soft tissue surgery, are the surgical gestures most frequently used to correct hallux valgus and hallux rigidus [3]. On the other hand, osteodesis uses cerclage structures between the first and second metatarsals to realign the first metatarsus and correct the deformation of the intermetatarsal angle. The first osteodesis technique was reported in 1961 [33]. Arthrodesis is another surgical procedure in which two bone pieces are fixed, anchoring a joint, this is a correction with high potential for treatment against hallux valgus [34]. Arthroplasty is a surgical procedure that involves replacing the diseased or damaged joint surface (bone and cartilage) with another material (metal, ceramic, polymer, etc.). This procedure is used in patients with advanced degrees pathologies such as hallux valgus, hallux rigidus, hallux [35]. Another surgical method is percutaneous surgery, which allows making minimal incisions without direct exposure of the surgical planes. This technique includes several surgical gestures because there is no surgical technique that alone can correct all the pathological elements of deformities of hallux valgus and hallux rigidus [2].

Conservative treatment is usually ineffective. The use of toe spreaders or bunion racks is useless. The same measures indicated in the bloodless treatment of first ray insufficiency syndrome may be recommended. Regarding surgical treatment, there is still no consensus on hallux valgus surgery. More than 100 interventions are described; Among them, those that alter the biomechanics of the foot usually give poor results, even achieving a relatively good aesthetic. It is also interesting to note that, among the multiple interventions that respect biomechanics, subjective results are good in more than 80% of cases. The percentage decreases on objective

assessment and radiology is often quite poor. Based on these facts, the simplest techniques with the shortest postoperative are preferable. It can be affirmed that in the case of hallux valgus, the complexity of the surgery is not proportional to the goodness of its results [27].

To date there is no technique that can be applied to the different types of hallux valgus and hallux rigidus. Hallux valgus is a very old pathology, due to this there are many conservative treatments that are not necessarily effective in curing the pathology, among them is to recommend the patient to wear shoes wide enough so they do not compress the toes and wear low heels, around 5 cm at most. It is also recommended to apply anti-inflammatory and pain relievers in the initial stages of hallux valgus in order to improve the walking process. Some doctors recommend using local ice for 20 minutes three times a day [4]. There are also exercises and massages for strengthening and stretching the first toe. Another alternative is surgical treatment, of which there are many techniques which can be classified into: Soft tissue procedures, osteotomies, arthrodesis, arthroplasties and combined procedures [3].

Surgical treatment is an alternative when conservative treatment has not given good results and therefore the surgical technique to be used must be adjusted to the needs of each patient. Despite the etiology, biomechanics, and the use of finite elements, this problem remains poorly understood [36].

1.3 Hallux rigidus.

1.3.1 Pathology.

Hallux rigidus is the second most frequent pathology of the first metatarsophalangeal joint after hallux valgus [6]. This pathology is an entity characterized by presenting permanent pain with a sensation of joint crunches when the first finger is mobilized, which increases with support and walking and is usually associated with a decrease in joint function, as well as the appearance of a lump or excrescence in the metatarsophalangeal dorsal region of the first ray [27]. Sesamoids are longer and the distance from the base of the proximal phalanx decreases as joint involvement progresses [6]. This pathology is generally associated with a limitation of the movement of the first ray of the foot, especially in dorsiflexion, medically called osteoarthritis of the metatarsophalangeal junction of the first toe [8]. The original description of this condition has been attributed to Davies-Colley, who called it hallux flexus in an article published in 1887. The name hallux rigidus was proposed four months later by Cotterill, and it remains the most common designation despite the defense of several authors by other terms such as: hallux limitus, hallux dolorosus, metatarsus non extensus, dorsal bunion, winkle-picker disease and metatarsus primus elevatus. The history of terminology was well summarized by Kelikian [6], [37].

The arc of mobility of the first metatarsophalangeal joint is 110 degrees, with a plantar flexion of 35 degrees and a dorsal flexion of 75 degrees. In hallux rigidus the range of motion decreases and a decrease in dorsal flexion, caused both by dorsal osteophytes and by the retraction of plantar soft tissues[6]. It is rare that hallux rigidus appears in young patients, being more normal in men between 40 and 60 years old. Its main symptom is pain in the toe pad, with a sensation of joint crunches, while joint mobility is diminished in its evolutionary course. The appearance of pain in the head of the fifth metatarsal is also very frequent. The existence of a lump in the dorsal region of the first metatarsophalangeal joint is a relatively frequent sign, especially in very advanced cases [27].

One of the reasons why hallux rigidus occurs is due to an imbalance of the soft tissues that alter the normal biomechanics of the first metatarsophalangeal joint. The proximal phalanx is progressively placed in a plantar position with respect to the metatarsal head, causing a gradual displacement of the center of rotation of the joint, clamping the joint dorsally during

movement in dorsiflexion. The repeated concentration of high demands on compression, in the dorsal portion of the head of the first metatarsal, causes the appearance of cartilaginous lesions and the progressive development of dorsal osteophytes evolve towards gradual articular degeneration, leading to total ankylosis [6]. Hallux rigidus is a degenerative disease that evolves over time. There are several classifications for the degree that the disease acquires. Núñez-Samper [27] In his biomechanics, medicine and foot surgery book, he says that hallux rigidus is a process that fundamentally evolves in three phases, each of which will present a different symptomatology and radiological semiology, which will condition treatment accordingly.

- Phase I. It is the beginning of the process, it presents in the patient an acute or subacute pain sporadically in the take-off stage of the foot, or when it makes free flexion-extension movements of the first toe. There is some limitation of joint mobility. Radiographically, a slight periarticular condensation and a decrease in the joint space appear, representing the onset of subchondral sclerosis with a minimum degree of osteophytosis, mainly on the lateral aspect, in the form of a roof, which gives a very typical appearance to the metatarsal head.

- Phase II. It is the phase of arthrosis or joint degeneration itself. The patient reports that he walks with the foot in supination, since the pain is constant, although of variable expression, ranging from intermittent to live, when the mobilization of the joint occurs. This is almost completely limited, while hyperkeratosis appears in the plantar support areas of the first and fifth metatarsophalangeal joints. Radiographically, there is disappearance of the joint line, with peripheral condensation of marginal osteophytosis with an eburnal appearance, both at the base of the phalanx and in the head of the metatarsal. Also, there is an irregularity of the edges of the sesamoid impeller.

- Phase III. It corresponds to the phase of ankylosis or complete stiffness of the joint that becomes a block; the pains are permanent due to joint hypertrophy and compression of the collateral nerve by an osteophyte. When supporting the foot, the pain is also evident in plantar hyperkeratosis. It is common to observe in this phase a retraction of the flexor tendon, typical of the first toe, which produces an entity called hallux rigidus flexus. The radiographic study is evident: complete disappearance of the joint, anarchic osteophytic hypertrophy with a sesamoideophalangeal bridge and hypercondensation of the peripheral articular bone, while the base of the first phalanx adopts a typical bell-shaped shape, corresponding proportionally to the metatarsal head.

Some other authors prefer to consider the classification of Coughlin et al. [8], [38] for their studies. These authors base their classification on finding subjective and objective radiographs and clinical data. This classification is summarized in Table 1.1, which is shown below. Anteroposterior, lateral, and weight bearing radiographs are used for Table 1.1.
Radiographs of the hallux rigidus appear in Figure 1.6 below. In part a, we can see an anterior posterior x-ray in charge of the feet, with complete loss of the joint space of the first metatarsophalangeal of both feet. Part b shows a load profile radiograph showing the tear-shaped dorsal osteophyte characteristic of hallux rigidus and part c shows an oblique radiograph where we can see the real joint space due to the absence of osteophyte interposition.
Another classification based on x-ray analysis is Regnauld's classification which mentions three degrees of hallux rigidus [39].

- Grade I. Condensation of bone around the joint. Slight narrowing of joint space. Sesamoids are regular but slightly enlarged.

- Grade II. Moderate osteophytes. Narrowing of joint space. Subchondral sclerosis or cysts. Hypertrophy and irregularity of sesamoids.

Tab. 1.1: **Clinical and radiological system for the evaluation of hallux rigidus by Coughlin and Shurnas.**

Grade	Dorsiflexion	Radiographic findings	Clinical findings
0	40-60 degrees and /or 10% to 20% loss compared with normal side	Normal	No pain; only stiffness and loss of motion on examination
1	30-40 degrees and/or 20% to 50% loss compared with normal side	Dorsal osteophyte is main finding, minimal joint-space narrowing, minimal periarticular sclerosis, minimal flattening of metatarsal head	Mild or occasional pain and stiffness, pain at extremes of dorsiflexion and/or plantar flexion on examination
2	10-30 degrees and/or 50% to 75% loss compared with normal side	Dorsal, lateral and possibly medial osteophytes giving flattened appearance to metatarsal head, no more than 1/4 of dorsal joint space involved on lateral radiograph mild to moderate joint space narrowing and sclerosis, sesamoids not usually involved	Moderate to severe pain and stiffness that may be constant; pain occurs just before maximum dorsiflexion and maximum plantar flexion on examination
3	$\leq$ 10 degrees and/or 75% to 100% loss compared with normal side. There is notable loss of metatarsophalangeal plantar flexion	Same as grade 2 but with substantial narrowing, possibly periarticular cystic changes, more than 1/4 of dorsal joint space involved on lateral radiograph, sesamoids enlarged and/or cystic and/or irregular	Nearly constant pain and substantial stiffness at extremes of range of motion but not at mid-range
4	Same as grade 3	Same as grade 3	Same as grade 3 but there is definite pain at mid-range of passive motion

- Grade III. Severe osteophytes. Complete disappearance of joint space. Degenerative hallux-metatarsosesamoid joint.

On the other hand, Hattrup and Johnson carry out another classification also based on the radiographic appearance, which also contains three grades [46].

- Grade 1. Degenerative changes with mild dorsal exostosis and good joint preservation.

- Grade 2. Degenerative arthritis with definite joint space narrowing accompanying the dorsal osteophyte and subchondral sclerosis Marked.

- Grade 3. Marked osteoarthritis with loss of the joint space and possible subchondral cysts.

As it can be seen the classification that Núñez-Samper mentions, the Regnauld classification and the Hattrup and Johnson classification are similar, but still there are authors who prefer to cite one instead of the other in their studies.

The American Orthopedic Foot and Ankle Society (AOFAS) [38] introduced a scale in 1994 to measure pain in patients at the metatarsophalangeal junction of the first toe. In the article titled Clinical Rating Systems for the Ankle-Hindfoot, Midfoot, Hallux and Lesser Toes [40], AOFAS proposes four scales for a better understanding with a simple way of describing the condition of the foot and ankle. In this article they mention that the scales should be applicable for different clinical situations such as evaluation of patients after arthrodesis, arthroplasties with implants and ligaments reconstruction. The scales can reach scores of up to 100 points where radiological data is not included so that the data is strictly clinical, they do not assign numerical values, preferring to assign results such as: excellent, good, fair and poor. The clinical factors that make up each scale are subjective and objective. The four scales presented in the article are: the ankle and forefoot scale, the midfoot scale, the hallux metatarsophalangeal-interphalangeal scale and the minor toes metatarsophalangeal-interphalangeal scale. The hallux metatarsophalangeal-interphalangeal scale section is described as a scale to measure the degree of the first metatarsal,
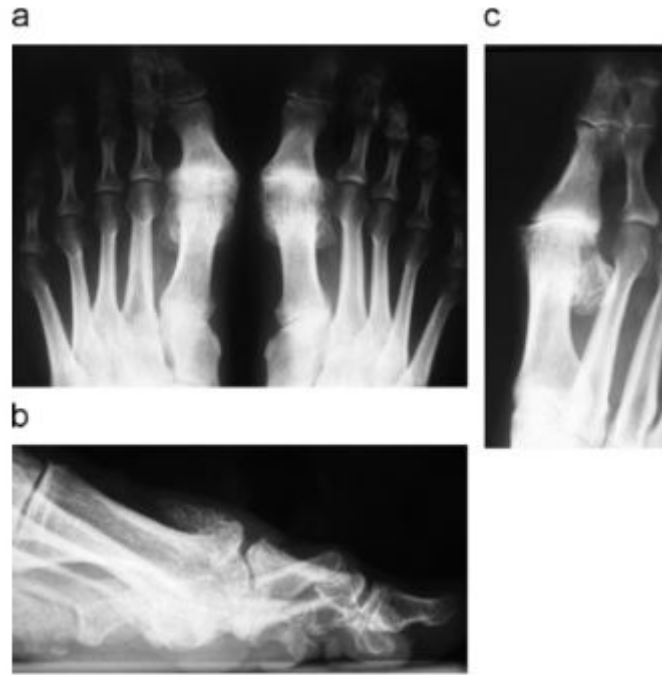
Fig. 1.6: X-rays of hallux rigidus [6].

metatarsophalangeal junction, proximal phalanx, distal phalanx, and interphalangeal junction of the first toe. and can be applied to hallux valgus, hallux varus, hallux, rigidus, osteoarthritis, traumatic or inflammatory osteoarthritis, interphalangeal hallux valgus, claw toe, hammer toe, metatarsophalangeal arthrodesis, cheilectomy, metatarsophalangeal implant arthroplasty, resection arthroplasty, instability or dislocation, interarticular and extra-articular fractures of the first metatarsal and phalanges of the first toe. On the scale, 100 points can be obtained if the patient is pain-free, has a complete metatarsophalangeal and interphalangeal range of motion, there is no metatarsophalangeal and interphalangeal instability, good alignment of the first ray of the foot, there is no limitation in daily or recreational activities and there is no limitation regarding footwear. In the scale, 40 points were assigned according to the pain that the patient may have, 45 points to the functionality of the first ray of foot and 15 points to the alignment of the first ray. Appendix III presents the four scales proposed by AOFAS in its article published in 1994.

1.3.2 *Etiology and etiopathogenesis.*

Hallux rigidus is a common form of osteoarthritis in the foot. The radiological signs of the disease can be recognized in 10 % of people between 20 and 34 years of age and in 44 % of people over 80 years of age. The exact cause of the disease is controversial. Coughlin et al. (2003) demonstrated that 80 % of all patients with bilateral hallux rigidus have a family history. Furthermore, in their study they were able to demonstrate that the majority of patients develop bilateral hallux rigidus over time. Some authors blame footwear, a narrow Achilles tendon, a long first toe, a flat foot particularly when the person wears rigid boots, a congenital flattening of the head of the first metatarsal, an osteochondritis dissecans on the head of the first metatarsal, or the belief of a spontaneous start [8], [37]. Another popular concept is that a first elevated ray, which is called metatarsus primus elevatus, results in hallux rigidus, while some authors are in favor of this theory, others oppose it. Coughlin et. al say that the normal elevation is considered to be ≤ 8 mm, and the normal inclination of the first metatarsal has been reported to be between 19 and 25 degrees and they propose that the metatarsus primus elevatus may be

a secondary change due to hallux rigidus, leaving the exact cause of hallux rigidus to remain controversial [6], [38]. In any case, it is well known that women currently develop a higher incidence than men and this occurs mainly after the age of 40 [6], [41]. The most common cause for unilateral hallux rigidus is the belief that it is trauma from an isolated injury or from a repetitive microtrauma, this may be a chondral injury and result in a progressive change in arthritis [8]. From the studies carried out by Rochera we can say that the abnormal increase in load on the metatarsal head is the most fundamental cause in the development of this pathology and that it appears in the first long and powerful metatarsals, with a metatarsal index plus shape. They would be metatarsals that had a proximal and distal physis during their development, most of them corresponding to males. Authors such as Viladot defend an etiology by microtrauma, which, produced by the use of the shoe, would act by striking the first toe against it, parallel to the second and with good muscular balance. On the other hand, De Donker and Kowalski, affirm that the cause of the production would be a muscular imbalance between the flexor long and short of the great toe with the extensors, which would produce decompensation and joint overload, causing a metabolic alteration of the cartilage with its consequent degeneration and osteoarthritis. Finally, it places the cause of production in metabolic disorders and osteoporosis, more or less discrete, produced in the course of trauma or microtrauma, infectious or inflammatory processes, or secondary to immobilizations. Either way, most of these concepts are theoretical and lack scientific evidence [27].

1.3.3 **Treatment.**

Conservative medical treatment, in principle, is palliative. The hygroma can be treated with keratolytic ointments, fundamentally avoiding infection. Retrocapital orthoses, over-lifting and unloading the joint, can be used in phase I. The use of a semi-cylindrical anterior heel can also be useful in the shoe [27]. In the absence of pain, the initial stages of the disease or in patients with surgical contraindications, conservative treatment is usually indicated. The placement of a template that produces an elevation of the metatarsal head artificially increasing the width of the dorsiflexion, can improve the patient's symptoms [6]. Some surgical techniques have been briefly described in the section that talks about treatment against hallux valgus, that is, because some surgical techniques are common for both diseases. Among the destructive surgical techniques we have arthrodesis, arthroplasty and cheilectomy, while as non-destructive surgical techniques there are many kinds of osteotomies [8]. Finally, to close this section about pathologies, we can say that in grade 0 and 1 of Coughlin and Shurnas, the treatment of choice is conservative. Grade 2 is the ideal indication for metatarsal osteotomies, which by lowering and shortening the metatarsal avoids transfer metatarsalgia and decompresses the metatarsophalangeal joint. Also in grade 2, cheilectomy can improve dorsiflexion of the metatarsophalangeal joint and painful symptoms. Cheilectomy is indicated in grade 3. Hemiarthroplasty implanted in the phalanx associated with joint cleaning is also indicated. In elderly patients, Keller's intervention or metatarsophalangeal arthroplasty is used with acceptable results. In grade 4, the technique of choice is metatarsophalangeal arthrodesis. Metatarsophalangeal arthroplasties are indicated in elderly patients with little functional demand: likewise, in patients with ankle involvement, we must avoid, as much as possible, arthrodesis of the metatarsophalangeal joint [6].

1.4 **History of the finite element method.**

The following is a brief historical account of the finite element method [42]. The idea of finite elements is over a century old. The idea came from two aspects, one is engineering, the other is mathematical. The engineers were inspired by the structures of the engineering

problems and used an intuitive approach to build the test functions. On the other hand, mathematicians introduced finite elements to solve differential equations and control the error of the test functions.

The classic variational engineering method was developed by Rayleigh over 140 years ago, which is called the Rayleigh method (John William Strutt, Third Baron of Rayleigh 1842-1919). Another variational method was developed by Walter Ritz (1878-1909) 105 years ago. Together these two methods are now called the Rayleigh-Ritz method, which is commonly used in deformable-body mechanics. Later John Hadji Argyris (1913-2004) in 1955 developed the guide of the continuous elements which is a matrix method used in mechanics. Richard Courant (1888-1972) specialized in applied mathematics combined engineering and mathematics, in 1943 he systematically studied continuous test functions. Olgierd Cecil Zienkiewicz (1921-2009) a mathematician and engineer developed in 1964 a continuous series test function which is one of the modern foundations of finite elements. Mathematician Carl Friedrich Gauss (1777-1855) developed the weighted residual method in 1795. Boris Galerkin (1871-1945) contributed greatly to the finite element method in 1915. The following people are pioneers in the field of finite elements. Courant, a German-born mathematician who later emigrated to the United States of America built an institute for applied mathematics in 1928. In 1964 the institute was called the Courant Institute for Mathematics Science, whose main line of research is that of finite elements. Courant's minimum principle is an important theorem that was named after him. Argyris is a Greek who emigrated to Germany and is a widely distinguished and recognized expert in computational science. He is hailed as one of the inventors of the finite element method. His contribution was the idea of the displacement matrix in mechanical analysis, which is a predecessor to the finite element method. In 1950 he became the director of the institute for applied computing at the University of Stuttgart and worked as director for almost 40 years. Zienkiewicz, an Englishman, was a professor in the civil engineering department at the University of Swansea. He founded a magazine for numerical methods in finite element analysis and received many honors. In 1967 he published his first monograph in the field of finite element analysis and is considered a classic. The three pioneers of finite element analysis lived quite a bit: Courant lived 84 years, Argyris lived 91 years, and Zienkiewicz lived 88 years. Finite element analysis is closely related to the development of computers. In the 1950s and 1960s there was a great development in computer science, which is a very important aspect in the field of finite element analysis.

In 1965 ASKA software was developed. The well-known MSC.NASTRAN was developed in 1966 and has since become an official program for NASA. All objects flying in the aerospace sector have to be analyzed with NASTRAN before their first flight. MARC is an excellent nonlinear analysis program and was developed in 1969. ANSYS software which is widely used in the fields of structure and heat transfer was created in 1970. ADINA which has wide advantages in solutions of non linear problems like contact or collision problems was created in 1975. DYNA2D and DINA3D which are commonly used in dynamic problems and collision among others was developed in 1978. For research and non-linear problem solving ABAQUS is an excellent program, this is widely used by researchers and universities, this was developed in 1979. COSMOS is a good extension for all forms of CAD software, as is PRO / E. There are also many programs developed for computers with fewer hardware requirements, for example, ALGOR which was created in 1984. There are also hundreds of finite element software packages used in engineering. Those mentioned above are the most well known.

The first applications of the method were in aeronautical engineering, a short time later it began to be applied in mechanical, civil, and naval engineering, among others. One of the advantages of simulations is that you can study a topic without having to be doing trial and error experimentally, which would be very expensive, as it is the case in aeronautics and biomechanics where trial and error experiments can cost a great deal, material loss and a large number of

lives, despite this, in order to carry out good research and to have more certainty in the results, it is recommended to correlate the computational results with experimental results.

In 1981 Sachio Nakamura presents what may be the first article of the foot by making a two-dimensional model and begins to assign mechanical properties to the components of the foot [12]. The first models were made in 2D, they only simulated bone tissue and did not differentiate cortical bone and trabecular bone, over time, more studies began to emerge on the foot, they began to consider different mechanical properties for cortical bone which it is less porous and has greater strength and trabecular bone that has a low modulus of elasticity and higher porosity [43]. Human gait is a dynamic problem, but some authors have divided it into several static problems for their study, some authors used 3 stages for walking and other authors have used 6 stages for human gait, so the dynamic problem could be simplified to 3 or 6 static problems which greatly reduces the computational cost. Other authors have carried out simulations where human gait is solved as a dynamic problem, gradually simulating the foot by adding ligaments, cartilage and tendons and the sole of the foot. These materials have been characterized in mechanical testing laboratories and these tests are carried out with corpses, which makes the simulations stray from reality. In itself, simulating a structure as complex as the human body is a great task in which much work remains to be done. One of the most recent and complete works on the foot is Enrique Morales Orcajo's doctoral thesis where he develops a model of finite elements of the foot complete and detailed in three dimensions. This model was created with real geometry differentiating cortical and trabecular bone, tendon, muscle, cartilage and fat. In this work, mechanical tests of the foot and plantar sole tendons were also carried out to determine their mechanical properties and computationally characterize their non-linear behavior [44]. On the other hand, finite element studies have also been carried out analyzing the foot with pathologies, as is the case of the master's final project by the aforementioned author where he simulates using a three-dimensional model to study the influence of the geometry of the proximal phalanx of the first toe in the formation of bunions. In this study a qualitative and quantitative description of the phalanges of the first toe provided by the dissection of cadavers is made [45].

1.5   *Objectives and scope of the thesis.*

The thesis presented performs a biomedical evaluation of three implants to correct the afore-mentioned pathologies, as well as pain when walking in the first ray of the foot, these implants are new surgical treatments of which there are few studies to date.

The general objective of this thesis is to make a biomechanical evaluation of three implants which can be used in a surgical procedure in the first ray of the foot to correct pathologies such as hallux valgus, hallux rigidus and pain in the metatarsophalangeal joint of the first toe. The biomechanical evaluation is made by means of a three-dimensional simulation of the foot considering cortical bone, trabecular bone, some ligaments, muscles and tendons, the other elements of the foot are not considered because the bones of the first ray are the most affected elements by the implant and making a more complex simulation greatly increases the computational cost. As the pathology is corrected by means of surgical treatment, the simulation has the geometry of a corrected foot, that is, the angle of the hallux, as well as the intermetatarsal angle, are within normal values. The biomechanical evaluation that is carried out also includes a study of implant fatigue, as there is currently no information on the subject.

The particular objectives of the thesis can be listed in the following way.

1. Give an explanation of hallux valgus and hallux rigidus pathologies, so that the solution to the problem is easy to understand.

2. Carry out a comprehensive study of the corrections made by the investigated implants

and their structural analysis.

3. Research the problem of fatigue in metals using a strain-based approach.

4. Carry out a biomechanical evaluation of the foot receiving each implant.

5. Obtain a fatigue analysis for biomechanical implants.

1.6 **Thesis description.**

This thesis is made up of 5 chapters and an appendix as shown.

In the first place, the first introductory chapter is exposed, with which an overview of the thesis work has been given, a brief definition and history of medical engineering, a description of the pathologies hallux valgus and hallux rigidus, a historical account of the finite element method up to our times and its application in biomechanics especially in the foot, as well as the objectives and scope of the thesis.

In chapter two a state of the art of the most used surgical corrections is elaborated in the application of the implants studied as treatment for hallux valgus and hallux rigidus, in which we choose cheilectomy, arthroplasty with implant and despite being a surgical procedure without implant we will study Keller resection arthroplasty. The finite element models of the foot and their evolution in recent years are also studied.

In chapter three, a biomechanical evaluation of the different types of arthroplasty is carried out. For this, several finite element models of the foot are developed, in total five models are presented: the first studies a healthy foot free of pathology, the second performs an hemiarthroplasty in the first proximal phalanx, the third analyzes an hemiarthroplasty in the first metatarsal, the fourth studies a total arthroplasty in the first metatarsophalangeal joint and the fifth performs a Keller resection arthroplasty.

Chapter four presents the development to obtain the curves, deformation versus fatigue life, $\varepsilon - N_f$ for the implants of the first metatarsophalangeal joint studied in this thesis. This is done from the deterministic results of the finite element models presented in the previous chapter. A brief explanation is made of the formulation of the Probabilistic Finite Element Method (PFEM) as well as the development of the Ramberg Osgood and Coffin-Basquin-Manson expressions for the construction of one step B models.

Chapter five makes a compilation of the conclusions and original contributions of this thesis work. It also comments on the future lines of research that are being opened after the development of this thesis.

Finally, Appendix A shows a brief explanation of the validation of the non-deterministic model developed in chapter four comparing the results obtained with a Monte Carlo simulation.

2. STATE OF THE ART.

2.1 Types of treatment for hallux valgus and hallux rigidus.

2.1.1 Types of treatment for hallux valgus.

In the previous chapter, treatment for hallux valgus was discussed and classified into two parts; conservative treatment and surgical treatment.As previously mentioned, conservative treatment is ineffective since it is only applied in the early stages of the disease, which is when the deformation is not so severe and there is no pain or in some cases of juvenile hallux valgus where conservative measures are applied that they tend to prevent the progression of the deformity, such as arch supports on flat feet, wide-fit footwear, etc. The indication for surgical treatment is frequently due to pain, caused by the pressure of the shoe on the medium area of the forefoot. Another indication for surgical treatment is the progression of the deformity. When the deformity is already sufficiently developed, conservative treatment usually does not produce results and that is when surgical treatment becomes an option [3], [4], [27]. Due to the above in this chapter we will focus only on surgical treatment.

Before discussing the techniques currently used for the correction of hallux valgus, we will examine the objectives of surgical treatment. [27].

1. Varus metatarsal correction. This correction can be achieved by simply acting on soft tissue or through osteotomies. When the deviation is due to the morphology of the wedge or due to its osteoarthritis, arthrodesis in anatomical position is recommended. If the metatarsal deviation is structured, an osteotomy should be used. This can be opening and be done in the first wedge, placing a graft obtained from the exostosis itself. In the metatarsal it can also be done at the base, in the diaphysis or in its distal part.

2. Hallux valgus correction. In cases where osteoarthritis has not appeared, it can be corrected, either by remodeling the base of the phalanx or by osteotomy according to Akin.

3. Bunion resection. It is a time prior to all other techniques; practiced in isolation, it is absolutely ineffective.

4. Correction of large deviations with osteoarthritis of the joint in older people.

   - Arthroplasty: Régnauld has recommended a technique by which a cartilaginous plug is removed from the base of the phalanx, the base of the phalanx is remodeled and then re-implanted, thus preserving a cartilaginous joint. According to Régnauld the recovery of movement is faster and more complete.

   - Arthrodesis: Recommended by Mann and Myerson, among others, it is in cases where the disease is more advanced, the most radical intervention and with more lasting results. In any case, its indication is limited because, depending on the angle at which the first toe is anchored, the patient may be forced to walk in varus. On the other hand, this same angle determines the height of the heel of the shoe. The intervention of choice in these cases is resection of the base of the phalanx with biological joint arthroplasty. Results are good about 75% of the time. The main

drawback, as we have said previously, is that when cutting the ligaments that join the sesamoids with the base of the phalanx, they are delayed.

5. Shortening of the great toe. Generally hallux valgus appears on Egyptian type feet with a very long first toe. The pressure of the toe of the shoe facilitates the advance of the deformity. In these cases it is recommended to shorten the toe. This is achieved in young people, either by amputating the distal phalanx or by Akin osteotomy. In cases of advanced osteoarthritis, resection of the base of the phalanx automatically corrects the deformity.

2.1.2 *Types of treatment for hallux rigidus.*

In the same way that as we discussed with hallux valgus, conservative treatment for hallux rigidus is only used in the absence of pain, which occurs only in the early stages of the disease. When the disease is advanced or produces pain, surgical treatment is the alternative, it is worth mentioning that surgical treatment for foot aesthetics alone is not a good solution [6], [8]. Because of this, in this section we will talk about the objectives of surgical treatment against hallux rigidus by means of some surgical techniques [27].

1. Remodeling or regularization of the articular surface. The objective of this treatment is limited to phases I and II according to the classification mentioned by Núñez-Samper. This process consists of regularizing the entire articular surface and especially the osteophytic crown. The requirement of this technique is that the articular surfaces that remain be homogeneous and regular.

2. Phalangeal resection. This type of treatment can be performed in phases I and II of the disease according to the classification mentioned by Núñez-Samper, sometimes it is usually done after a bone remodeling has not given the expected results.

3. Epiphysis resection. This indication is usually recommended for phases I and II according to the classification mentioned by Núñez-Samper, Régnauld proposed this technique, referring to the resection of the epiphysis of the phalanx when there is still a healthy cartilage area, a regularization of the metatarsal head and an osteocartilaginous graft carved into the resected base is implanted.

4. Complete fixation of the joint. In this type of treatment Andreasi mentions that the pain disappears and recommends it as a treatment for phase III according to the classification that Núñez-Samper mentions, it is used as an alternative to other treatments. Joint fixation can be carried out by different surgical methods: osteosynthesis with screws, external mini-fixators, Barouk staples, etc.

5. Implants or Prosthesis. One of the most numerous options is the use of implants for diseases such as hallux rigidus, hallux valgus and other foot pathologies, arthroplasties are usually done so that the implant works as a spacer with a discreet hinge effect that partially supplants the joint mobility. The material to be used can be Silflex, as Lawrence advocates for his prosthesis, or the silicone used by Swanson, both in its partial and in its total version, with titanium reinforcements in the intraosseous arms, and whose use this option of Treatment should be restricted to phase III according to the classification mentioned by Núñez-Samper.

2.2 Implants for the treatment of the first ray of the foot.

Implant arthroplasty has been available for more than 60 years and has undergone great changes and improvements with advanced technologies as well as a greater appreciation of the functional biomechanics of the first metatarsophalangeal joint. These implants are not organic so they do not share the same biomechanical properties and elastic modulus of healthy hyaline cartilage on viable subchondral bone [7]. First toe implant arthroplasty dates back to early 1950s. The first reported design was derived from acrylic methacrylate anchored with bone cement in 1951 by Endler. This implant was intended to restore the base of the proximal phalanx [47]. Also around this time, Townley and Taranow introduced the BioPro proximal phalanx hemiarthroplasty implant (BioPro, Port Huron, MI). The implant, which is available in 3 uniformly graduated sizes, is designed to replace only the articular surface of the proximal phalanx, with minimal resection of bone mass. This particular implant paved the way for the future development of metallic unipolar hemiarthroplasty devices [48]. In 1952 Swanson [49] presented hemi implants for the first ray of the foot and 1964 Seeburger [50]. developed metal alloy hemi implants for the first metatarsophalangeal joint. Both Seeburger and Swanson were unsuccessful due to the types of materials used. Implant arthroplasty didn't really catch on until the mid-1960s and early 1970s, when Swanson redesigned his original implant device to include the use of silicone. The first ray implant consisted of a silicone cap on a single stem that was intended to act as a stabilizing spacer after a Keller resection arthroplasty was performed [49]. After disappointing initial results plagued by material fractures, foreign body reactions, stiffness, and permanent deformation leading to high failure rates, double-stem (bipolar) implants such as the Laporta, Suter, and Lawrenc designs were introduced [51], [52], [53]. Although they had slightly different methods of achieving dorsiflexion, these implants were designed to retain normal function of the flexor hallux brevis and sesamoid apparatus [52]. Although initial results were promising with respect to pain relief, longer follow-up reports revealed a high incidence of exogenous bone formation around the implant radiographically, painful keratotic transfer lesions to the minor metatarsophalangeal junctions, and limited amounts of plantar flexion. , with the frequency of failures, these were related to the duration of implant use [54], [55]. Due to the apparent limitations of the initial silicone implants, unipolar and bipolar systems have been developed different types of materials such as; metallic, ceramic, polymer and metal alloy [56]. Since then, several metallic hemi implant and total arthroplasty devices have been developed and have been reported to have varying degrees of success relative to other joint destruction procedures [54]. When determining which side of the joint to replace, the most accepted practice is to assess the degree of destruction of the articular surface of both the proximal phalanx base and the metatarsal head and replace the surface that appears to have the most damage. Below is a brief description of the hemi implants that appear in figure 2.1 which are currently used and are designed to be placed in the first proximal phalanx [7].

- Cannulated Hemi Implant (CHI) System (Vilex, McMinnville, TN) - The CHI System has 2 different options to choose from based on the deterioration of the articular cartilage in the joint. Vilex CHI has hemi-implants available in elliptical and concave shapes to replace the base of the proximal phalanx. There are also spherical and convex shapes to replace the metatarsal to resurface the metatarsal head. All implants are cannulated to allow precise positioning within the joint. There are also 2 positioning holes to allow the implant to be sutured to the soft tissue, if desired by the surgeon.

- AnaToemic Phalangeal Hemiprosthesis (Arthrex, Naples, FL) - This hemi implant re-shapes the proximal phalanx and promotes a 2.4mm head. According to the manufacturer with this head size minimal resection of the proximal phalanx base is required, allowing patients to maintain flexor insertion. It is composed of cobalt-chromium and uses a pilot punch to precisely place the implant.

Company	Proprietary Name	Image	Placement method	Material Type	Advancement
Vilex	**Cannulated Hemi**		Cannulated screw fit	Titanium	Cannulated Implantation
Arthrex	**AnaToemic**		Press fit	Co-Cr-Mo	Low profile
Biopro	**Great Toe**		Press fit	Co-Cr-Mo	Longest follow-up studies
Integra	**K2 Hemi Toe**		Press fit	Co-Cr-Mo	Anatomically shaped
Metasurg	**Biomotion Cannulated**		Cannulated screw fit	Titanium	Cannulated Implantation
OrthoPro	**Metal Hemi**		Press fit	Titanium	Dorsally elevated stem
Osteomed	**Hemi Great Toe**		Press fit	Co-Cr-Mo	Anatomically shaped plantarly
Tornier	**Futura Metal Hemi**		Press fit	Co-Cr-Mo	Trapezoidal shaped
Trilliant	**3S Hemi**		Press fit	Co-Cr-Mo	Tri-spade stem, anatomically shaped
Wright Medical	**LPT2**		Press fit	Co-Cr-Mo	Straight and angled options
Integra	**Movement Great toe**		Press fit	Co-CR-Mo	Use reamer for less bone resection
Solana	**Phalangeal Decompression Implant**		Press fit	Co-CR-Mo	Anatomic design

Fig. 2.1: Hemi implants for the first proximal phalanx currently used [7].

- BioPro GREAT TOE (BioPro, Port Huron, MI) - The BioPro is a hemi implant that repairs the base of the proximal phalanx and has been around since its introduction in 1952. It is available in porous and non-porous cobalt chrome. It is indicated to replace the base of the proximal phalanx and has a diamond-shaped stem that provides intramedullary fixation.

- Integra K2 Hemi Toe Implant System (Integra, Plainsboro, NJ) - The K2 Hemi is made from cobalt chrome with a titanium plasma coated stem. On the underside of the implant base there is a small groove for the tendon of the flexor hallux longus. It also has a suture hole that allows the short flexor hallux to be sutured to the implant to add bending power to the proximal phalanx. There is a cutting guide that allows you to take the exact amount of bone needed to place the implant, which is 2 mm wide.

- BioMotion First MPJ Cannulated Hemi System (Metasurg, Houston, TX) - The BioMotion is designed for the proximal phalanx and offers the minimal bone resection necessary to maintain flexor tendon attachment sites. It is a cannulated implant that allows precise alignment. It has a tapered stem and offers 5 color-coded sizes.

- Metal Hemi (OrthroPro, Salt Lake City, UT) - The Metal Hemi is a titanium implant used to replace the base of the proximal phalanx. According to the manufacturer, the

implant stem is dorsally elevated to allow better and more precise positioning and has a plantar fin to prevent rotation.

- Hemi Great Toe Implant (OsteoMed, Addison, TX) - According to the manufacturer, this is an anatomically based design that focuses on alignment to allow for an improved, pain-free range of motion. The Hemi instrument tray includes tests, calipers, awl, and impactor for convenient device placement. It is available in four implant sizes and is low profile, allowing minimal bone resection during implantation.

- Futura Metal Hemi Toe (MHT) (Tornier, Bloomington, MN): The MHT features a cobalt chrome, single-stemmed resurfacing prosthesis for the base of the proximal phalanx that has a titanium plasma coating along the intramedullary stem to promote osseous integration. It has a trapezoidal articular surface to be congruent with the metatarsal head and is rounded dorsally to decrease impingement on the metatarsal head. It has a thinned inferior surface to preserve the flexor hallucis brevis attachment site. The stem is trapezoidal and angled to protect the plantar cortex.

- 3S Hemi Implant (Trilliant Surgical, Houston, TX) - Designed to feature a stem for maximum implant-to-bone contact and promotes an anatomical concave shape. It is made of cobalt chrome and has a color-coded instrumentation kit.

- LPT2 Great Toe Implant (Wright Medical, Arlington, TN) - The LPT2 implant is a titanium implant that resurfaces the base of the proximal phalanx and comes exclusively in straight or angled designs. The angled implant can correct or accommodate an increased proximal joint adjustment angle at the metatarsal head. The implant also has fabricated suture fasteners if necessary. If using the implant at an angle to address and increase the proximal joint placement angle, it is important to place the widest part laterally.

In the same way, a brief description is made of the hemi implants designed to be placed in the head of the first metatarsal shown in figure 2.2.

- Arthrosurface HemiCAP Toe DF Resurfacing System (Arthrosurface, Franklin, MA): Arthrosurface HemiCAP is indicated for reshaping of the first metatarsal head. It is a 1-component, 2-part implant with a spongy tapered post and 2 designs (with and without dorsal phalanx) for an articular resurfacing cap. According to the manufacturer, it is designed to provide stable and immobile implant fixture and is made of a cobalt chromium alloy with a titanium surface coating and a tapered titanium alloy post. The metatarsal head can be decompressed prior to implant insertion with the included metatarsal head reamers.

- EnCompass Metatarsal Resurfacing Implant (OsteoMed, Addison, TX) - The EnCompass Metatarsal Resurfacing Implant is designed to replace the metatarsal head. It has a concave spherical surface that is coated with titanium plasma and hydroxyapatite. It comes in various sizes, is one-piece, and has a proximal stem that attaches to the metatarsal canal. It has a 4-fin stem to provide stability and prevent rotation.

- Metatarsal Decompression Implant System (MDI) (Solana Surgical, Memphis, TN) - The MDI is made of titanium with a cobalt chrome coating. There are 4 sizes available and it can provide up to 3mm of metatarsal decompression. The implant is oval in shape, with a toroidal articular surface of the head to distribute gait forces. According to the manufacturer, it mainly repairs the upper two-thirds of the metatarsal head in an attempt to avoid scarring and capsular adhesions of the plantar capsular tissue. The proximal stem is conical and rectangular distally to prevent rotation.

	Company	Proprietary Name	Image	Placement method	Material Type	Advancement
Metatarsal Head Resurfacing	Arthrosurface	**Hemicap**		Press fit on post	Co-Cr-Mo	Dorsal phalange
	Osteomed	**Encompass**		Press fit	Co-Cr-Mo, Ti	Single piece low profile stem
	Solana	**Metatarsal Decompression Implant**		Press fit	Co-Cr-Mo	Dorsal 2/3 met-head decompression
	Vilex	**Cannulated Hemi**		Cannulated screw fit	Titanium	Vilex
	Integra	**Movement Great Toe**		Press Fit	Co-Cr-Mo	Dorsal phalange. Surgeon also has option to resurface the base of the proximal phalanx

Fig. 2.2: Hemi implants for the first metatarsal currently used [7].

- CHI System (Vilex, McMinnville, TN): This implant has been previously defined in the anterior section of hemi implants for the first proximal phalanx.

Various attempts have been made to design total metatarsal joint replacements since they were first introduced more than 50 years ago; but to date, none have achieved wide acceptance. Artificial replacement of the first metatarsophalangeal joint has not been established as a standard of care for osteoarthritis of the first toe. Despite their initial success in relieving symptoms, first and second generation joint replacements with a flexible, hinged silicone were abandoned due to poor durability and a fairly high failure rate. Third generation implants were redesigned for insertion with titanium grommets to reduce stress applied to the implant-bone interface in an attempt to increase arthroplasty survival. Below is Figure 2.3 showing some of the current options for implant of total arthroplasty in the first metatarsophalangeal joint.

- Integra MOVEMENT Great Toe System (Integra, Plainsboro, NJ): The Movement Great Toe System allows the surgeon to determine intraoperatively the degree of cartilage wear and to decide whether a hemiarthroplasty versus a total arthroplasty is more appropriate or not. The implants have a cobalt chromium articular surface, with titanium plasma spray that favors bone integration. It has a 4-fin cylindrical stem for added stability. The metatarsal implant specifically features a dorsal ridge to help prevent osteophyte formation. The proximal phalanx implant is reamed in place to avoid impaired insertion of the flexor hallux brevis while minimizing bone resection. It also has suture holes to reattach the flexors if the flexor apparatus is compromised.

- The Integra Kinetik Great Toe Implant System (Integra, Plainsboro, NJ): The Kinetik Great Toe is an unrestricted 2-piece implant for total replacement of the first metatarsophalangeal joint. This 2-component system offers interchangeable components and a dorsal flange on a metatarsal component that extends the dorsal range of motion.

Company	Name	Image	Cement	Material Type	Number of components
Integra	Kinetic Great Toe		Press fit	Cr-Co-Ti, PE	2
Integra	Movement Great Toe		Press fit	Cr-Co-Ti, PE	2
Merete	ToeMobile		Press fit	Cr-Co-Ti, PE	2
Osteomed	Bio-Action		Cement	Cr-Co-Ti, PE	2
Osteomed	Reflexion		Cement	Cr-Co-Ti, PE	3
Tornier	Futura classic flexible		Press fit	Silicone without grommets	1
Tornier	Futura primus flexible		Press fit	Silicone with grommets	1
Wright Medical	Swanson Flexible		Press fit	Silicone with grommets	1

Fig. 2.3: Currently Used Total Arthroplasty Implant [7].

- ToeMobile Anatomic Great Toe Resurfacing System (Merete Medical, New Windsor, NY) - The ToeMobile is a 2-piece unrestricted prosthesis that replaces the first metatarsophalangeal joint by fully functional preservation of the joint while maintaining the sesamoid complex. The prosthesis consists of an anatomically shaped, polished metatarsal implant made of Cobalt-Chromium-Molybdenum (CoCrMo), which slides over a polyethylene inlay that is pre-assembled into a conical-shaped phalangeal component made of titanium alloy. Ti-6Al-4V.

- The OsteoMed Bio-Action Toe Great Toe Implant (OsteoMed, Addison, TX) - The Bio-Action Toe is no longer available on the market. One study reviewed 36 Bio-Action Toe implants (in 32 patients) in an average of 47 months. A significant improvement in dorsiflexion and range of motion of the first metatarsophalangeal joint was observed.

- The Osteomed ReFlexion 1st MPJ Implant System (OsteoMed, Addison, TX) - This device is a 3-piece unrestricted implant system for primary and revision reconstruction of the first metatarsophalangeal joint with a cone-to-cone implant design. It has replaced the Bio-Action Great Toe implant in the OsteoMed portfolio. All components are interchangeable and are available in 3 sizes. The 17 degree orientation of the metatarsal component adapts to the declination angle of the metatarsal head.

- The Futura Primus Flexible Great Toe (model FGT) (Tornier, Bloomington, MN): The Futura Primus implant is a third generation Silastic prosthesis designed to complement the

arthroplasty of the first metatarsophalangeal joint. The implant is made of ULTRASIL medical grade silicone elastomer and includes titanium washers. The underside of the distal hinge abutment is angled to minimize interference with the insertion site of the flexor hallux brevis and the sesamoid apparatus.

- The Futura Classic Flexible Great Toe (Tornier, Bloomington, MN) - The Futura Flexible Great Toe implant is also a third generation prosthesis designed to complement the arthroplasty of the first metatarsophalangeal joint. Constructed of medical grade ULTRASIL silicone elastomer, the Classic offers Futura's patented axial displacement hinge and other advanced design features, while maintaining the surgical technique of previous generation joint replacements.

- Swanson Titanium Great Toe Implant (Wright Medical, Arlington, TN) - This is a stemmed intramedullary implant that replaces the proximal third of the proximal phalanx. The implant is made to preserve joint space by being surrounded by a fibrous support capsule. It is available in 5 sizes.

2.3 Surgical techniques researched.

2.3.1 Cheilectomy.

The technique of cheilectomy in a procedure was first described by DuVries in 1959, but it was not until 1979 that the procedure began to gain popularity when it was introduced by Mann et al [37]. In this technique, in addition to osteophyte removal, the base of the proximal phalanx and the dorsal head of the metatarsal are also resected. Therefore, the procedure can be classified as a partially destructive technique because severe removal can result in subluxation of the metatarsophalangeal junction. In addition to osteophyte removal, the phalanx base is also resected. proximal and dorsal head of metatarsal. Arthrodesis or arthroplasty are procedures that are considered more difficult to perform compared to cheilectomy although there are only retrospective studies comparing cheilectomy with other surgical procedures and there is no consistent evidence that cheilectomy is superior to other surgical techniques. This is commonly used to treat low degrees of hallux rigidus. Figure 2.4 presents a typical cheilectomy design.

Fig. 2.4: Cheilectomy design [8].

Michael J. Coughlin and Paul S. Shurnas [38] describe the technique as follows: Cheilectomy is performed with the use of general anesthesia and a tourniquet is performed with an Esmark bandage. A longitudinal incision of approximately 3 cm is centered over the metatarsophalangeal junction and deepened through the capsule medially from the extensor hallux longus. The capsule is preserved for later repair. The hypertrophic synovial tissue and the free bodies are completely debrided from the junction and the percentage of viable cartilage remaining in the metatarsal head is estimated. The proximal phalanx is flexed plantar by exposing the head of the metatarsal. An osteotome is used to dorsally remove the lateral, dorsal, and medial osteophytes along 25 to 33% of the metatarsal head. Usually all or almost all of the surface

of the poor cartilage of the metatarsal head is resected. At least 70 degrees in dorsiflexion must be achieved intraoperatively. The osteophytes are then dorsally removed from the base of the proximal phalanx and the junction is washed. Bone wax is applied to the dorsal region of the metatarsal head. The capsule under the long hallux extensor tendon is repaired with interrupted absorbable sutures and the skin is routinely closed. At the end of the surgery, a gauze tape is applied and this is changed every 10 days. Passive movement exercises begin 10 days after surgery. The patient is allowed to walk after the operation with the use of a rigid sole post-operative shoe bearing only the own weight that can be tolerated.

Roger A. Mann et al [37] treated 28 patients with 34 cheilectomies between January 1976 and December 1981. Of the 28 patients, 3 lost follow-up. The average follow-up was 56 months with a range of 30 to 100 months. There were 5 men and 20 women. The average age was 56 years with a range of 30 to 80 years. 6 patients had a bilateral injury. The preoperative arc of movement of the first metatarsophalangeal junction was 29 degrees with a range of 5 to 65 degrees. The improvement of the patients was evident from two to three months, but some patients continued to improve for 20 months after the operation. At the end of the evaluation, patients reported pain relief and improvement in range of motion. The range of motion of the first metatarsophalangeal junction improved after surgery in 23 of the 31 feet. The postoperative average of the arc of movement was 48 degrees with a range of 5 to 80 degrees. Footwear problems continued in 4 patients, but 21 patients were able to wear normal footwear.

Wieske Beertema et al [39] published a study of 28 patients who underwent a cheilectomy. The average age was 49 years with a range of 22-72 years. The average follow-up was 8 years with a range of 2-12 years. Of the 28 patients, 16 had hallux rigidus in grade I and 7 in grade II according to the Regnauld classification, of 5 patients their data was lost to follow-up. The average of the AOFAS scale after cheilectomy was 87 points for patients with grade I and 82 points for patients with grade II. The average range of motion and dorsiflexion of the first metatarsophalangeal junction was 61 ± 9.1 degrees with a range of 40-80 degrees and 47 ± 8.5 degrees with a range of 30-60 degrees for grade I respectively and grade II it was 46 ± 23.9 degrees with a range of 0-80 degrees and 41 ± 20.1 degrees with a range of 0-70 degrees.

In the article by Michael J. Coughlin and Paul S. Shurnas [38], they report 53 patients who were treated with cheilectomy. 13 patients underwent bilateral surgery. The average follow-up was 9.6 with a range of 2.3-20.3 years. The mean declination angle of the first metatarsal was 20.4 degrees with a range of 15-27 degrees before surgery and 21.1 degrees with a range of 12-30 degrees after surgery. The average angle of the hallux valgus was 12.2 degrees with a range of 0-20 degrees before cheilectomy, and afterwards it was 12.6 degrees with a range of 0-24 degrees. The mean of the intermetatarsal angle 1-2 was 7.3 degrees with a range of 2-24 degrees before the operation and 7.7 degrees with a range of 2-15 degrees after the operation. In 6 patients, 7 failed cheilectomies resulted after follow-up and other surgical procedures had to be performed for the patients.

Cheilectomy may be a good choice for patients with grade I or grade II hallux rigidus. It is a simple and safe procedure that preserves the metatarsophalangeal junction [39].

2.3.2 *Hemiarthroplasty in first proximal phalanx.*

Hemiarthroplasty of the first proximal phalanx is a surgical procedure that inserts an implant into the proximal head of the first phalanx, thus allowing the proximal phalanx and the first metatarsal to slide together [57]. Although the instrumentation and insertion method varies between manufactures, the procedure typically involves a resection and decompression of the articular surface of the base of the proximal phalanx, in addition to the resection and remodeling of the first proximal phalanx head and resection of any periarticular spur formation. The prosthesis is then implanted using the specific technique associated with the particular device

being used [7]. Connor Delman describes this surgical procedure as follows [9]: The procedure is performed with the patient in the supine position and under general anesthesia, using a thigh tourniquet or with an ankle block using a pediatric ankle tourniquet. The first metatarsophalangeal joint is exposed through a dorsal longitudinal incision followed by an eccentrically placed longitudinal capsular incision. The capsule is released with preservation of the collateral ligaments and plantar capsule.

Dorsal osteophytes are removed from the proximal phalanx and dorsal metatarsal head, and the medial prominence of the metatarsal head is resected. About 20% to 30% of the articular surface can be resected and is often needed to achieve adequate postoperative dorsiflexion. A Freer elevator is placed under the metatarsal head to release plantar adhesions. A cut is made perpendicular to the long axis of the proximal phalanx, resecting an amount of bone corresponding to the width of the implant (2.4 mm). See figure 2.5. A centralizing hole is drilled,
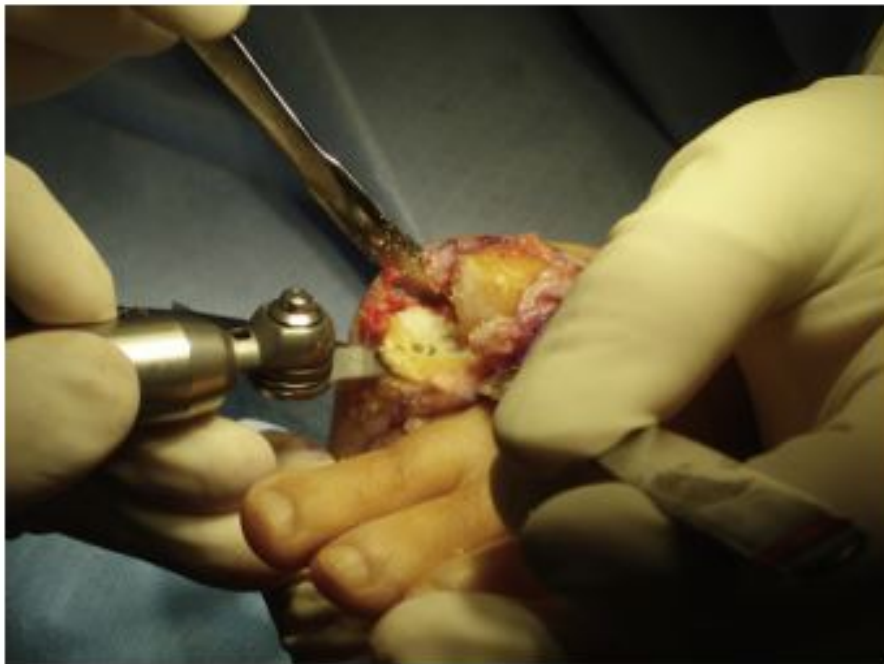
Fig. 2.5: Cut corresponding to the width of the implant in proximal phalanx [9].

and a small Hoke osteotome is used to create medial and lateral keel entry points, following which the keel punch is placed into the proximal phalanx. See figure 2.6. A trial implant is placed to check size, fit, and range of motion. The final implant is then inserted with thumb pressure and carefully seated with an impactor. See figure 2.7. The medial capsule is reefed if necessary, and the dorsal capsule is closed with absorbable suture. Range of motion is checked, the skin is closed, and a light compressive dressing is applied. Postoperative radiographs are obtained at the 6-week follow-up visit. See figure 2.8.

Eric Giza et al. [58] report 22 hemiarthroplasties in the first proximal phalanx in 20 patients. Preoperative radiographs revealed 14 cases of grade 3 and 8 cases of grade 4 of hallux rigidus, according to the classification of Coughlin and Shurnas. The average dorsiflexion of the first metatarsophalangeal joint improved from 41 with a standard deviation of 11 degrees to 49 with a standard deviation of 10 degrees in 1 year. The average score of the AOFAS scale improved from 61 points (range: 35−80) to 86 points (range: 75−95). The VAS pain scale improved from 4.7 with a standard deviation of 2.6 points to 2.5 with a standard deviation of 1.9 points. One patient developed metatarsalgia in the second metatarsophalangeal joint and only required conservative treatment. Konkel et al. followed up 23 patients for 72 months (17 had hallux rigidus grade 3, and 6 had hallux rigidus grade 4). The average age was 62 years. There were
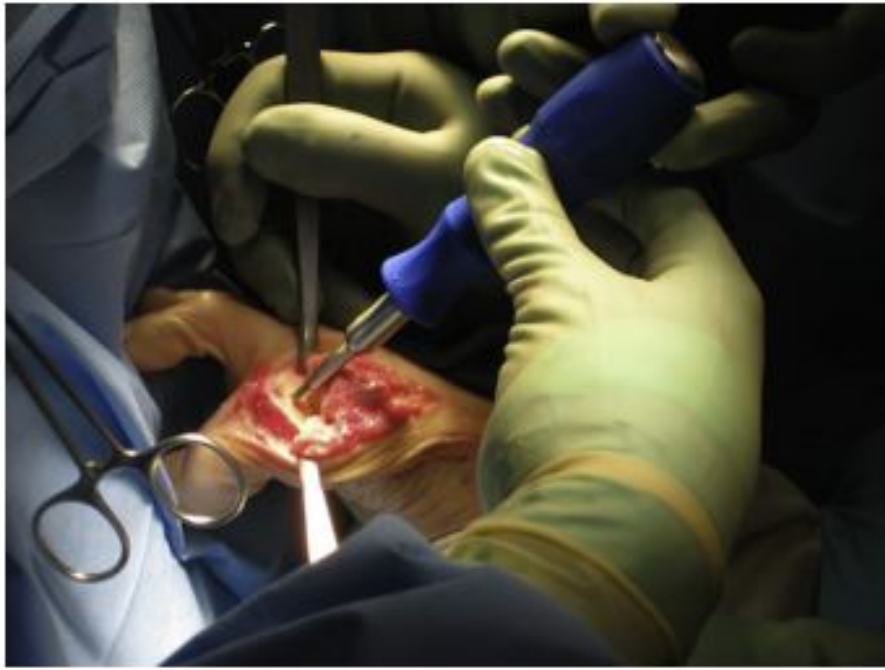
Fig. 2.6: Placement of keel punch into the proximal phalanx before implant insertion [9].

two cases of mild transfer metatarsalgia and two of mild clawing of the great toe. The average plantar flexion increased from 1 degree with a range of (-15 to 15) to 13 degrees with a range of (-20 to 30). For dorsiflexion, there was an average improvement from 16 (5 to 50) to 60 (20 to 85) degrees. In the score of the AOFAS scale the change was from 19 (17 to 50) to 89 (40 to 100) points. At the end of the follow-up there was a 68% of recurrent dorsal osteophytes, the recurrence was mild in 10 patients, moderate in 4, and severe in 6, while 8 patients had no recurrence. There were three unsatisfied patients; a hard-working man in the construction industry, a woman who worked in a marketing industry and had to wear designer shoes, and another man who worked as a machinist in a factory and had to stand all day [59].

2.3.3 Hemiarthroplasty in first metatarsal bone.

Hemiarthroplasty of the first metatarsal bone is a surgical procedure that inserts an implant in the head of the first metatarsal, thus providing a solution to those cases where there is a localized osteochondral lesion of this metatarsal head [6]. This procedure is aimed at restoring the articular surface on the first metatarsal head. Technically, less bone is removed with resurfacing, allowing for additional options for reconstruction if future surgery is warranted secondary to implant failure. Implant insertion requires minimal bone resection of the joint and does not destabilize the intrinsic muscle insertion into the proximal phalanx [60]. Alex J. Kline [10] describes the surgical procedure as follows. The patient is placed in a supine position on the operating table with the operative extremity in a well-padded position. The procedure can be done with either a regional block and a calf tourniquet or an ankle block with an Esmarch bandage wrapped around the ankle. A dorsal incision is made over the first metatarsolphalangeal joint and slightly medial to the extensor hallucis longus tendon. The subcutaneous tissues are spread gently to expose the dorsal joint capsule with care to protect the dorsomedial branch of the superficial peroneal nerve. The extensor hallucis tendon is left free from the capsule and retracted laterally to keep the tendon within its sheath if possible. A longitudinal arthrotomy is made along the medial border of the joint with the incision as medial as possible but avoiding injury to the dorsomedial branch of the superficial peroneal nerve. The capsule and collateral
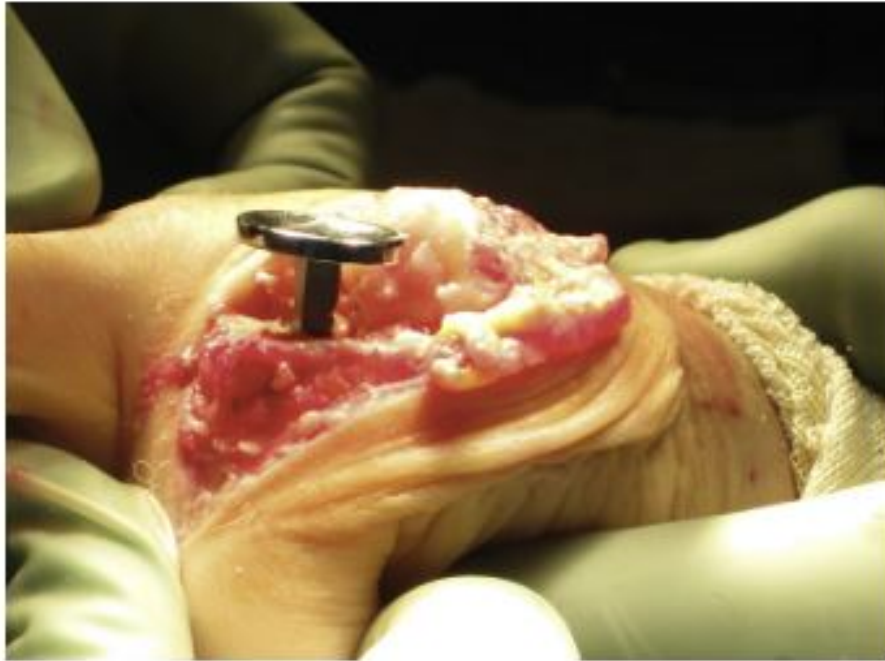
Fig. 2.7: Implant positioning in the proximal phalanx before final insertion with thumb pressure [9].

ligaments are released off the metatarsal head with subperiosteal dissection similar to what is done with total knee arthroplasty. The collateral ligaments, sesamoid suspension ligaments, and capsule should be completely released so that the entire joint, including the sesamoids, is easily visualized as it is shown in figure 2.9.

It is very important to visualize the cristae of the sesamoid articulation because this is the landmark for sizing of the implant. In advanced hallux rigidus, the sesamoids and flexor hallucis brevis have fibrotic adhesions to the metatarsal head, which limits dorsiflexion postoperatively. Care should be taken to avoid damaging the sesamoid articulation with the plantar metatarsal head. The insertions of the plantar plate and flexor hallucis brevis tendon are then released from the proximal portion of the proximal phalanx using subperiosteal dissection similar to a hamstring release in a contracted knee joint when doing knee replacement as it is shown in figure 2.10. This step has a similar effect in the sense that it will release the contracture but allow for the tendons and plantar plate to reattach in a less-contracted position. As the bone remains in place, the tendons scar down or reinsert into the remaining proximal phalanx. There are strips of the flexor hallucis brevis that are attached to the flexor hallucis longus, which will hold the tendon in its proper orientation until it can secure itself get back to the bone of the proximal phalanx. From experience of performing over 500 implant surgeries, it is the opinion of the senior author that if 90 degrees of dorsiflexion of the first metatarsophalangeal joint has not been achieved with the ankle in neutral dorsiflexion at the completion of the operation, to include implant positioning, then further soft tissue release is needed to ensure adequate postoperative motion.

Once the joint is exposed and adequate soft tissue release is completed, resurfacing of the metatarsal head is completed in a stepwise manner as described by the manufacturer (Arthrosurface). A drill guide is used to place a pin within the shaft of the first metatarsal using a guide on the implant set. Often, wear of the metatarsal head is asymmetrical and so the pin needs to be placed within the center of the metatarsal shaft in both the sagittal and coronal planes. Fluoroscopy may be needed to verify adequate position of the pin. A cannulated double-step drill is inserted over the guide wire, and the metatarsal head is drilled until the proximal shoulder of the drill is flushed with the plantar articular surface of the metatarsal head.
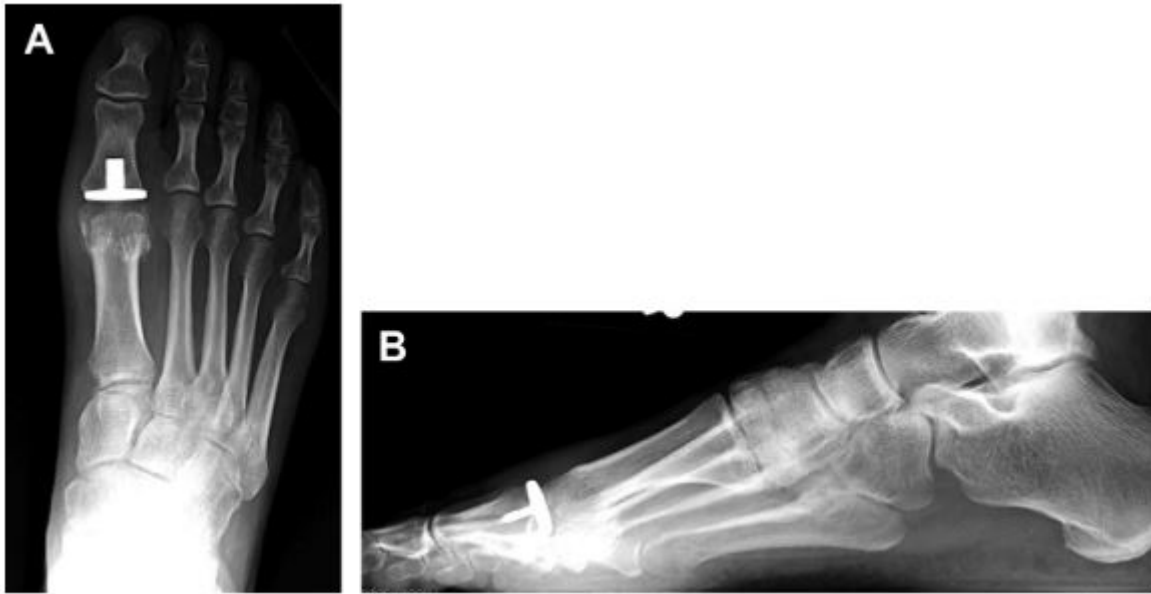
Fig. 2.8: Postoperative anteroposterior (A) and lateral (B) radiographs of the foot [9].

In most instances, the plantar articular surface is the only normal surface, so this surface is used for determination of the depth of the taper post placement. The tap is removed, and the taper post is inserted over the guide wire. The taper post is inserted until the etched line on the driver is flushed with the plantar articular surface of the metatarsal head. If one chooses to decompress the joint by slightly shortening the metatarsal, then the taper post is inserted 1 or 2 mm deeper than this. The metatarsal head articular geometry is checked with mapping measuring guides, and the final size of the implant determined. The appropriate implant is chosen, and the metatarsal head resurfaced with 2 reamers to match the shape of the implant. The trail implant is then placed onto the taper post, and the final position of the implant is checked to ensure adequacy of coverage as can be seen in figure 2.11. With the trial implant in place, any bone around the implant is removed from the medial, lateral, and dorsal side as it is shown in figure 2.12. Once this is completed, the trial implant is removed and the final implant is impacted onto the taper post with gentle blows to lock the morse taper. As stated before, at this point, the range of motion of the metatarsophalangeal joint is tested with the ankle in neutral dorsiflexion. If the first metatarsophalangeal joint does not have the same range of motion as the second metatarsophalangeal joint, then further soft tissue releases are needed until the 2 are equal to ensure adequate postoperative range of motion of the arthroplasty. The key pearls to success with this technique include adequate soft tissue release, addressing sesamoid arthritis, and treating arthrosis of the phalangeal side. The most common reason for failure is persistent stiffness and pain because of failure of adequate soft tissue release. The metatarsal head must undergo release of all the collateral ligaments so that the entire distal 3 cm of the metatarsal head is completely released of all soft tissue attachments. There is still an intraosseous blood supply so the risk of avascular necrosis is minimal. The authors have not seen any in their experience. The proximal phalanx should also be released of its soft tissue attachments. This is a disease of soft tissue contractures on the plantar surface so failure to release these tissues will result in recurrence of pain and stiffness. Cock-up toe or other deformities have not been seen with this aggressive soft tissue release.

Persistent sesamoid arthritis is another concern when resurfacing the metatarsal head. Once the implant is in place, sesamoid arthritis can be addressed by placing a soft tissue graft between the sesamoids and plantar metatarsal head using a "boxing glove" technique. The graft is placed over the implant on the metatarsal head and covers the entire remaining articular

Fig. 2.9: The entire metatarsal head is degloved for 2 cm proximal to the joint line to ensure adequate release of the collateral ligaments [10].

surface of the plantar metatarsal and sutured in place.

For significant arthritis of the phalangeal base cheilectomy is performed at the phalangeal base and the dorsal capsule of the first metatarsophalangeal joint is transferred to the base of the proximal phalanx as shown in figure 2.13.

Ulusal et al. used the HemiCAP®resurfacing implant by Arthrosurface in their study and report 14 patiends with no bilateral case of hallux rigidus, of the 14 patients, 5 were male and 9 were female, with a mean age of 58.7 ± 7.4 with a range from 52 to 75 years. The mean preoperative VAS score for pain was 8.4 ± 0.9 with a range from 7 to 10 cm and had decreased to 1.21 ± 1.2 with a range from 0 to 5 cm at the final follow-up visit. The mean preoperative AOFAS score was 33.9 ± 9.8 with a range from 22 to 59 points and had increased to 81.6 ± 10.1 with a range from 54 to 96 points at the final follow-up visit. The mean preoperative of the range of motion in the first metatarsophalangeal join was 22.8^o with a range from 15° to 45° and had increased to 69.6^o with a range form 50° to 90° at the final follow-up. One patient's implant was removed, and arthrodesis of the first metatarsophalangeal join was performed because of ongoing pain and immobility [61].

2.3.4 *Arthroplasty in the first metatarsophalangeal joint.*

Arthroplasty in the first metatarsophalangeal joint is a surgical procedure that replaces the first metatarsophalangeal joint with an artificial joint. There are many types of implants for the first metatarsophalangeal joint. Some manufacturers have produced one-piece implants commonly made of silicone, some others have produced two-piece implants made of ceramic materials, and there are also manufacturers that have produced three-component implants, two metallic, generally chrome-cobalt or titanium, which are inserted into the metatarsal head and proximal phalanx to facilitate osseointegration and a further component made of polyethylene that serves as a spacer between the two metal pieces and is inserted into the phalangeal component [6]. Several attempts have been made to design total metatarsal joint replacements since first being introduced more than 50 years ago; but to date, none have reached wide acceptance [7]. Alex J. Kline [Kline2015] describes the surgical procedure in the same way as hemiarthroplasty in the first metatarsal discussed in the previous section, but at the end the phalangeal side is resur-

Fig. 2.10: The insertions of the flexor hallucis brevis and plantar plate are released off the plantar aspect of the proximal phalanx with subperiosteal dissection [10].

faced with an implant. The ToeMotion (Arthrosurface) is a metal-backed polyethylene implant designed to resurface the proximal phalangeal side if the disease has progressed significantly to this area, this can be seen in Figure 2.14.

Wenjay Sung et al. reviewed medical records of consecutive adult patients who underwent a total first metatarsophalangeal joint arthroplasty using double-stem silicone implants with titanium grommets from January 1979 until December 2002 at the Weil Foot and Ankle Institute. The average age of the patients was 58.8 years (range 29–75 years) at time of operation and 66.0 (range 34–86 years) at time of last follow-up visit. Of the 63 patients, 6 were men, and 57 were women, and of the 92 feet included, there were 50 right feet, compared with 42 left feet. The average interval follow-up after surgery for all 63 patients was 86.7 months (range 24.5–333.9 months). The average American Orthopaedic Foot and Ankle Society Hallux-Metatarsophalangeal Interphalangeal Scale was 82.4 (range 55–100) with a standard deviation of 12.0. Total range of motion was recorded postoperatively at final follow-up for an average of 56.6° (45.6° of dorsiflexion and 10.0° of plantarflexion). Complications in the postoperative period were found in 10 cases. This included 5 ulcerations, 3 unresolved neuritis, and 2 incisional dehiscence complications. There were 13 cases of surgical revision at an average of 5.1 years (range 1–10 years) after surgery. Nine cases involved worn or failed implants that were replaced. There were 4 cases where the implant was removed. Of those 4 implant removals, two required amputation of the first ray [62].

2.3.5 *Keller's resection arthroplasty.*

Resection of the proximal half of the proximal phalanx of hallux was first described by Davies-Colley in 1887 as a treatment for hallux valgus [46]. In 1904, in an attempt to improve the results of the surgical technique, Captain William L. Keller removed the proximal phalanx and resected the middle eminence of hallux in three patients. This was the first documented data of the surgical technique known as Keller′s resection arthroplasty, then in 1912 he published results of his operation in 26 patients of which 24 had excellent results [11], [63]. This technique can be used for both hallux valgus and hallux rigidus and provides early symptomatic relief and a minimal rehabilitation program [39]. One of the advantages of this technique is the

Fig. 2.11: Placement of the trial implant onto the taper post before to resection of any excess bone [10].

conservation of movement in the metatarsophalangeal junction, especially in older people [63], [64]. Currently, several doctors use this procedure in relatively active patients. In these patients, pain and deformity limit their activities. Keller's resection arthroplasty provides correction and reduction of pain to allow patients to resume their activities. The recovery period is shorter and less complicated when compared to other techniques such as metatarsophalangeal junction arthrodesis and implant arthroplasty [11]. It is currently indicated for the last stages of diseases as an alternative to implant arthroplasty or arthrodesis. It is recommended for patients with advanced age, diabetics or with major vascular disorders. Insufficient resection runs the risk of producing a painful stiffness of the metatarsophalangeal joint, always associated with a release of sesamoids and joint cleaning [6]. When the resection is not carried out successfully, there is a risk of producing transfer metatarsalgias, plantar calluses of the second metatarsophalangeal junction, loss of flexor power in the hallux, hammering in the upper part of the hallux, weakness in the toe-off phase of the gait, excessive shortening in first ray of foot or claw toe of hallux interphalangeal junction [46], [11], [64] [65].

Despite being a procedure that is more than a century old, it has not changed over time. Modifications to the technique have arisen, which have received other names. Stephen V. Corey [11] describes the technique as follows: The first metatarsophalangeal joint is approached through a standard curvilinear dorsomedial skin incision. Dissection is then carried down to the level of the deep tissue and joint capsule. Next, a proximally based U capsulotomy is performed and carried out over to the central aspect of the phalangeal base. The capsule is reflected proximally exposing the base of the proximal phalanx and head of the first metatarsal. An aggressive resection of the medial eminence of the first metatarsal head is then performed. Preservation of the cristae is not important since we are not trying to maintain joint alignment. In cases of hallux valgus attention is directed into the first intermetatarsal space where the adductor tendon is identified and freed from its attachment into the sesamoid apparatus and base of the proximal phalanx. The fibular collateral ligament is then identified and released. At this time, an attempt is made to restore the sesamoid apparatus to a center position under the first metatarsal head. Positioning of the sesamoids is important in hallux valgus because of the path of the long flexor tendon. If the long flexor tendon is not centered back under the first

Fig. 2.12: The trial implant in place and after resection of the excess bone around the trial implant. Note the plantar surface is untouched. [10].

metatarsal head it will continue to be a deforming force and hallux valgus is likely to reoccur. If the sesamoids are unable to be mobilized or osseous hypertrophy is present, the fibular sesamoid should be excised. Attention is then turned to the base of the proximal phalanx where the proximal one third is identified at the notch on the hallux. Care is taken at this time to be sure that the resection of this base is perpendicular to the long axis of the shaft. An intraoperative photograph of the arthroplasty is shown in figure 2.15. Problems can arise when bone resection is made parallel to the articular surface of the proximal phalanx. The hallux is then held in proper alignment with approximately 1 cm gapping maintained between the proximal phalanx and the first metatarsal head. At this time, if there is significant pull or tension on the hallux an extensor hallucis brevis tenotomy can be performed. If sufficient tension continues causing either dorsal or abductory forces, the extensor hallucis longus tendon can then be lengthened using an open Z pattern. The flexor hallucis longus tendon is then identified and a small drill hole is made in the central plantar aspect of the shaft of the proximal phalanx. The toe is then distracted into position and a braided nonabsorbable suture is made to secure the tendon to the proximal phalanx though the drill hole. The first metatarsal head is remodeled both dorsally and medially in order to create a smooth rounded surface. Prior to placing a K-wire, the joint capsule is then interposed in the space from dorsal medial to plantar lateral. The capsule is then draped over the first metatarsal head and anchored to the deep fascial area at the plantar lateral aspect of the joint. The capsule will later be secured with the use of the K-wire. The intermetatarsal angle is then compressed and the hallux is held in a rectus position. Once adequate position is obtained, a 0.062-inch K-wire is retrograded out the distal aspect of the hallux and then back across the metatarsophalangeal joint into the first metatarsal head and shaft. Position at this point is very important and the phalanx should be placed in straight alignment with a slight dorsal position. Following observation of satisfactory position, the subcutaneous tissue and skin are subsequently closed. Figure 2.16 shows an x-ray after Keller's arthroplasty resection and Figure 2.17 shows a photo of a foot during postoperative follow-up. Postoperatively, the patient is placed in a bandage and a surgical shoe with 0.5 inch felt ending in the digital sulcus to prevent pressure on plantar hallux pulp. The patient is also instructed to walk flatfooted. The K-wire is left in place for 3 weeks and subsequently
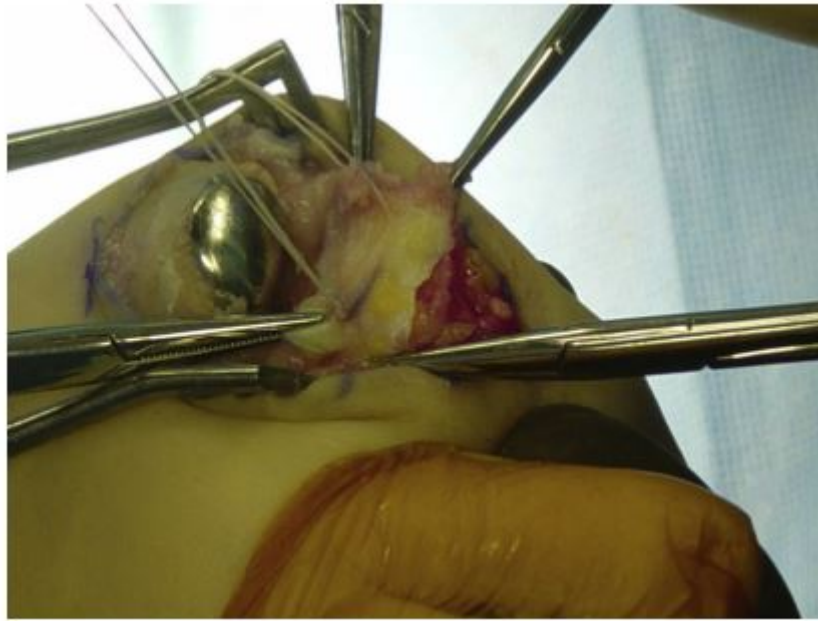
Fig. 2.13: A portion of the dorsal capsule is being attached to the proximal phalanx using 2 absorbable suture anchors. [10].

pulled. Following the K-wire removal, the patient is kept in a bunion splint for 2 to 3 more weeks for continued splinting. Range of motion exercises are begun immediately after removal of the pin and continued throughout the entire postoperative course.

A. Putti et al. performed a study with 46 feet who underwent Keller's resection arthroplasty. The operation was carried out between April 1993 and July 1997. The duration of follow-up after surgery was 1-7 years [63]. The indication for surgery on all feet was painful hallux valgus associated with hallux rigidus. Patients with only primary diagnoses of hallux valgus, hallux rigidus, or only diagnoses of underlying rheumatoid arthritis were excluded from the study. The study included 30 women and 2 men. 19 right feet and 27 left feet were operated. The average age at surgery was 62.5 ± 6.9 years, with a range of 50-83 years. The patients were divided into two groups. The final results were compared in 32 patients younger than 65 years and 14 patients older than 65 years. The results were approved by the Local Ethics Committee. 44 feet had significant pain at the metatarsophalangeal joint of the great toe before the operation. Of those, 22 feet continued to experience some degree of pain after the operation. In 35 feet, patients showed concern about the appearance of the great toe before the operation. A satisfactory appearance of the great toe after the operation was found at 41 feet. Problems with the use of regular footwear, platform footwear, was recorded at 39 feet before the operation and in 6 cases the patients were wearing a pre-operative footwear model. After the operation in 31 of the 39 feet, patients were able to wear regular footwear, while in 8 feet they indicated that they could not use regular footwear. Two patients were unable to wear regular footwear post-operatively despite indicating that they were able to wear pre-operatively without the need for modified footwear. In 17 feet, pain was found in the lower part of the lesser toes before the operation, of those 8 they continued with similar symptoms. In a total of 18 feet of the 46 feet evaluated, metatarsalgia was found after the operation. In 39% of the feet the subjective result was found to be excellent, in 37% it was found to be good, in 22% it was reported as regular and in 2% the results were poor. The average metatarsophalangeal angle of the great toe was 29.2° with a range of 11 to 38° before the operation. After the operation the average was 17.2° with a range of 4 to 50°. The change in the metatarsophalangeal angle range was 15 to 34° with an average angle change of $11.8 \pm 10.9°$. The average pre-operative

Fig. 2.14: The phalangeal side has been resurfaced with a metal-backed polyethylene surface, which is secured to the phalangeal with a taper post as in the metatarsal head. [10].

intermetatarsal angle between the first and second metatarsals was 13.8° with a range of 3 to 30°. After the operation the average was 10.3° with a range of 8 to 20° and The range change in the intermetatarsal angle was 8 to 20° with an average change angle of $4 \pm 5.2°$.

Another study by Coutts et al. [46] treated 131 feet from 104 patients between 1997 and 2007 for hallux rigidus with Keller resection arthroplasty. For this study of the 131 ft 89 were lost to follow up, 13 patients died. 12 did not attend the follow-up or did not want to take part in the study and 37 patients had their notes destroyed. Unfortunately the health trust policy states that if the patient has no contact or inquiries in 8 years then the patient's medical notes must be destroyed. In all cases the procedure was developed by second author Timothy E. Kilmartin.

42 patients attended the revision, 8 male feet with a total of 6 males and 34 female feet with a total of 26 females, the follow-up of patients was 92 months. The mean age of follow-up was 69 years with 8 months in a range of 52-86 years of age. Dorsoplantar, lateral and weight bearing radiographs confirmed the presence of grade III in hallux rigidus according to the Hattrup and Johnson scale classification. Of the participants, 76% presented complete satisfaction with the results of the operation, 21.5% presented satisfaction with reservations and 2.5% dissatisfaction. The average of the results of the scale proposed by the AOFAS for the metatarsophalangeal junction of the first toe was 38 points for 29 feet, after three months it was 89 points for 21 feet and in the final revision 89 points for 42 feet. Passive range of motion using a digital goniometer was 48.2 degrees of extension and 11.3 degrees of flexion. Active flexion defined as the ability of the patient to lift a paper towel with hallux while keeping the foot in the plantigrade position was positive in 62% of the feet.

Beertema et al [39] conducted a study with patients who had operations between 1990 and 2000 for symptomatic hallux rigidus or hallux valgus / rigidus. The patients had a minimum follow-up of 2 years and were seen by the researcher Wieske Beertema who was not the person who performed the surgeries. 28 patients underwent the Keller procedure. The age range was 31 to 77 years. Most of the patients demonstrated grade II hallux rigidus in the Regnauld classification. The average of the scale proposed by the AOFAS for grades I, II and III was 94, 83 and 87, respectively, and the average in the VAS scale was 0.4, 1.6 and 2.3. Only one grade I and one grade II patient stated that they would not undergo the same procedure again. One

Fig. 2.15: Intraoperative photo showing the position of arthroplasty. [11].

patient in each grade reported good satisfaction; 8.7.1 7.9 respectively. 4 patients were able to walk for a time limit of one hour. The mean range of motion and dorsiflexion of the hallux metatarsophalangeal junction in grade I was; 70 $\pm$ 8.2 degrees with a range of 60-80 degrees and 47 $\pm$ 4.7 degrees with a range of 40-50 degrees, respectively. For patients with grades II it was; 57 $\pm$ 18.5 degrees with a range of 10-85 degrees and 43 $\pm$ 16.1 degrees with a range of 10-65 degrees. For patients with grade III it was; 65 $\pm$ 11.2 degrees with a range of 50-80 degrees and 56 $\pm$ 6.5 degrees with a range of 50-65 degrees. None of the 28 patients required a second operation. 6 patients reported some instability and only 7% developed metatarsalgia.
An important risk of the Keller procedure is an excessive cut in the first toe with the possibility of reducing joint instability and impairing the thrust of the take-off phase of gait, resulting in transfer metatarsalgia. As we have seen, the Keller procedure is a very old but very effective procedure in people with hallux valgus and hallux rigidus, it can be used in the initial stages of the diseases, but it is more recommended in the more advanced stages. The main technical complication is the development of transfer metatarsalgia. Due to its complications, some specialists recommend this procedure in older people with low functional demands. Despite this, the technique has been working for more than a century.

2.4 Finite element Analysis.

2.4.1 Finite element method.

The finite element method was developed in the 1950s. M.J. Turner, R.W. Clough, H.C. Martin and L.J. Topp published in 1956 an article entitled "Stiffness and Deflection Analysis of Complex Structures" where a method is exposed in which the stiffness of the complete structure is obtained by adding the stiffnesses of the individual units. The basic conditions of continuity and equilibrium are established at selected points (nodes) in the structure and any physically possible support condition can be taken into account, but the term finite elements is not

Fig. 2.16: Immediate postoperative radiograph showing alignment [11].

mentioned. [66]. Ray Clough was a professor at Berkeley University and subsequently wrote an article that used the term "finite elements" for the first time, and was credited with being one of the founders of the method. Berkeley was the center of finite element research for many years. This research coincided with the rapid growth of computer power, and the method quickly became widely used in the nuclear power, defense, automotive and aeronautics industries. [67]. The method was initially termed matrix analysis of structures. Later, it was extended to include the analysis of continuum structures. Since continuum structures have complex geometries, they had to be subdivided into simple components or "elements" interconnected at nodes [68]. A physical phenomenon usually occurs in a continuum of matter (solid, liquid, or gas) involving several field variables. A continuum with a known boundary is called a domain. The field variables change from point to point, thus possessing an infinite number of solutions in the domain. The basis of finite element analysis relies on the decomposition of the domain into a finite number of subdomains (elements) for which the systematic approximate solution is constructed by applying the variational or weighted residual methods. The finite element analysis method requires the following major steps [18]:

- Discretization of the domain into a finite number of subdomains (elements).

- Selection of interpolation functions.

- Development of the element matrix for the subdomain (element).

- Assembly of the element matrices for each subdomain to obtain the global matrix for the entire domain.

- Imposition of the boundary conditions.

- Solution of equations.

Fig. 2.17: Postoperative clinical view [11].

- Additional computations (if desired).

Although finite element analysis started in the field of structural engineering, the method can be used in different engineering disciplines as shown in Table 2.1. Due to the wide field of application, this method has become a powerful tool in industry and research. This thesis

Tab. 2.1: Degrees of freedom and force vectors in finite element analysis for different engineering disciplines [18].

Discipline	Degree of freedom	Force vector
Structural/solids	Displacement	Mechanical forces
Heat conduction	Temperature	Heat flux
Acoustic fluid	Displacement potential	Particle velocity
Potential flow	Pressure	Particle velocity
General flows	Velocity	Fluxes
Electrostatics	Electric potential	Charge density
Magnetostatics	Magnetic potential	Magnetic intensity

focuses on the discipline of biomechanics by performing finite element analysis for the foot of a person weighing 60 kg in the take-off position after having performed the different types of arthroplasties discussed above. All analyzes are linear elastic and mainly three different types of elements are used. 3D bar elements are elements in three-dimensional space that can only withstand axial load without risk of buckling and are used to simulate the behavior of the foot's thin ligaments and plantar fascia. The 3D beam elements are three-dimensional elements capable of withstanding flexion and are used to simulate the behavior of some foot muscles. Finally, the tetrahedral elements are used for cortical and trabecular bones, as well as for the cartilage and implants studied in this thesis. Next, the formulation of the stiffness equations and simple examples in structural engineering for the three types of elements used are carried out.

2.4.2 *Finite element models of the foot.*

As previously mentioned, the finite element method appeared in the 50's, but it was not until the 80's that the first finite element model of the foot appeared where a foot is analyzed in the

mid-stance position during a variety of footwear conditions. The results of this nonlinear analysis warrant more detailed and realistic modeling of shoe mechanics, and systematic efforts to correlate physical measurements and clinical experience with trends indicated by finite element analyzes [12]. Later in 1993 and 1996 K.M. Patil presented a two-dimensional model of a normal foot in the three phases of quasi-static gait: heel-strike, mid-stance, and push-off. This model included cartilage and ligaments and was used to simulate muscle paralysis and its effect on the distribution of principal efforts. Subsequently, the model was used to analyze the stresses on the deformed feet of three patients suffering from leprosy with complete paralysis of certain muscles [69], [13]. In 1997, Lemmon presented a finite element model representing a sagittal section through the second metatarsal bone with dorsal and plantar soft tissue. This extends from the proximal end of the second metatarsal to the joint space at the second metatarsophalangeal joint. The metatarsal geometry was obtained by scanning a video image of a typical second metatarsal from a postmortem skeletal specimen. Their approach considered the hyperelastic properties of the soft tissue of the foot, the accommodative orthoses constantly reduced the peak plantar pressures, the peak pressure decreased as the thickness of the insole increased [70]. In 2000 Gefen et al. provided significant advances in the description of the stress distribution for various support subphases, which established the basis in the material properties, loads and constraints of the finite element models of the foot [71]. In the early 2000s, 3D foot models were developed with significant simplifications. Jacob et al. in his model treated the lateral metatarsals and medial metatarsals as single bodies, Other authors such as Bandak et al. and Guo et al. simplified the geometry by fixing the midfoot and forefoot joints while Cheung et al. facilitated the use of 3D foot models to analyze the internal stress and strain distributions of the foot structure. Based on the boundary conditions and material properties proposed by these researchers, a large number of foot models with more precise geometries have been used in recent years in many different applications [44], [72], [73], [74].

In 2006 Xiao-Qun Dai et al. created a 3D finite element model to simulate the contact between the foot, the sock and the insole. The biomechanical effects of wearing socks with different combinations of friction properties on the plantar contact of the foot were investigated. The dynamic plantar pressure and the shear stress during the stance phases of the gait were studied using finite element computations. Three cases were simulated, one barefoot with a high coefficient of friction against the insole (0.54) and two with socks, one with a high coefficient of friction against the skin (0.54) and a low coefficient of friction against the insole (0.04 and another with an opposite frictional properties assignment. The results showed that wearing low-friction socks against the skin of the foot was more effective in reducing the plantar shear force on the skin than the sock with low friction against the insole. The risk of walking barefoot in the development of blisters and ulcers related to plantar shear can be reduced by wearing socks, especially those with little friction against the skin of the foot [75].

J.T-M Cheung published in 2007 a study where the biomechanical effects of midfoot fusion were investigated using the finite element approach. Two different types of midfoot fusion were studied during the heel strike, mid stance and push off phases. This 3D model contained 28 linearly elastic bones, 72 ligaments and the plantar fascia, said structure was embedded in a volume of hyperelastic soft tissue simulating foot fat. From their research they conclude that midfoot fusion may induce abnormal stresses and loads in the adjacent forefoot and rearfoot joints, so midfoot fusion should be done with caution to minimize possible adverse biomechanical effects [76].

During 2008, Jia Yu et al. presented an anatomically detailed 3D finite element model of the female foot and ankle along with a high heel support to investigate the plantar contact pressure and internal load responses of the bone and soft tissue structures of the foot with different heights of heel during simulated standing. The results showed an increase in stresses in the first metatarsophalangeal joint and a decrease in efforts in the plantar fascia. The study concludes

by saying that increased stresses in the first ray of the foot during prolonged standing with high heels can contribute to the progressive deformity of hallux valgus. However, reduced tension strain in the plantar fascia with heel lift can help relieve pain and inflammation associated with plantar fasciitis [77].

J. Bayod et al. compared in 2009 using finite element simulations two surgical procedures used as treatment for claw toe; flexor digitorum longus tendon transfer and transfer of the flexor digitorum brevis. The study shows that both techniques reduce the level of stresses compared to the non-operated pathological foot, demonstrating that both techniques are effective in the treatment of claw toe deformity [78].

Sung-Jae Lee et al. developed in 2010 a three-dimensional and non-linear finite element model of a human foot complex with comprehensive skeletal and soft-tissue components. The model was validated by experimental data of subject-specific barefoot plantar pressure measurements. The preliminary results indicate that large von Mises stress occurs where plantar soft-tissue contacts with geometrically irregular bony structures, thus internal stress distribution within the plantar soft-tissue was dramatically influenced by bony prominences due to stress concentration. The lateral sesamoid bone associated with the head of the first metatarisan showed the greatest stress concentration effect [14].

Ya-Bo Yan et al. presented in 2011 a finite element modeling of a 3D coupled foot-boot model. The boot was represented by assembling the finite element models of the upper, insole, midsole and sole built based on the finite element model of the foot-ankle, and finally the coupled foot-boot model was generated by assembling the models of the lower limb and boot. In this study, the foot and ankle finite element model was validated during standing. There was good agreement on the general patterns of distribution of the predicted and measured plantar pressure published in the literature [79].

Emmanuel Brilakis et al. conducted in 2012 an investigation where the objective was to evaluate the effects of maintaining different postures of the foot during the healing of fifth metatarsal fractures for 3 types of common fractures. 30 finite element 3D models were analyzed that took into account the type of fracture, the posture of the foot and the stage of healing. The research results indicate that the clinical observations and standard therapeutic options in the literature are in agreement with the results observed in this research [80].

Ming Zhang et al. in 2013 they showed a three-dimensional finite element model of the coupled foot-ankle-shoe complex. Interfacial contact simulation was used to complete the contact placement process between the top of the foot and the shoe. Three main phases of the gait were simulated; heel strike, midstance, and push off, to investigate the biomechanical response of walking in high-heeled shoes. It was found that the contact pressure in all metatarsophalangeal joints intensified and reached its maximum in the push off phase during locomotion, while the first metatarsophalangeal joint had the highest magnitude. The first and fifth metatarsophalangeal joints had greater movements in the transverse plane between all metatarsophalangeal joints, indicating that these two joints flex more significantly by toe box restraint during locomotion [81]

A.K.-L. Leung et al. In 2014 they published an investigation about first ray hypermobility of the foot using finite element analysis. A three-dimensional foot model was constructed from a 28-year-old woman using magnetic resonance images. All foot and ankle bones, including two sesamoids and encapsulated bulk tissue, were modeled as 3D solid parts, joining with the ligaments as connecting muscle shell elements. The stance phase of the gait was simulated using the boundary and load conditions obtained from the analysis of the gait of the same subject. Compared to the normal foot, the hypermobile foot had higher resulting metatarsocuneiform and metatarsophalangeal joint forces. The predicted results represented a possible risk of joint problems and metatarsus primus varus [82].

Duo Wai-Chi Wong et al. in 2015 they explored functional restoration and the risk of nonunion

after performing a metatarsocuneiform atrodesis using finite element analysis. A 3D foot model was constructed from a 28-year-old woman using magnetic resonance imaging. Parts of the first metatarsal and cuneiform were cut and the bone graft was assigned with the same rigidity as the adjacent bones to simulate metatarsocuneiform arthrodesis surgery. The results showed that the main efforts of the third metatarsal in the midstance and push off positions increased after the operation, while those of the second metatarsal decreased. The operation reduced the medial deviation of the first metatarsal head during the push off phase. The bone graft may experience tensile stresses on the underside. In conclusion, the increased efforts in the first metatarsal and the reduction in the medial excursion of the first metatarsal head after sham operation reflected that metatarsocuneiform arthrodesis could restore the load-bearing function of the first ray [30].

Zahari Taha et al. in 2016 they worked on a finite element analysis of a human foot model to study the dynamic behavior and internal loading conditions during the neutral position on flat ground. The foot structure is simulated to aid in the design of an instrumented footwear insole. A finite element model of a human foot was generated and the load condition during neutral standing was used to evaluate the stress distribution. The results showed maximum pressures in the first metatarsal, the fifth metatarsal and below the heel. The study offered a preliminary computational model, which is capable of estimating the integral plantar pressure and is intended to help scientists investigate the plantar pressure of the foot, as well as develop custom insoles [83].

Martinez Bocanegra et al. In 2017, they carried out a structural biomechanical analysis of a restorative arthroplasty of the first metatarsophalangeal joint, and analyzed the interaction between bone and medical grade silicone implants. For this, a simulation of a foot with Swanson and Tornier joint implants was performed to evaluate the distribution of stresses and deformations during toe-off. The main stresses obtained for the first metatarsal with both implants suggest that failure is induced in this bone because the values exceed the tensile strength reported for the trabecular phalanx, which may be related to osteolysis. The stress and strain values obtained in this study suggest that arthroplasty surgery with the Swanson implant is more likely to cause postoperative complications compared to the Tornier implant [84].

Yubo Fan et al. in 2018 they evaluated the effect of distal osteotomy in postoperative hallux valgus, using experimental measurement and finite element modeling of the foot to compare the biomechanical behavior of the first ray in pre / postoperative hallux valgus. The results showed that compared to preoperative hallux valgus, plantar pressure decreased and redistributed in the region of the second metatarsal. The osteotomy was helpful for the stability of the first ray [85].

Ming Zhang et al. In 2019 they examined and compared arch deformity and plantar fascia tension between different running gait techniques using a computational modeling approach. A three-dimensional finite element foot model was reconstructed from the MRI of a healthy runner. The foot model included twenty bones, soft tissue, ligaments, tendons, and plantar fascia. Time series data for segmental kinematics, foot muscle strength, and ankle joint reaction force were derived from a same-participant musculoskeletal model based on motion capture analysis. The rearfoot strike and the forefoot strike were simulated using an explicit dynamic solver. The results showed that, compared to the rearfoot strike, the forefoot strike reduced the height of the arch of the foot and increased the angle of the medial longitudinal arch. The forefoot strike also increased the tension of the flat connective tissue and increased the traction force of the plantar fascia [86].

Christian Cifuentes-De la Portilla et al in 2020 used an innovative finite element model to evaluate some flatfoot scenarios treated with isolated hindfoot arthrodesis and triple arthrodesis. When arthrodesis are performed in situ, the talonavicular seems a good option, possibly superior to the subtalar and at least three times as high. Calcaneal-cuboid arthrodesis significantly

reduces stresses on the plantar fascia and elastic ligament, but concentrates higher stresses around the fused joint [15].

As mentioned above, around 40 years have passed since finite element analysis began to be used to simulate the biomechanical behavior of the foot. Figure 2.18 shows how finite element models have evolved decade by decade.
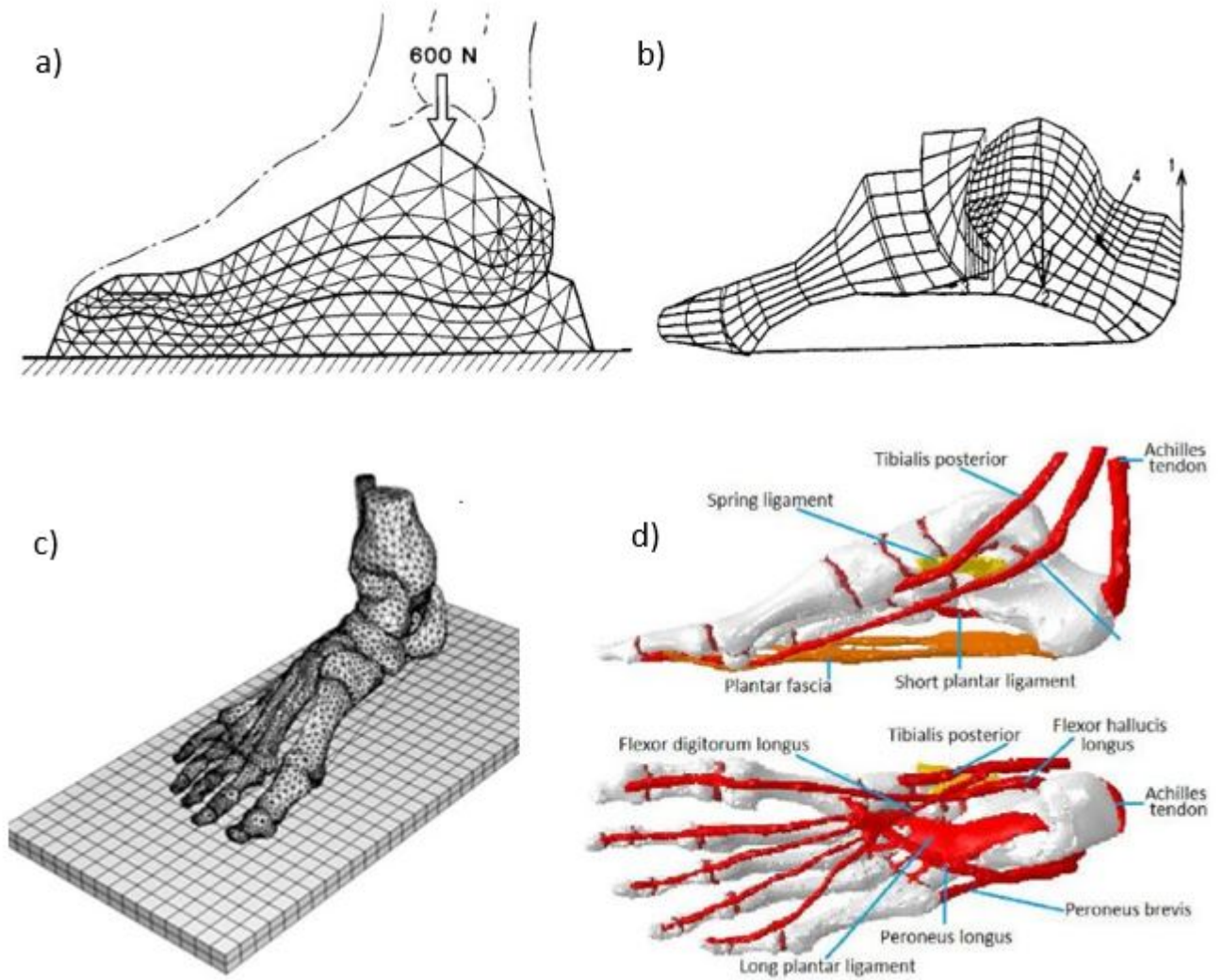
Fig. 2.18: Evolution of finite element models of the foot in the last 40 years [12], [13], [14], [15].

3. BIOMECHANICAL EVALUATION OF ARTHROPLASTY IN THE FIRST METATARSOPHALANGEAL JOINT.

3.1 *Arthroplasty models for the first ray of the foot.*

This chapter shows the finite element models developed in this thesis to study the biomechanics of the foot after having developed an arthroplasty procedure in the first metatarsophalangeal joint. This surgical technique remains controversial. It has the advantage of being a technique that allows to relieve pain and restore mobility to dorsiflexion of the first metatarsophalangeal joint, but it also has the disadvantage of being a destructive procedure and is considered one of the last treatment options for hallux valgus and hallux. rigidus [9].

To date, there are no scientific articles that show a biomechanical evaluation for the implants studied in this thesis. Finite element models are a good technique to understand the effects that undergoing arthroplasty in the first metatarsophalangeal joint can have and are cheaper and easier to perform than experimental ones (either in vivo or in cadavers).

One of the objectives of this work is to understand the effect on biomechanics generated by different types of arthroplasty in the first ray of the foot. To do this, displacements and stresses will be compared in 5 finite element models; The first of them is a healthy and pathology-free model, followed by a hemiarthroplasty model in the first proximal phalanx, then a hemiarthroplasty model is presented in the first metatarsal, then a total arthroplasty model is presented, finally and despite Since it is a surgical procedure without an implant, a Keller resection arthroplasty model is exposed.

The arthroplasty process consists of aligning the first ray of the foot, in the case of hallux rigidus the osteophytes are removed. A resection is made in the proximal area of the first phalanx and/or the head of the first metatarsal, taking care not to damage the sesamoids. If this is the case, the implant is inserted, and some muscles and tendons are disconnected. Forces and displacements of the five models presented are analyzed during toe-off to evaluate the effects of the surgical procedure on the biomechanics of the gait, especially in the first ray of the foot. The healthy model induces stresses and deformations that correspond to the biomechanics of the foot in the literature in the toe-off position, and the arthroplasty models induce stresses and displacements that allow us to know how the implants work and how the biomechanics of gait changes with the arthroplasty procedure, especially knowing whether or not there are consequences in the biomechanics of the first ray of the foot.

3.1.1 *Healthy model.*

For the development of the bones of this healthy model, a foot of a 36-year-old person weighing 60 kg and free of pathologies was scanned. 93 CT scans were needed for the foot scan. These radiographs were taken every 2 mm. The creation of volumes was done using the extrapolation program g1.exe provided by the Advanced Informatics Group of the University of Zaragoza GIGA. For the creation of bones, a differentiation was made between cortical bone and trabecular bone. The model contains 28 cortical and trabecular bones. These are: calcaneus, talus, cuboid, navicular, 3 cuneiforms, 5 metatarsals, 2 phalanges of the hallux, 12 phalanges of the lesser toes and two sesamoids embedded in the first metatarsal. Cartilage was created

by covering the spaces of the joints of the bones and its function is to cushion the pressure of the articular surfaces so that they can slide or move without friction between them. The model includes the posterior, exterior and interosseous talo-calcaneal, inferior, superior, interosseous and external calcaneal-scaphoid ligaments, tarsal-metatarsal and intermetatarsal joints, Lisfranc ligaments, calcaneo-cuboid ligaments and calcaneal-scaphoid ligaments. All of these have been named as thin ligaments. The model also contains short and long plantar ligaments and plantar fascia ligaments which will be referred to as plantar ligaments. The healthy model also contains the following muscles and tendons; abductor hallux, adductor hallux, extensor hallucis longus, extensor hallucis longus expansion, flexor hallucis brevis, flexor hallucis longus, extensor hallucis brevis, flexor digitorum brevis, flexor digitorum longus and capsularis. The model is presented in the toe-off phase because in this phase the maximum stresses are developed in the first ray of the foot [43], [45]. For bones and cartilage, we use tetrahedral elements due is a good type of element to mesh complicated geometries, for muscles and tendons we use beam elements because they experiment directly a pretension force due to the position of toe-off and for thin ligaments, plantar ligaments, and plantar fascia we use bar elements due they only suffer small displacements in their extreme nodes when the model is loaded [78], [84], [87], [88],[89], [90]. Thin ligaments have a cross section of 0.045 mm2, long ligaments a cross section with an area of 7.35 mm2, Muscles and tendons have a circular cross section with a radius of 2 mm. The maximum element size in the model is 3 mm, the minimum is 0.31 mm, and the average size is 1.78 mm, thus solving the model's convergence problem. This model contains 150,594 nodes and 802,294 elements of which are; 992 1D, 4,109 2D and 797,193 3D. Figure 3.1 shows the elements of this first model.
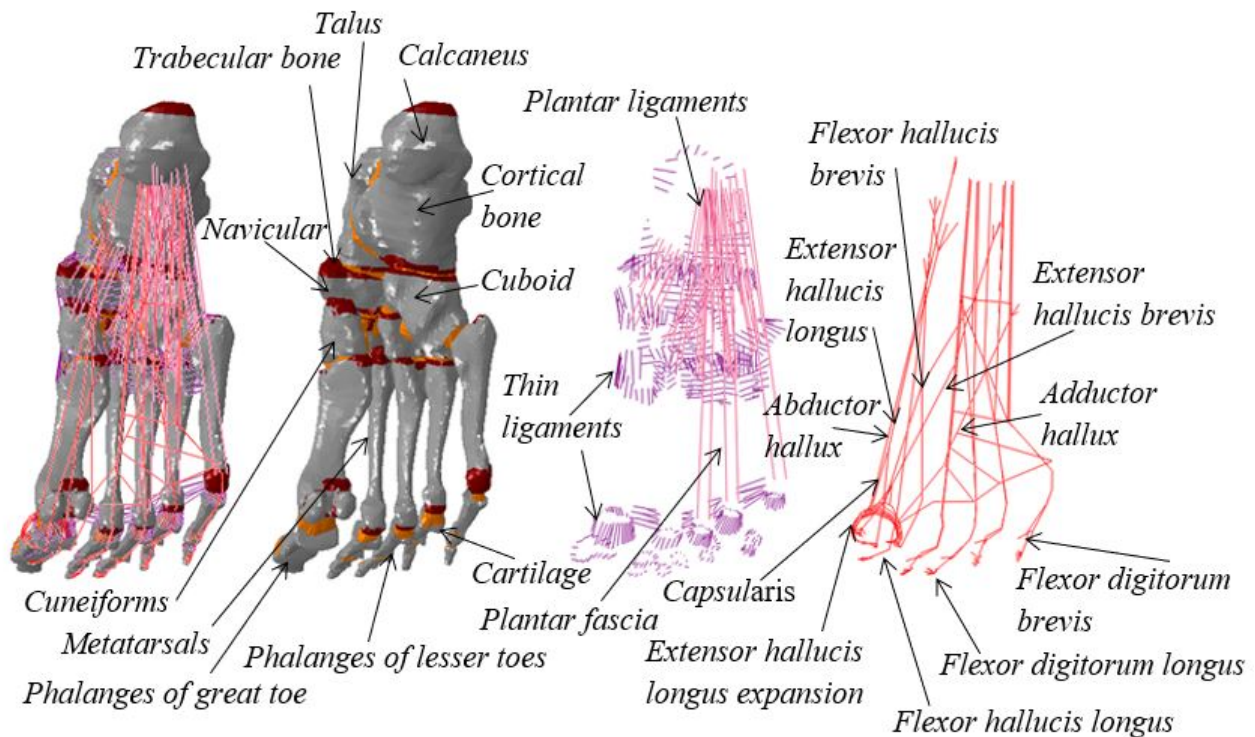
Fig. 3.1: Elements of the healthy model.

3.1.2 *Model of hemiarthroplasty in the first proximal phalanx.*

The second model presented in this chapter contains the insertion of an hemi implant in the proximal phalanx of the great toe. This implan is the AnaToemics® Phalangeal Prosthesis by

Arthrex. To obtain the implant volume, a 3D scanner provided by the University of Zaragoza was used. The implant was placed in the model with the help of Softimage 2015. According to the surgical procedure, a cut of approximately 2 to 3 mm is made in the proximal part of the first phalanx to then introduce the implant. To make this cut in the proximal phalanx, Mimics 10.0 was used. The mesh of the hemiarthroplasty model in the first proximal phalanx was performed with ICEM CFD 17.2 from ANSYS, with a maximum and minimum element size of 3.8 mm and 0.18 mm respectively in the entire model, with an average size of 1.13 mm. In the implant, the maximum and minimum element size was 3 mm and 0.42 mm, respectively, with an average element size of 1 mm. In this way, the geometry of the first ray was preserved after the surgical procedure had been developed, in addition to solving the model convergence problem. When the maximum, minimum and average size of the element in the implant is 5 mm, 0.7 mm and 1.7 mm respectively, there are no significant changes in the calculations of stresses and strains in the implant. To maintain the geometry of the soft tissues, the MATLAB R2013b programming was used to insert muscles, tendons and ligaments, calculating the minimum distance of the nodes of the healthy model with the nodes of the hemiarthroplasty model in the first proximal phalanx.

For this model with implant in the first proximal phalanx, some muscles and tendons, as well as some ligaments, have been removed from the first metatarsophalangeal joint as part of the hemiarthroplasty process [91]. Figure 3.2 shows the elements of the model with the implant and figure 3.3 shows the AnaToemics®Phalangeal Prosthesis hemi implant and its mesh, it should be noted that in the part of the implant (spikes) inserted in the trabecular bone of the first proximal phalanx, stresses and strains are small values, so the mesh size adequately solves the model convergence problem. The hemiarthroplasty model in the first proximal phalanx contains 1,836,607 elements of which are; 849 1D, 93499 2D and 1742259 3D, the model contains 329,159 nodes.
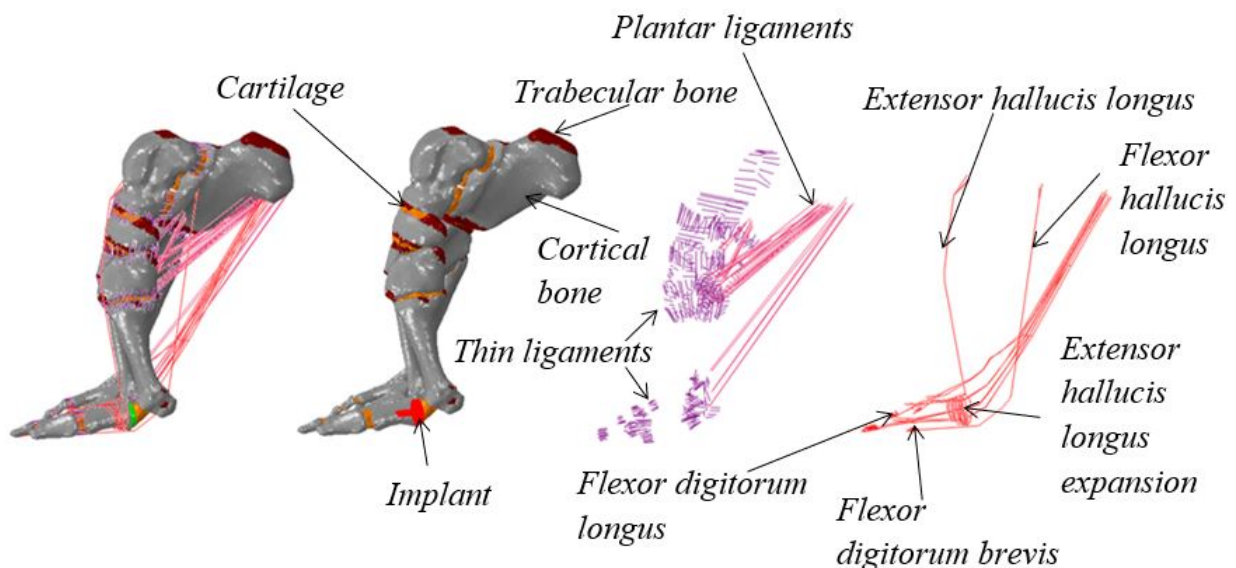
Fig. 3.2: Elements of the model of hemiarthroplasty in the first proximal phalanx.

3.1.3 *Model of hemiarthroplasty in the first metatarsal.*

The third model presented in this chapter contains the insertion of an hemi implant in the first metatarsal bone. This implant is the Arthrosurface HemiCAP® Toe DF. This model has been developed in the Applied Mechanics and Bioengineering (AMB) group of the University

Fig. 3.3: Hemi implant AnaToemics®Phalangeal Prosthesis and its mesh.

of Zaragoza. To develop the model, 93 computed tomographies separated every 2 mm were generated in DICOM format. To generate the volumes from the tomographies, the volume extrapolation program called g1.exe was used, developed by the Advanced Computing Group (GIGA) of the University of Zaragoza (same procedure as the healthy model). The 93 CT scans were processed in MIMICS 10.0 software to make volumes of cortical and trabecular bones, as well as cartilage in .STL format. The implant was placed using the Softimage 2015 software and the resection in the first metatarsal bone was performed with MIMICS 10.0. The mesh for the model was generated with the ANSYS ICEM CFD 17.2 software. The maximum and minimum element size in the implant were 8.69 mm and 0.129 mm respectively, with a mean element size of 0.85 mm. In the implant, the maximum element size was 0.5 mm, thus avoiding the loss of geometry due to meshing and thus solving the problem of mesh convergence. The model of hemiarthroplasty in the first metatarsal contains 28 cortical and trabecular bones and also contains cartilage that serve as a connection between the bones. These bones are: calcaneus, talus, cuboid, navicular, 3 cuneiforms, 5 metatarsals, 2 major phalanges, 12 minor phalanges, and 2 sesamoids embedded in the first metatarsal. After obtaining the mesh of bones, cartilage and implant with tetrahedral elements, programming in MATLAB R2013b was used to add soft tissues such as: fine ligaments, plantar ligaments, muscles and tendons. In this model with implant in the first metatarsal the thin ligaments between the first metatarsal and the first proximal phalanx, as well as the muscles and tendons; flexor hallucis brevis, capsularis, extensor hallucis brevis, adductor hallux and abductor hallux were disinserted on the recommendation of podiatrist Dr. Ricardo Becerro de Bengoa Vallejo [91]. This model of hemiarthroplasty in the first metatarsal bone contains 611,349 nodes and 3386,602 elements of which 851 are 1D, 57623 are 2D and 3328,128 are 3D. Figure 3.4 shows the elements for this model with hemiarthroplasty in the first metatarsal, and figure 3.5 shows the implant and the mesh generated by it.

3.1.4 *Model of total arthroplasty in the first metatarsophalangeal joint.*

The fourth model presented in this chapter contains the insertion of the Arthrosurface® ToeMotion® Modular Restoration System implant which has components that insert into the first proximal phalanx as well as the first metatarsal. 93 CT scans were required every 2 mm for the foot scan (healthy model). The volumes of cortical and trabecular bones as well as cartilage were obtained by processing the tomographies in DICOM format with the MIMICS 10.0 software. To obtain the volumes of the implant components, a 3D scanner provided by
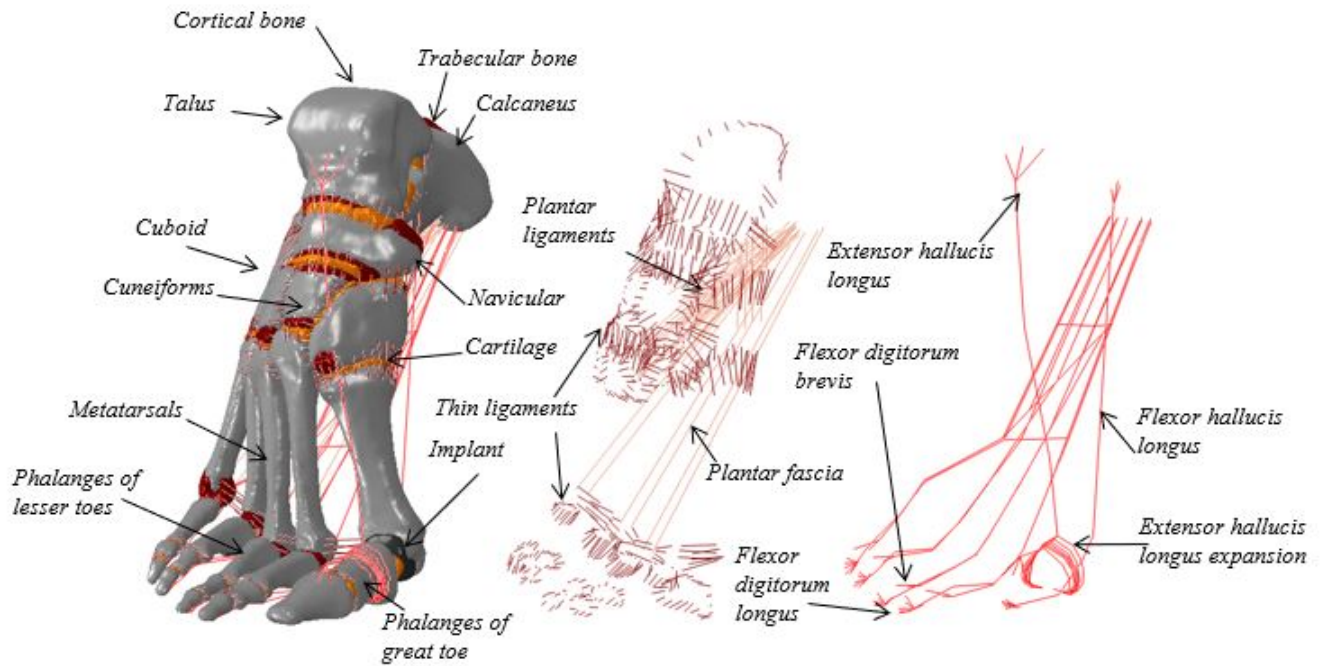
Fig. 3.4: Elements of the model of hemiarthroplasty in the first metatarsal.

the University of Zaragoza was used. For the insertion of muscles, tendons and ligaments, programming was carried out in MATLAB R2013b in the same way as in the hemiarthroplasty models. The implant placement in the model according to the surgical procedure was done with the Softimage 2015 software. The cuts in bones and cartilage of the model according to the arthroplasty procedure were carried out by performing boolean subtraction operations with the MIMICS 10.0 software. The mesh of bones, cartilage and implant (tetrahedra) was performed with the ANSYS ICEM CFD 17.2 software, having a maximum and minimum size in the model of 3.8 mm and 0.19 mm, respectively, having an average element size of 1.09 mm. In implants, the maximum and minimum element size are 1.9 mm and 0.27 mm, respectively, with an average size of 0.66 mm, thus solving the model's convergence problem in addition to preserving the geometry of the first metatarsophalangeal joint after the development of the aforementioned procedure. Part of the arthroplasty process in the model consists in disconnecting some muscles and tendons, while the following muscles and tendons remain connected; extensor hallucis longus, extensor hallucis longus expansion, flexor hallucis longus, flexor digitorum brevis and flexor digitorum longus. This model of total arthroplasty in the first metatarsophalangeal joint contains 381,046 nodes and 2108,347 elements of which 851 are 1D, 48009 are 2D and 2059,487 are 3D elements. Figure 3.6 shows the elements of the model and figure 3.7 shows the Arthrosurface® ToeMotion® Modular Restoration System implant and its mesh.

3.1.5 *Model of Keller resection arthroplasty.*

The last model presented in this chapter analyzes a foot in the toe-off position after a Keller resection arthroplasty has been developed. From the 93 computational tomographies in DICOM format, the volumes of the 28 cortical and trabecular bones, as well as those of the cartilage, were obtained. The resection cut of the proximal part of the first phalanx was made using the MIMICS 10.0 software. The dead tissue filling that is made in the area of the cut of the first phalanx was made using the same geometry cut in the first phalanx. The meshing of the tetrahedral elements of the model includes the cortical and trabecular bones as well as the

Fig. 3.5: Arthrosurface HemiCAP®Toe DF hemi implant and its mesh.
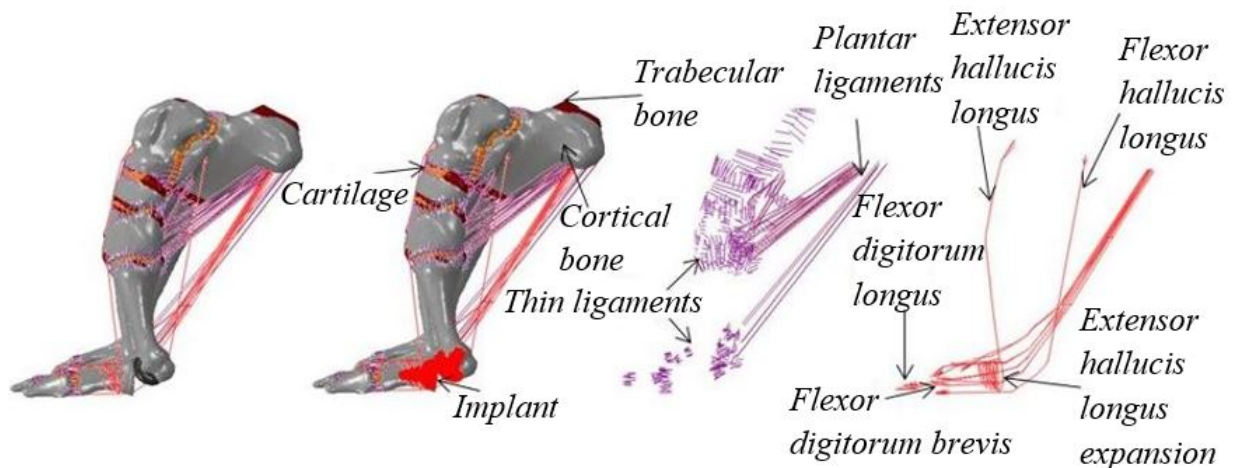
Fig. 3.6: Elements of the model of arthroplasty.

cartilage and dead tissue filling. Tetrahedral elements were generated with ICEM CFD 17.2 from ANSYS. The maximum and minimum element size were 4.53 mm and 0.15 mm respectively with an average size of 1.07 mm. MATLAB R2013b programming was used to insert muscle tendons and ligaments into the model. The muscles, tendons and ligaments that are disinserted in the model are the same as in the other arthroplasty procedures described previously. This Keller resection model contains 412,680 nodes and 2,256,585 elements of which 851 are 1D, 61,450 are 2D, and 2194284 are 3D. In figure 3.8 the elements of the model can be seen in figure 3.9 the cut in the proximal phalanx due to the surgical procedure is shown.

3.2 *Mechanical properties and boundary conditions.*

The mechanical properties, as well as the boundary and load conditions used in the five models presented in this chapter, are the same, so they are only defined once [84], [87]. All the elements were considered as homogeneous, isotropic and linearly deformable elastic because there are only small displacements and small deformations. For cortical bone, trabecular bone, muscles, thin ligaments and plantar ligaments, a modulus of elasticity of 17000, 700, 450, 260

Fig. 3.7: Arthrosurface® ToeMotion® Modular Restoration System implant and its mesh.

and 350 MPa respectively has been used, all elements mentioned above have a Poisson's ratio of 0.3. For cartilage, a Young's modulus of 10 MPa and a Poisson's ratio of 0.4 were used. The Arthrex AnaToemics®Phalangeal Prosthesis hemi implant that is inserted into the first proximal phalanx is made of cobalt chromium (Co-Cr) and a modulus of elasticity of 210 MPa with a Poisson's ratio of 0.29 has been considered for this material. The Arthrosurface HemiCAP®Toe DF hemi implant that is inserted into the first metarsian is made up of two parts. The joint reshaping component is made of cobalt chromium alloy (Co-Cr) and the conical post is made of titanium alloy (Ti-6Al-4V), for this material we use a modulus of elasticity of 113.8 GPa and a Poisson's ratio. of 0.29. The Arthrosurface® ToeMotion® Modular Restoration System total arthroplasty implant has 4 components, the two components that are inserted into the metatarsal are the Arthrosurface HemiCAP®Toe DF hemi implant and the two components that are inserted into the first proximal phalanx are two materials; the conical post is made of titanium alloy (Ti-6Al-4V) and the joint reshaping component is made of ultra molecular weight polyethylene (UHMW-PE) which has an elastic modulus of 650 Mpa with a Poisson's ratio of 0.30. The Keller resection model does not contain implants; however, for the filling material in the first proximal phalanx, as it is dead tissue, a Young's modulus of 1 MPa and a Poisson's ratio of 0.45 have been considered. The summary of the mechanical properties of the five models presented in this chapter can be seen in table 3.1 [43], [92], [93], [94], [95].

Some authors divide the human gait cycle in 3 steps while others do it in 6 steps and still others in 8 steps. Regardless of the gait cycle classification taken, it is well documented that maximum stresses in the first ray of the foot occur during toe-off [87]. The models presented are in the toe-off stage and correspond to a person weighing 60 kg. The analysis was performed in the Abaqus 6.13-5 software. Two steps were used for the analysis. In the first step, a pretension force of 2% is added to the muscles. The pretension loads were calculated with cadavers, muscles were cut in the toe-off position and their elongation was measured after the cut, thus calculating their stress and pretension force. In flexor digitorum longus and flexor digitorum brevis, a pretension force of 22 N was obtained in each muscle. For the remaining muscles the pretension force obtained was 11 N [45]. In this first step of the analysis, a fixed support was used on the insertion surface of the Achilles tendon (one of the tendons that mechanically generates the greatest reaction against the person's own weight) and the first two
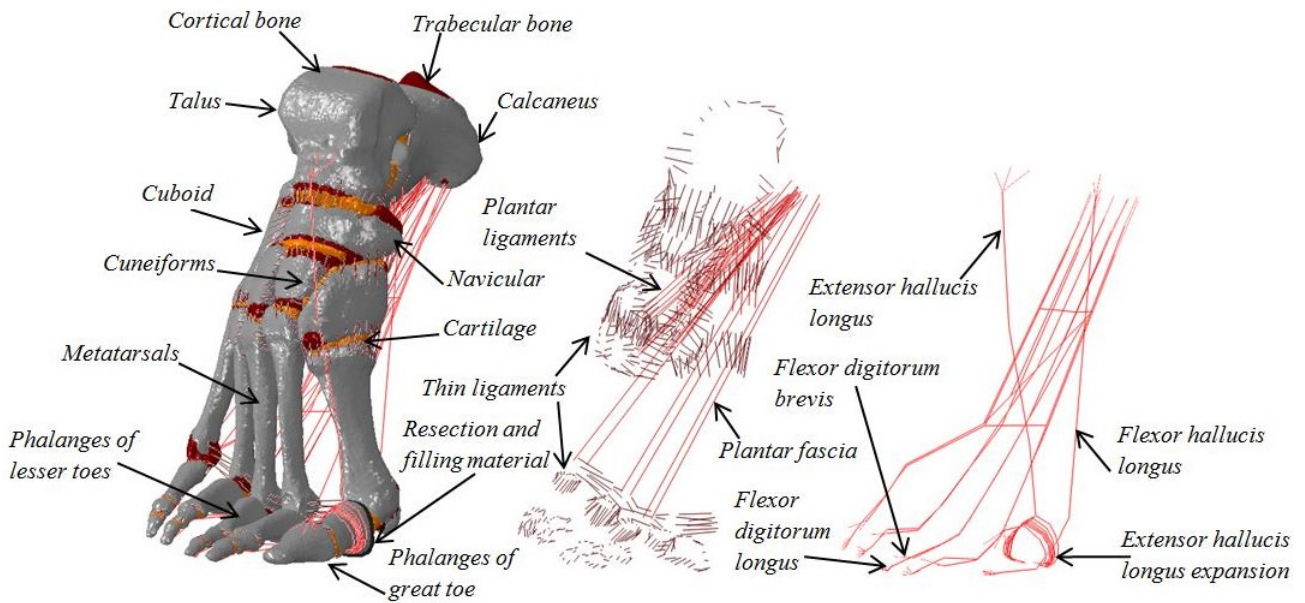
Fig. 3.8: Elements of the model of Keller resection..

Tab. 3.1: Mechanical properties of bones, soft tissues and implants.

Materials	Elasticity modulus (MPa)	Poisson's ratio
Cortical bone	17000	0.3
Trabecular bone	700	0.3
Cartilage	10	0.4
Muscles	450	0.3
Thin ligaments	260	0.3
Plantar ligaments	350	0.3
Filling material	1	0.45
Hemi implant in proximal phalanx (CoCr)	210000	0.29
Hemi implant head in metatarsal (CoCr)	210000	0.29
Hemi implant pin in metatarsal (Ti-6Al-4V)	113800	0.34
Hemi implant in proximal phalanx (UHMW-PE)	650	0.3
Hemi implant in proximal phalanx (Ti-6Al-4V)	113800	0.34

proximal phalanges. Translation and rotation in the vertical axis were restricted for the distal phalanges of the lesser toes. In the second Step, the pretension forces are maintained and the weight of the person is added considering a force of 1805 N decomposed in the global axes of the model as can be seen in figure 3.10, said load was applied in a group of 361 nodes in the area where the tibia and fibula contact the talus. The boundary conditions are the same as in step 1 but adding a fixed support on the proximal phalanx of the third toe [78].

3.3 Results of models of arthroplasty in the first ray of the foot.

3.3.1 Results of the healthy model.

In this healthy model, the maximum absolute principal stresses appear in the calcaneus, in the area of the insertion surface of the Achilles tendon, which is a fixed support in the model. For the first ray of the foot, the first distal phalanx acquires a movement in the sagittal plane. This movement is due to the reaction of force that the ground exerts on the person and produces a forward impulse, giving directionality to the march [96]. In Figure 3.11, we can see this
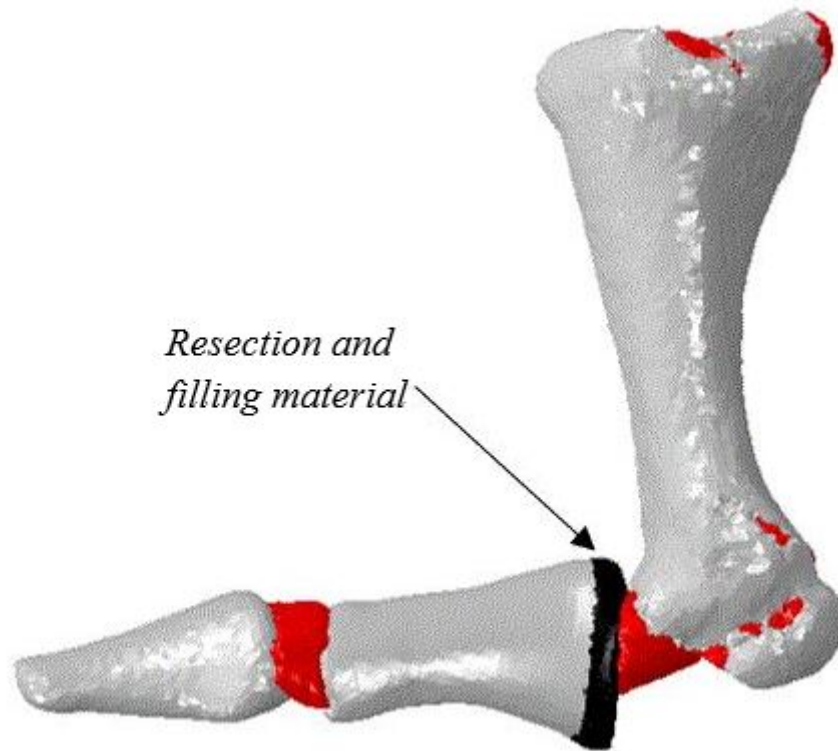
Fig. 3.9: First ray of the foot in Keller resection model.

movement, which is commonly known as the passive Windlass mechanism, and we can also see the principal stresses for this healthy model of the foot.

For the first distal phalanx, the maximum concentration of major stress occurs in the dorsal area, where the tendons of the extensor hallucis longus act. Major stress concentrations appear at the support points for the second and third ray of the foot. For the first ray of the foot, the maximum concentration of principal stresses does not occur in the support points, it occurs in the part where extensor hallucis longus expansion acts. The maximum displacement occurs in the phalanges of the fifth ray of the foot. For rays 2 and 3 of the foot, compression stresses appear in the plantar area, while tension stresses appear in the dorsal part. Figure 3.12 shows the displacements in the first ray of the foot and it is observed that the maximum displacement is 9 mm, as mentioned, this occurs in the distal phalanx as a consequence of the passive Windlass mechanism.

3.3.2 Results of the model of hemiarthroplasty in the first proximal phalanx.

For the second model presented in this chapter, the principal stress concentrations appear in the second ray of the foot and calcaneus. For the first ray of the foot, the greatest concentration of principal stresses appears at the points of support. The stresses and displacements in the first ray of the foot are small values compared to those occurring in the minor rays. For the second and third ray, the highest stress concentration occurs in the proximal phalanges, in the proximal plantar area. Tensile stresses appear in rays 2 and 3 in the dorsal part and compression stresses appear in the plantar area. The greatest displacement occurs in the third and fifth ray of the foot in the area of the phalanges. The function of the passive Windlass mechanism is lost. The forces and displacements mentioned above can be seen in figure 3.13. Figure 3.14 shows the maximum von Mises stress on the implant, which is 27 MPa. The maximum principal tensile stress is 29 MPa and occurs at the base of the implant spike. The highest value of the principal stress in compresion in the implant is 27 MPa and appears in the oval part.
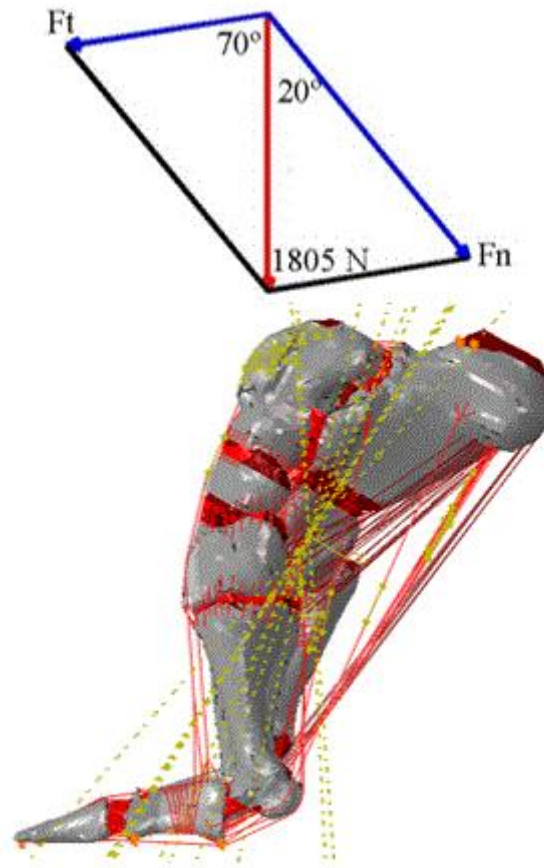
Fig. 3.10: Boundary and loading conditions for foot models.

3.3.3 Results of the model of hemiarthroplasty in the first metatarsal.

In the figure. 3.15 you can see the absolute maximum values of the principal stresses for the hemiarthroplasty model in the first metatarsal. The maximum absolute principal stresses appear on the calcaneus in the area of the insertion surface of the Achilles tendon which is a fixed support on the model. It can be noted that rays 2 and 3 are responsible for transmitting the load in the take-off stage when a hemiarthroplasty has been developed in the first metatarsal bone. Regarding the proximal phalanges of the second and third rays of the foot, the dorsal area is working in tension (positive stresses) and the plantar area is working in compression (negative stresses).

Regarding the first ray of the foot, only at the support points a small concentration of effort appears. The displacements in the first ray of the foot are nulls, while the displacements in the lesser toes are responsible for carrying out the impulse produced in the human gait cycle in the take-off stage. The passive Windlass mechanism is lost in this first metatarsal hemiarthroplasty model.

In figure 3.15 it can be seen that forces with values greater than those of the first ray appear in the second ray of the foot. The maximum value of the principal stresses in the toes appears in the second proximal phalanx in the area of the points of support. Figure 3.16 shows the von Mises and principal stresses values in the Arthrosurface HemiCAP®Toe DF hemi implant. The absolute greatest value of minimum principal stress in the implant is 51 MPa (compressive stress). The maximum principal stress in the implant is 70 MPa, both stresses occur in the articular component of the implant. The maximum value of von Mises stress in the implant was 49 MPa.
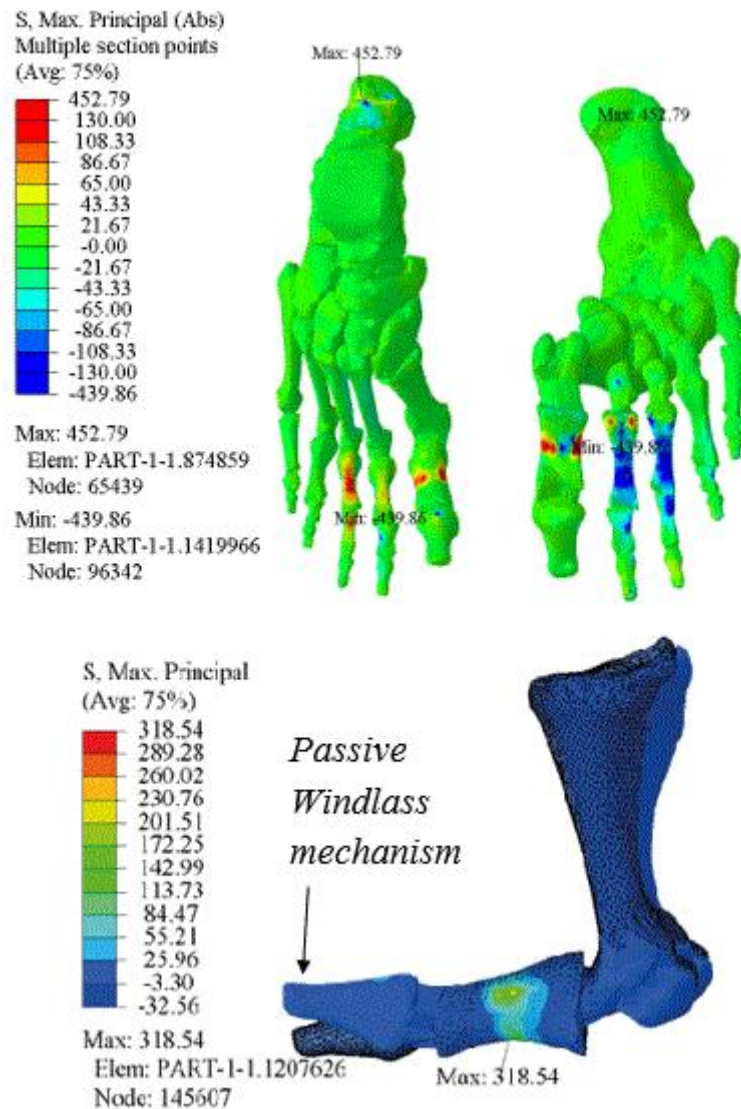
Fig. 3.11: Principal stresses in healthy model.

3.3.4 *Results of the model of total arthroplasty in the first metatarsophalangeal joint.*

The results of the total arthroplasty model in the first ray of the foot show a higher concentration of principal stresses on the calcaneus in the area of the insertion surface of the Achilles heel. Concentrations of stress appear at the support points of the first proximal phalanx. Displacements in the first distal phalanx are zero. Rays 2 and 3 of the foot obtain compression stresses in the plantar area and tension stresses in the dorsal area. Concentrations of stress appear at the support points of the second and third ray. Figure 3.17 shows the principal stresses for this total arthroplasty model.

The highest von mises stress in implants is 716 MPa and this occurs in the articular component of the first metatarsal in the area of contact with the UHMW-PE component. For the articular component that is inserted into the first proximal phalanx, the highest von Mises stress is 549 MPa on the surface that contacts the articular component of the first metatarsal. The maximum principal tensile stress in the articular component of the first metarsian is 889 MPa while the maximum principal compressive stress is 391 MPa. In the articular component of the first proximal phalanx, the maximum principal tensile stress is 375 MPa. and the maximum principal compressive stress is 376 MPa. The stresses on the implants can be seen in
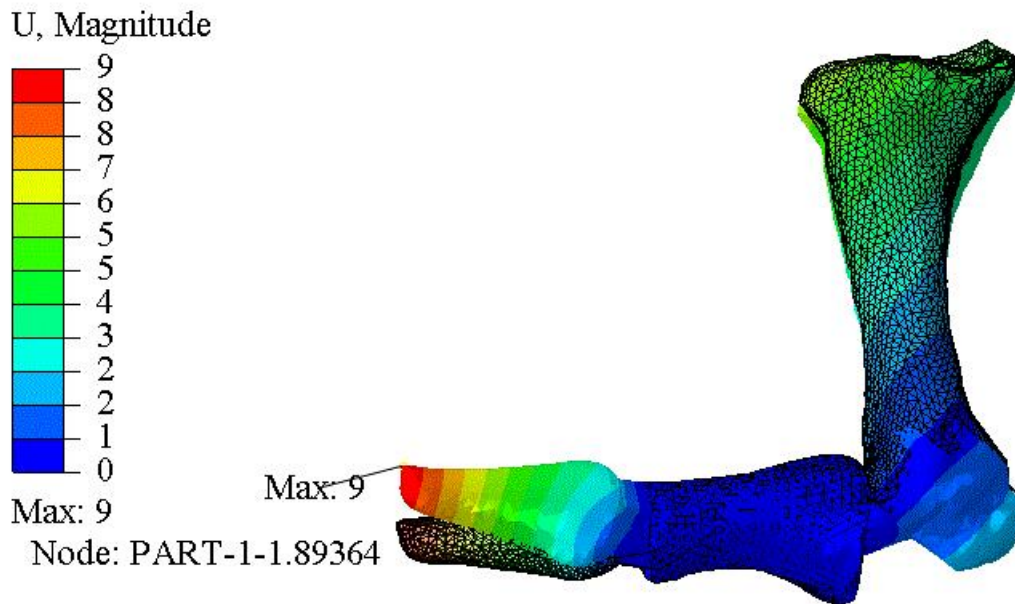
Fig. 3.12: Displacements in the first ray of the foot for the healthy model.

figure 3.18.

3.3.5 *Results of the model of Keller resection arthroplasty.*

The results of this last model presented in this chapter show the maximum principal stresses in the insertion zone of the Achilles tendon in the calcaneus in the nodes that have support restrictions in the model. For the first ray of the foot, small concentrations of stresses appear only at the support points of the first proximal phalanx. Displacements of the first distal phalanx are nulls. The maximum displacement occurs in the fifth ray of the foot. At the support points of the second and third ray of the foot stresses concentration occurs. The plantar area of the second and third ray of the foot works in compression and the dorsal area works in tension. The principal stresses for the Keller resection atroplasty model are shown in Figure 3.19.

3.4 **Discussion of results.**

In this chapter, finite element models of a foot have been presented after different types of arthroplasty have been developed in the first metatarsophalangeal joint. If a Keller resection arthroplasty is developed, joint remodeling consists of making a cut of the proximal part of the first phalanx, if a hemiarthroplasty is performed, remodeling consists of inserting an implant in the first metatarsal or in the first proximal phalanx while If a total arthroplasty is done, the joint is replaced by an artificial one, inserting implants in both the proximal phalanx and the metatarsal. Regardless of the type of joint remodeling, the arthroplasty process in the finite element models of the foot investigated in this thesis consists of disinseting the muscles and tendons of; hallux abductor, hallux adductor, capsularis, flexor hallucis brevis and extensor hallucis brevis as well as the thin ligaments between the metatarsal and proximal phalanx. Being in this way connected the muscles and tendons of; extensor hallucis longus, extensor hallucis longus expansion, flexor hallucis longus, flexor digitorum longus, and flexor digitotum brevis.

The results of the healthy model show displacements in the sagittal plane for the first distal

S, Max. Principal (Abs)
Multiple section points
(Avg: 75%)

Min: -657.70   Min: -657.70

1348.38
80.00
66.67
53.33
40.00
26.67
13.33
-0.00
-13.33
-26.67
-40.00
-53.33
-66.67
-80.00
-657.70

Max: 1348.38
  Elem: PART-1-1.1515995
  Node: 28958

Min: -657.70
  Elem: PART-1-1.574829
  Node: 116882

Max: 1348.38   Max: 1348.38

S, Max. Principal
(Avg: 75%)

93.07
82.71
72.35
61.99
51.63
41.27
30.91
20.55
10.19
-0.17
-10.53
-20.89
-31.25

Passive Windlass mechanism is lost

Fig. 3.13: Principal stresses in model of hemiarthroplasty in the first proximal phalanx.

phalanx, this displacement of the distal phalanx during the toe-off position is known as passive Windlass mechanism. In all the arthroplasty models presented in this chapter, the distal phalanx displacements are zero. In order to understand how implants work when they are overloaded, we simulate the foot during the toe-off position, loading 1, 2 and 2.5 times the weight of the person. The upper part of figure 3.20 shows the displacements of the healthy model under the three loading conditions. The lower part shows the displacements for the three loading conditions in the model with the implant in the first proximal phalanx. The units of the displacements are millimeters. The distribution of stresses and displacements in the three load conditions analyzed was similar. The higher load value conditions the higher stress and displacement values in the model. The displacement values in the lesser toes are increased when the loading condition are increased, but for the healthy model the displacements of the distal phalanx of the great toe obtained the same value in the three conditions of load. In the hemiarthroplasty model, the displacement values in the first distal phalanx are zero under all loading conditions. The same results occur for the other arthroplasty models.

The principal stresses in the first ray of the foot for the healthy model show stress concentrations in the proximal phalanx in the area where the muscles and tendons of the extensor hallucis longus expansion act. For the distal phalanx the highest stress concentrations occur in
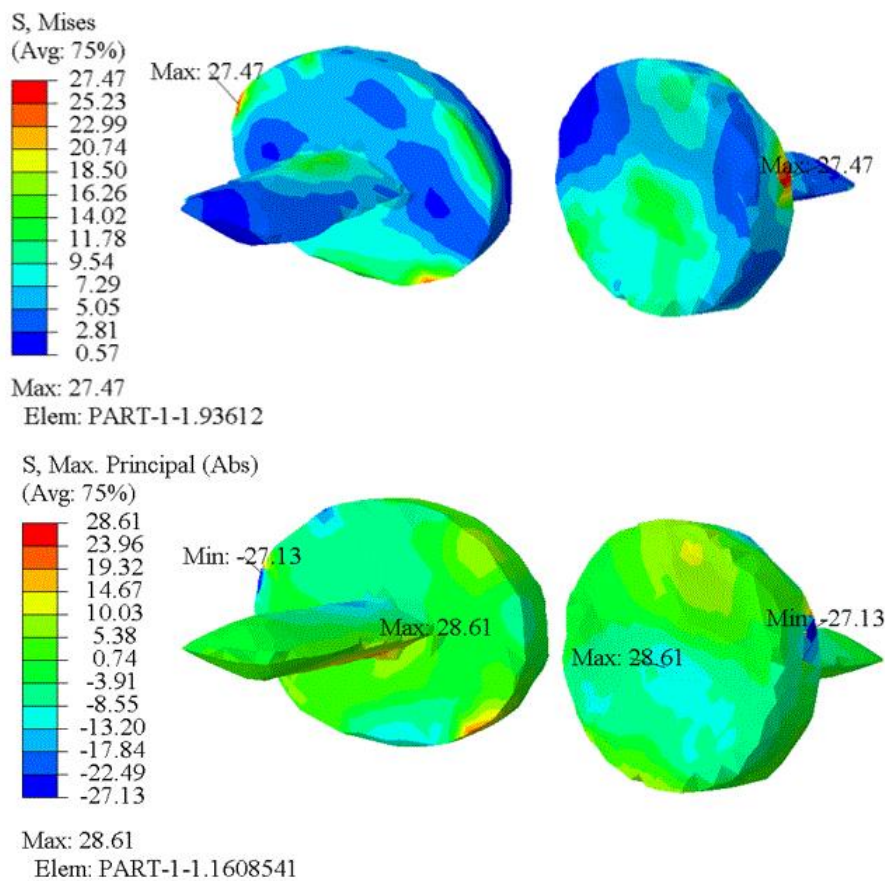
Fig. 3.14: Von Mises and principal stresses in Arthrex AnaToemics®Phalangeal Prosthesis hemi implant.

the area of the extensor hallucis longus tendons, while for the arthroplasty models the stress concentrations occur only at the support points of the first proximal phalanx. The stresses of the first ray of the foot decrease with the arthroplasty process, which can be translated as pain relief in the first metatarsophalangeal joint, but it is also a loss of load capacity for the first ray. In all the models presented in this chapter, for rays 2 and 3 compression stresses in the plantar area and tension stresses in the dorsal area appeared. The greatest concentration of stresses for rays 2 and 3 occurs at the support points of the proximal phalanges and after the arthroplasty process these stresses increase considerably, which can cause postoperative complications such as metatarsalgia, claw toe, hammer toe or tendonitis of the lesses toes [90], [78], [89].

For soft and hard tissues, the maximum principal stresses have been reported, while for implants, being used ductile metals and plastics, Von Mises stresses have been reported. Table 3.2 shows the Von Mises stresses for the implants investigated. For hemi implants, the reported stresses are small values compared to their elastic limit, while for the total arthroplasty implant the stresses in the implants generate plasticity, this indicates that the life of this implant will be much shorter than that of the other two.

Tab. 3.2: Von Mises stresses in implants.

Implant	Von Mises stress (MPa)
AnaToemics®Phalangeal Prosthesis	27
HemiCAP®Toe DF	49
ToeMotion® Modular Restoration System (metatarsal component)	716
ToeMotion® Modular Restoration System (phalanx component)	549
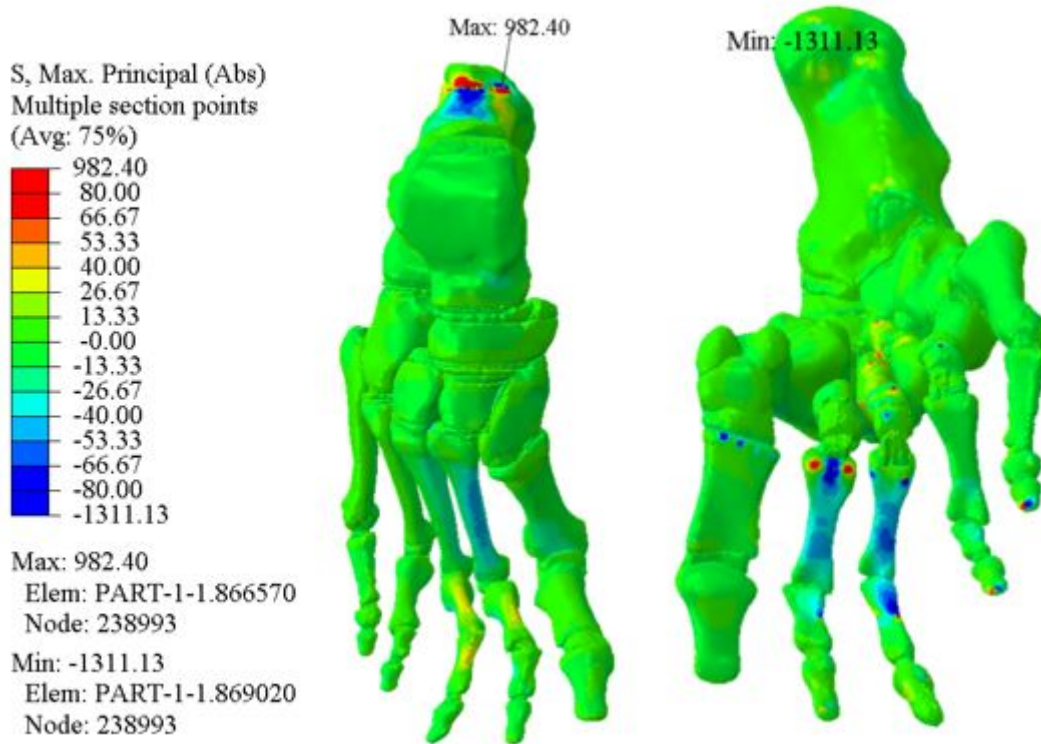
Fig. 3.15: Principal stresses in model of hemiarthroplasty in the first metatarsal.
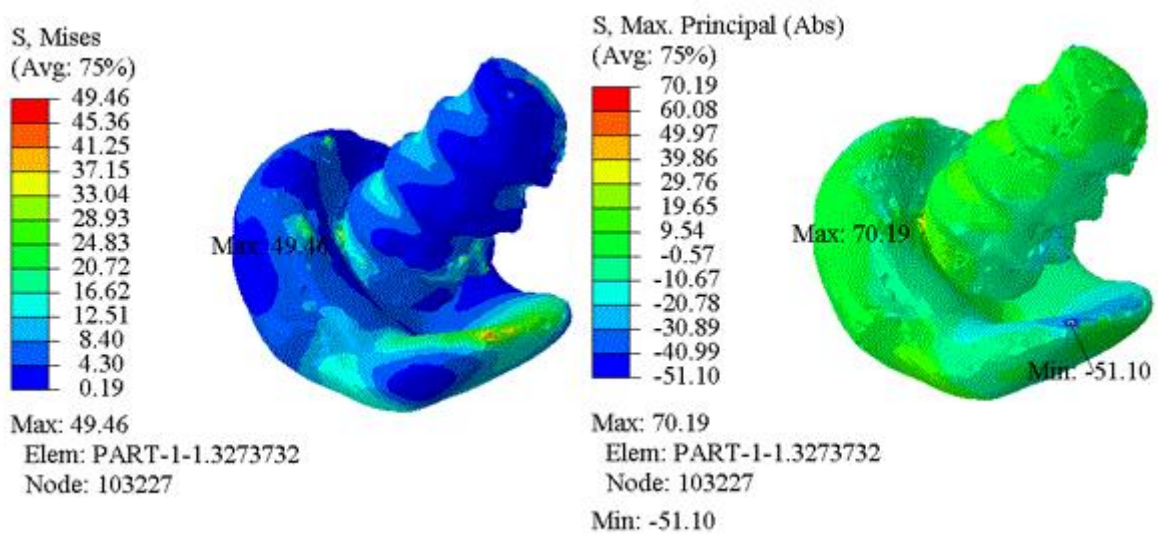
Fig. 3.16: Von Mises and principal stresses in Arthrosurface HemiCAP®Toe DF hemi implant.
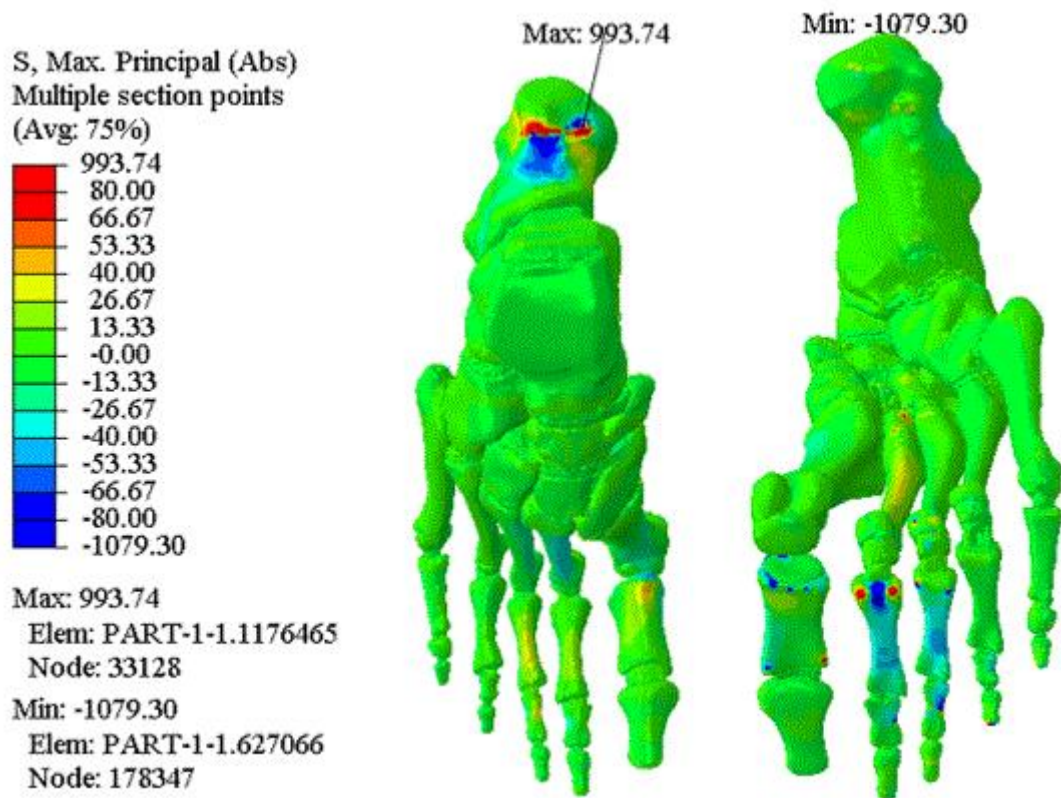
Fig. 3.17: Principal stresses in model of total arthroplasty.
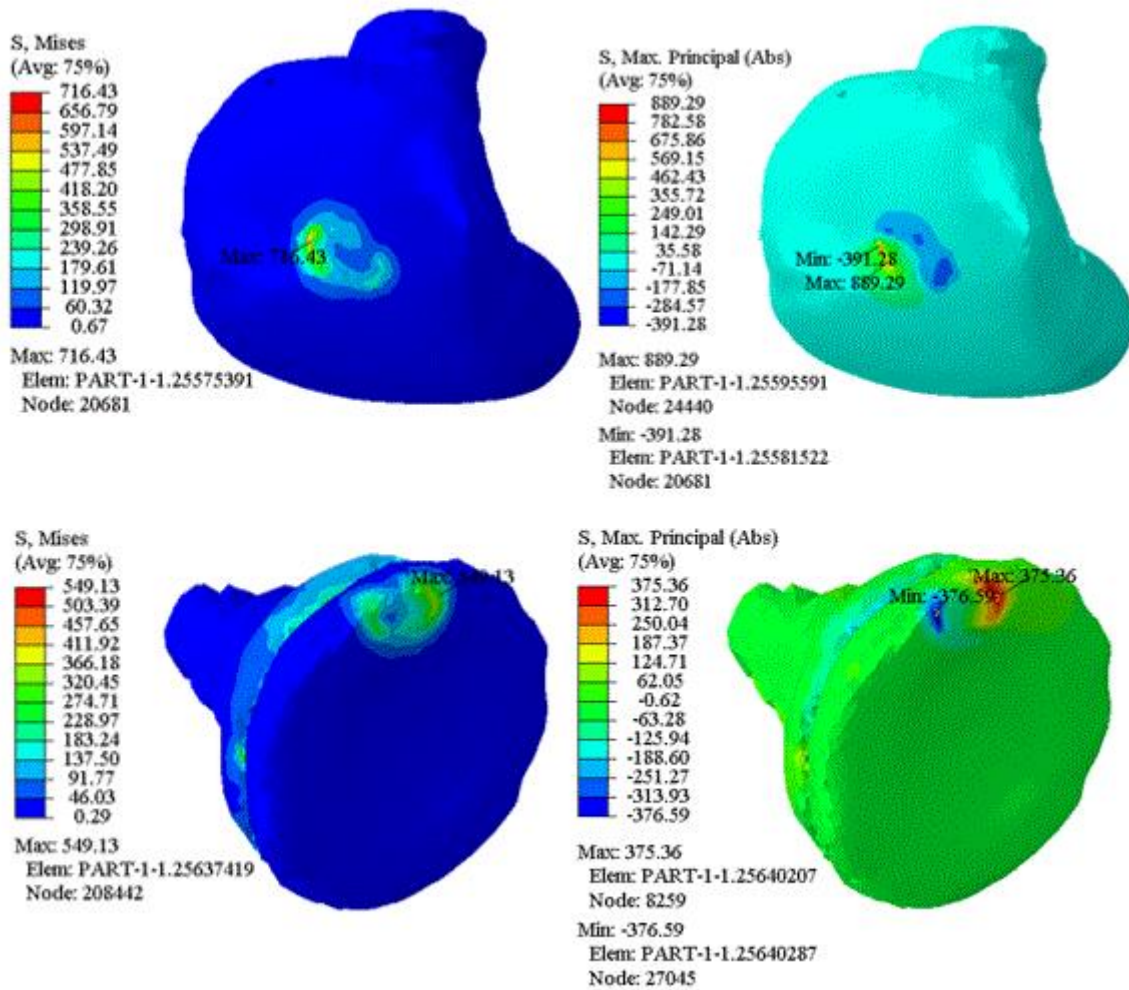
Fig. 3.18: Von Mises and principal stresses in Arthrosurface® ToeMotion® Modular Restoration System.
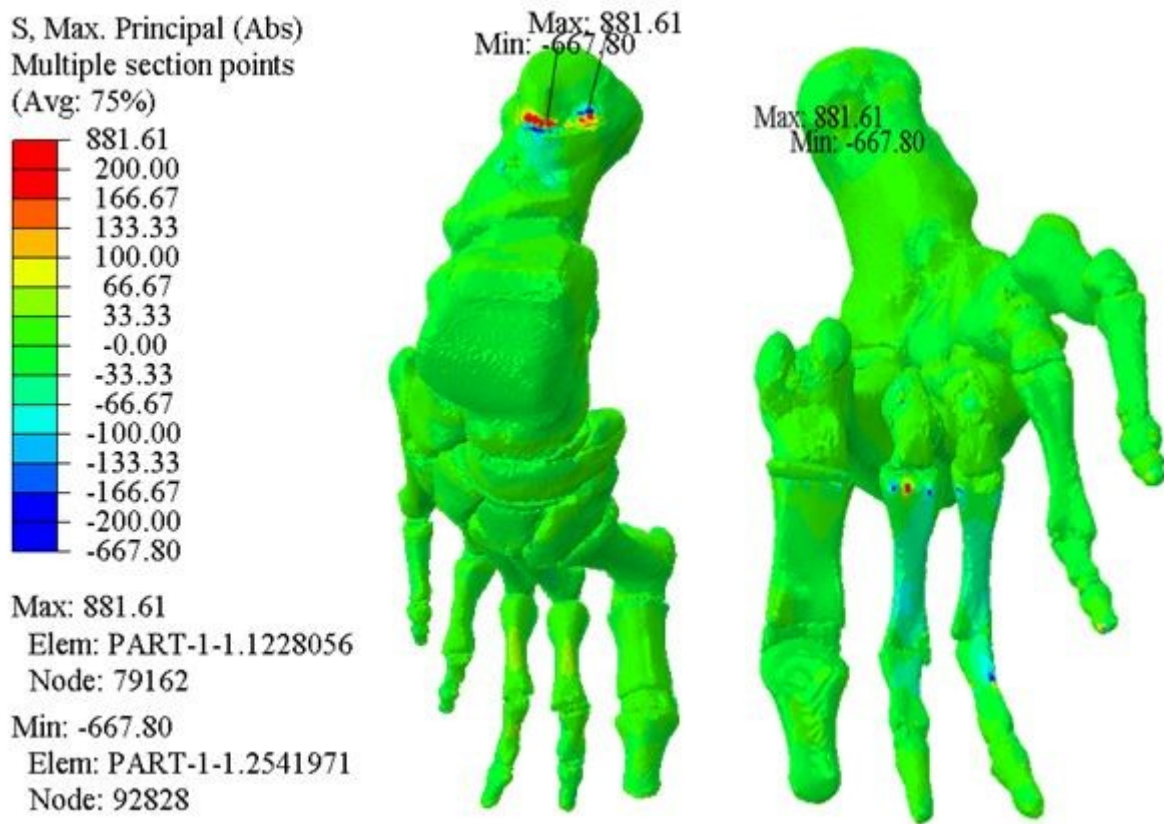
Fig. 3.19: Principal stresses in model of Keller resection arthroplasty.
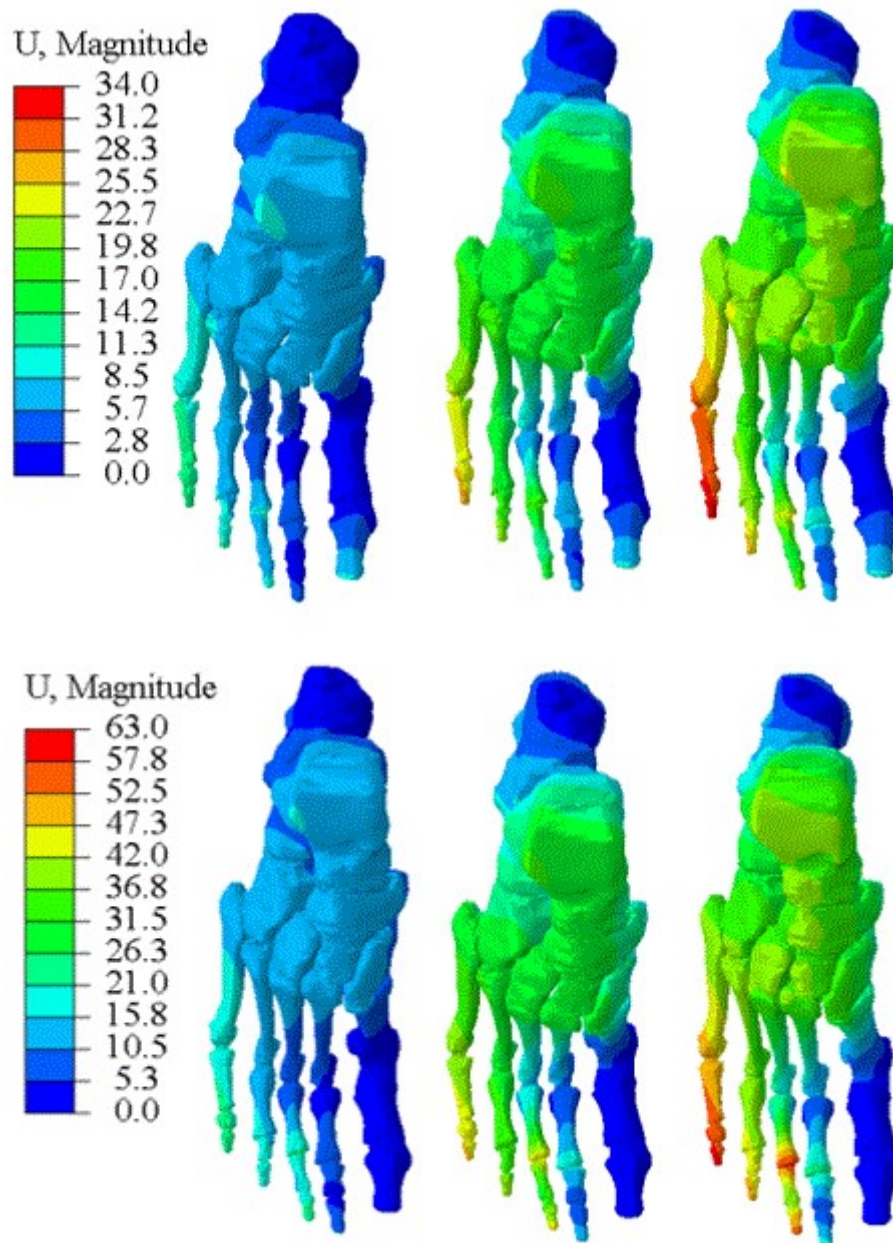
Fig. 3.20: Displacement values for healthy model (upper part) and hemiarthroplasty model (lower part) for all loading conditions.

4. ε-N_F CURVES AND ONE-STEP B MODELS FOR IMPLANTS IN THE FIRST METATARSOPHALANGEAL JOINT.

4.1 Introduction.

The strain-based approach to fatigue considers plastic deformation that can occur in localized regions where fatigue cracks begin. This type of procedure allows detailed consideration of fatigue situations involving local plasticity, which is often the case for ductile metals with relatively short lives. Either way, the approach also applies when there is little plasticity throughout life, making it a comprehensive approach that can be used in place of stress-based methods. The strain-based method was initially developed in the late 1950s and early 1960s in response to the need to analyze fatigue problems involving relatively short service life. The particular applications were nuclear reactors and jet engines, specifically, cyclic loads associated with their operating cycles, especially cyclic thermal stresses. Subsequently, it became clear that the service loads of many machines, vehicles, and structures include occasional severe events that can best be assessed with a stress-based approach. In mechanical tests to obtain the strain-life curve, the axial load is generally applied to samples with straight cylindrical test sections. In long lives where there is little plastic deformation, the tests can be performed under stress control, which is then essentially equivalent to deformation control. The number of cycles to failure N_f is generally defined as the occurrence of substantial cracking of the sample. A schematic diagram of a strain-life curve, plotted on log-log scales, is shown in Figure 4.1 [16]. It can be seen that when elastic deformation predominates in the problem, the energy lost due to the load and discharge hysteresis cycles is low and the value of the number of fatigue life cycles N_f is higher, while when the problem is dominated by plastic deformation the energy lost by the hysteresis cycles is greater and the value of the number of fatigue life cycles N_f is less.

This chapter describes the obtaining of the ε-N_f curves for each implant studied in the previous chapter through the use of probabilistic finite elements, and which corresponds to the adaptation of the work carried out by Bogdanoff and Kozin to the concept of fatigue in the stage of nucleation. This approach is based on the construction of non-linear accumulated damage models based on Markoff chains, through the use of estimators of the variables that characterize this process [97].

We will use the methodology proposed by J.A. Bea [98] where we start from probabilistic finite element results to develop statistical estimators starting from expressions also known as Neuber, Ramberg-Osgood and Coffin-Basquin-Manson. In the following sections, the general equations of the probabilistic finite element method are formulated and the coefficients of the Neuber, Ramber-Osgood and Coffin-Basquin-Manson expressions are obtained to determine the mean value of the number of life cycles and their variance of each implant studied in this thesis.
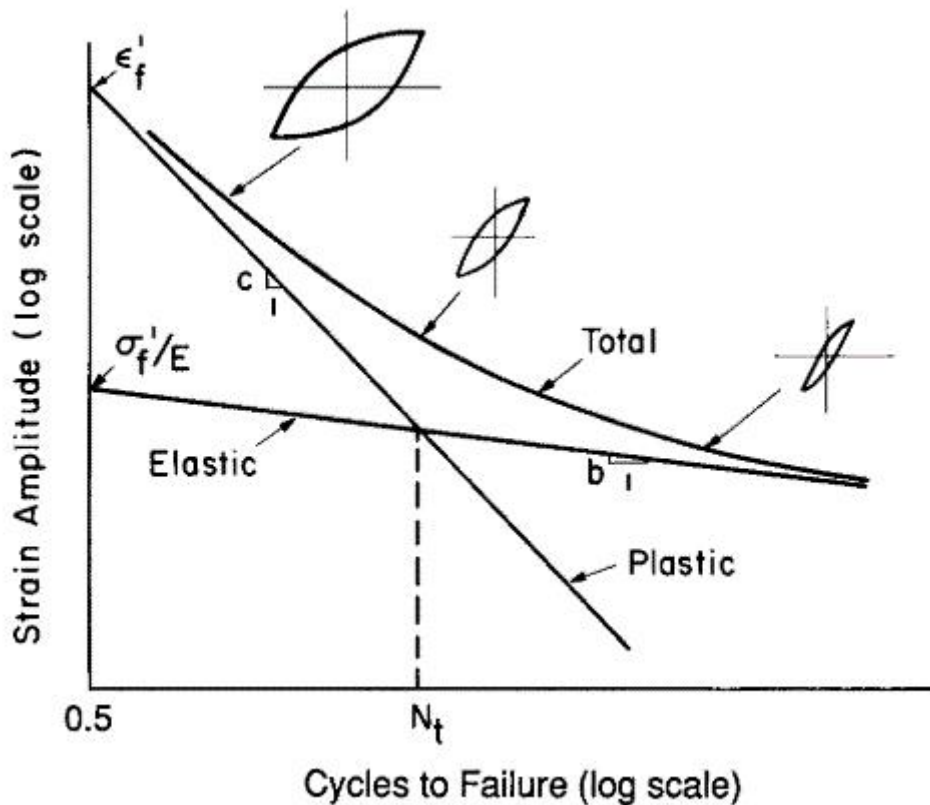
Fig. 4.1: Elastic, plastic and total deformation curve versus life [16].

4.2 Formulation of the finite element method.

4.2.1 General formulation of finite elements.

We will use the virtual work method to obtain in a general way the formulation of the finite elements by making an equality between the virtual internal deformation work and the external forces of a deformable body [99].

$$-\delta\boldsymbol{u}^T\boldsymbol{r} = \int_V \delta\boldsymbol{u}^T\boldsymbol{b}dV + \int_A \delta\boldsymbol{u}^T\boldsymbol{t}dA - \int_V \delta\boldsymbol{\varepsilon}^T\boldsymbol{\sigma}dV \qquad (4.1)$$

where $\delta\boldsymbol{u}^T$ can be any virtual displacement, $\delta\boldsymbol{\varepsilon}^T$ is the matrix of virtual deformations, $\boldsymbol{r}$ is the vector of external real forces applied at the nodes of the structure, $\boldsymbol{b}$ the vector of real mass forces, $\boldsymbol{t}$ is the vector of real surface forces that current in the domain contour and $\boldsymbol{\sigma}$ is the vector associated with the real stress tensor in the solid.
The element displacement field is defined as

$$\boldsymbol{U}^e = \boldsymbol{N}\boldsymbol{a}^e \qquad (4.2)$$

where $\boldsymbol{N}$ is called a matrix of shape functions and $\boldsymbol{U}^e$ is the element domain vector of displacements. We also define the element deformation matrix as

$$\varepsilon = \boldsymbol{B}\boldsymbol{a}^e \qquad (4.3)$$

where $\boldsymbol{B}$ is called the kinematic operator. In the same way, we have the vector of element stresses that is nothing more than multiplying to the left of the vector of element strains by the constitutive matrix of the material $\boldsymbol{D}$.

$$\boldsymbol{\sigma} = \boldsymbol{D}\boldsymbol{B}\boldsymbol{a}^e \qquad (4.4)$$

Applying equation (4.1) in an elementary way, equations (4.2) to (4.4) can be introduced, thus having the matrix formulation of the problem

$$\boldsymbol{K}^e \boldsymbol{a}^e = \boldsymbol{q}^e \tag{4.5}$$

where the element stiffness matrix $\boldsymbol{K}^e$ is defined as

$$\boldsymbol{K}^e = \int_V \boldsymbol{B}^T \boldsymbol{D} \boldsymbol{B} dV \tag{4.6}$$

Assuming that there are no initial stresses and deformations in the solid, the vector of element loads $\boldsymbol{q}^e$ is defined.

$$\boldsymbol{q}^e = \int_V \boldsymbol{N}^T \boldsymbol{b} dV + \int_A \boldsymbol{N}^T \boldsymbol{t} dA \tag{4.7}$$

The concept of the finite element method starts from formulating the stiffness equation in an elementary way, expression (4.5), and then formulating the stiffness equation in global form [100]. In order to obtain the equation of the stiffness in the entire structure, we add in an assembled manner according to the global degrees of freedom of the model; the stiffness matrix of each element, the vector of loads of each element and the vector of nodal displacements of each element, having then

$$\boldsymbol{K} = \sum_{e=1}^{NE} \boldsymbol{K}^e = \boldsymbol{K}^{e1} + \boldsymbol{K}^{e2} + \cdots + \boldsymbol{K}^{eNE}$$

$$\boldsymbol{Q} = \sum_{e=1}^{NE} \boldsymbol{q}^e = \boldsymbol{q}^{e1} + \boldsymbol{q}^{e2} + \cdots + \boldsymbol{q}^{eNE}$$

$$\boldsymbol{U} = \sum_{e=1}^{NE} \boldsymbol{a}^e = \boldsymbol{a}^{e1} + \boldsymbol{a}^{e2} + \cdots + \boldsymbol{a}^{eNE}$$

$$\boldsymbol{Q} = \boldsymbol{K}\boldsymbol{U} \tag{4.8}$$

Equation (4.8) is the stiffness equation applied to the entire structure and NE is the number of elements in the structure. It is worth to noted that the loads vector has known elements, which are the forces applied to the structure, and has unknown elements, which are the reactions of the structure or the forces necessary to achieve the displacements imposed on the structure. The division of the loads vector remains as

$$[\boldsymbol{Q}] = \begin{bmatrix} \boldsymbol{Q}_k \\ \boldsymbol{Q}_u \end{bmatrix} \tag{4.9}$$

where $\boldsymbol{Q}_k$ represents the known forces of the structure and $\boldsymbol{Q}_u$ are the unknown forces of the structure. Consequently we will also have known displacements and unknown displacements in the structure. Known displacements are often called restricted displacements of the structure and do not necessarily have to be equal to zero. The unknown displacements are generally the unknowns of the problem to be solved, having

$$[\boldsymbol{U}] = \begin{bmatrix} \boldsymbol{U}_u \\ \boldsymbol{U}_k \end{bmatrix} \tag{4.10}$$

where $\boldsymbol{U}_u$ represents the unknown displacements of the structure and $\boldsymbol{U}_k$ represents the known displacements of the structure. By making these partitions of force vector and displacement vector, the stiffness equation remains

$$\begin{bmatrix} \boldsymbol{Q}_k \\ \boldsymbol{Q}_u \end{bmatrix} = \begin{bmatrix} \boldsymbol{K}_{11} & \boldsymbol{K}_{12} \\ \boldsymbol{K}_{21} & \boldsymbol{K}_{22} \end{bmatrix} \begin{bmatrix} \boldsymbol{U}_u \\ \boldsymbol{U}_k \end{bmatrix} \tag{4.11}$$

Writing these equations simultaneously we have

$$Q_k = K_{11}U_u + K_{12}U_k \tag{4.11a}$$

$$Q_u = K_{21}U_u + K_{22}U_k \tag{4.11b}$$

From equation (4.11a) we solve for the unknown displacements having

$$U_u = K_{11}^{-1}[Q_k - K_{12}U_k] \tag{4.12}$$

After obtaining all the nodal displacements, we proceed to calculate the external loads in the structure, this is to directly solve the equation (4.11b). These two operations are commonly known as *process*, according to finite element software, everything before the process is called *modeling* and everything after the process is known as *post-processing*.

4.2.2 *First-order formulation of probabilistic finite element method.*

As an approach to the fatigue crack nucleation, the Probabilistic Finite Element Method (PFEM) will be used. In particular, the perturbation method in which Taylor series expansions of an elastostatic problem are used with respect to its random variables. As a result of this analysis, the sensitivities of the response variables of the system are obtained with respect to the random variables introduced as data of the problem [97].
We define the infinitesimal sensitivity of a function $S(\alpha_1)$ with respect to each of its independent variables as

$$\textit{Sensitivity of } S \textit{ with respect to } \alpha_1 = \ \partial S(\alpha_1)/\partial \alpha_1 \tag{4.13}$$

The computed sensitivities allow to evaluate the optimization problem related to an objective variable S. Starting from the stiffness equation in element form where the stiffness matrix now depends on the random variables $\alpha_i (i = 1, 2, \ldots, N)$, it is possible to apply the first-order Taylor series expansion to $\boldsymbol{K}$, $\boldsymbol{u}$ and $\boldsymbol{q}$, with respect to all the random variables α_i around their mean values $\alpha_i{}^0$, that is

$$\mathbf{K} = \boldsymbol{K^0} + \sum_{i=1}^{N} \boldsymbol{K_i^I}\left(\alpha_i - \alpha_i{}^0\right) + \text{...} \tag{4.14}$$

$$\mathbf{u} = \boldsymbol{u^0} + \sum_{i=1}^{N} \boldsymbol{u_i^I}\left(\alpha_i - \alpha_i{}^0\right) + \text{...} \tag{4.15}$$

$$\mathbf{q} = \boldsymbol{q^0} + \sum_{i=1}^{N} \boldsymbol{q_i^I}\left(\alpha_i - \alpha_i{}^0\right) + \text{...} \tag{4.16}$$

where $\boldsymbol{K^0}$, $\boldsymbol{u^0}$ and $\boldsymbol{q^0}$ correspond to the values of the functions evaluated in the mean values of their variables and $\boldsymbol{K_i^I}$, $\boldsymbol{u_i^I}$ and $\boldsymbol{q_i^I}$, are the first partial derivative with respect to α_i and evaluated at $\alpha_i = \alpha_i{}^0$ having the partial derivative vectors as

$$\boldsymbol{K_i^I} = \left.\frac{\partial \boldsymbol{K}}{\partial \alpha_i}\right|_{\alpha_i = \alpha_i{}^0} \tag{4.17}$$

$$\boldsymbol{u_i^I} = \left.\frac{\partial \boldsymbol{u}}{\partial \alpha_i}\right|_{\alpha_i = \alpha_i{}^0} \tag{4.18}$$

$$\boldsymbol{q_i^I} = \left.\frac{\partial \boldsymbol{q}}{\partial \alpha_i}\right|_{\alpha_i = \alpha_i{}^0} \tag{4.19}$$

with $\alpha = [\alpha_1, \alpha_2 \ldots \alpha_N]^T$.

To obtain the sensitivities we derive the equilibrium equation with respect to the random variables $\alpha_i (i = 1, 2, \ldots, N)$ obtaining

$$\frac{\partial \boldsymbol{K}}{\partial \alpha_i} \boldsymbol{u} + \boldsymbol{K} \frac{\partial \boldsymbol{u}}{\partial \alpha_i} = \frac{\partial \boldsymbol{q}}{\partial \alpha_i} \tag{4.20}$$

and now it is possible to isolate from the equation the sensitivity of the displacements with respect to the random variables, leaving

$$\frac{\partial \boldsymbol{u}}{\partial \alpha_i} = \boldsymbol{K}^{-1} \left[\frac{\partial \boldsymbol{q}}{\partial \alpha_i} - \frac{\partial \boldsymbol{K}}{\partial \alpha_i} \boldsymbol{u} \right] \tag{4.21}$$

To obtain the displacements, deformations and stresses, we use the elementary relationships between deformations, stresses and nodal displacements shown above, having the expressions

$$\boldsymbol{u_e} = \boldsymbol{u_e}^0 + \sum_{i=1}^{N} \boldsymbol{u_{ei}^I} \left(\alpha_i - \alpha_i{}^0 \right) + \ldots \tag{4.22}$$

$$\boldsymbol{\varepsilon_e} = \boldsymbol{\varepsilon_e}^0 + \sum_{i=1}^{N} \boldsymbol{\varepsilon_{ei}^I} \left(\alpha_i - \alpha_i{}^0 \right) + \ldots \tag{4.23}$$

where

$$\boldsymbol{\varepsilon_e}^0 = \boldsymbol{B_e} \boldsymbol{u_e}^0 \tag{4.24}$$

$$\boldsymbol{\varepsilon_{ei}^I} = \boldsymbol{B_e} \, \boldsymbol{u_{ei}^I} \tag{4.25}$$

while for the stress tensor we have

$$\boldsymbol{\sigma_e} = \boldsymbol{\sigma_e}^0 + \sum_{i=1}^{N} \boldsymbol{\sigma_{ei}^I} \left(\alpha_i - \alpha_i{}^0 \right) + \ldots \tag{4.26}$$

where

$$\boldsymbol{\sigma_e^0} = \boldsymbol{D_e}^0 \boldsymbol{\varepsilon_e}^0 \tag{4.27}$$

$$\boldsymbol{\sigma_{ei}^I} = \boldsymbol{D_e}^0 \boldsymbol{\varepsilon_{ei}^I} + \boldsymbol{D_{ei}^I} \boldsymbol{\varepsilon_e}^0 \tag{4.28}$$

$$\boldsymbol{D_e} = \boldsymbol{D_e}^0 + \sum_{i=1}^{N} \boldsymbol{D_{ei}^I} \left(\alpha_i - \alpha_i{}^0 \right) + \ldots \tag{4.29}$$

$$\boldsymbol{D_{ei}^I} = \left. \frac{\partial \boldsymbol{D_e}}{\partial \alpha_i} \right|_{\alpha_i = \alpha_i{}^0} \tag{4.30}$$

The Probabilistic Finite Element Method (PFEM) has a non-deterministic character so it seeks to obtain in a first order approach the expectation and covariance operators of the vectors $\boldsymbol{u}$, $\boldsymbol{\varepsilon}$ and $\boldsymbol{\sigma}$. The expectation operator on these vectors results in another vector with the expected mean value of each of the components of the given vector, while the covariance operator results in a matrix whose main diagonal is composed of each of the variances of each of the components of the given vector. Applying the expectation and covariance operators to the vectors $\boldsymbol{u}$, $\boldsymbol{\varepsilon}$ and $\boldsymbol{\sigma}$ we have

$$E\left[\boldsymbol{u_e}\right] = \boldsymbol{u_e}^0 \tag{4.31}$$

$$[Cov\,[\boldsymbol{u_e}, \boldsymbol{u_e}] = E\left[(\boldsymbol{u_e} - E(\boldsymbol{u_e}))\,(\boldsymbol{u_e} - E(\boldsymbol{u_e}))^T\right] = \sum_{i=1}^{N}\sum_{j=1}^{N} \boldsymbol{u_{ei}^I}(\boldsymbol{u_{ej}^I})^{\boldsymbol{T}}\left\{E\,[\alpha_i\alpha_j] - \alpha_i{}^0\alpha_j{}^0\right\}$$

(4.32)

$$Var\,[\boldsymbol{u_e}, \boldsymbol{u_e}] = \sum_{i=1}^{N}\sum_{j=1}^{N} diag\left[\boldsymbol{u_{ei}^I}(\boldsymbol{u_{ej}^I})^{\boldsymbol{T}}\left\{E\,[\alpha_i\alpha_j] - \alpha_i{}^0\alpha_j{}^0\right\}\right]$$

(4.33)

$$E\,[\boldsymbol{\varepsilon_e}] = \boldsymbol{\varepsilon_e}{}^{\boldsymbol{0}}$$

(4.34)

$$[Cov\,[\boldsymbol{\varepsilon_e}, \boldsymbol{\varepsilon_e}] = E\left[(\boldsymbol{\varepsilon_e} - E(\boldsymbol{\varepsilon_e}))\,(\boldsymbol{\varepsilon_e} - E(\boldsymbol{\varepsilon_e}))^T\right] = \sum_{i=1}^{N}\sum_{j=1}^{N} \boldsymbol{\varepsilon_{ei}^I}(\boldsymbol{\varepsilon_{ej}^I})^{\boldsymbol{T}}\left\{E\,[\alpha_i\alpha_j] - \alpha_i{}^0\alpha_j{}^0\right\}$$

(4.35)

$$Var\,[\boldsymbol{\varepsilon_e}, \boldsymbol{\varepsilon_e}] = \sum_{i=1}^{N}\sum_{j=1}^{N} diag\left[\boldsymbol{\varepsilon_{ei}^I}(\boldsymbol{\varepsilon_{ej}^I})^{\boldsymbol{T}}\left\{E\,[\alpha_i\alpha_j] - \alpha_i{}^0\alpha_j{}^0\right\}\right]$$

(4.36)

$$E\,[\boldsymbol{\sigma_e}] = \boldsymbol{\sigma_e}{}^{\boldsymbol{0}}$$

(4.37)

$$[Cov\,[\boldsymbol{\sigma_e}, \boldsymbol{\sigma_e}] = E\left[(\boldsymbol{\sigma_e} - E(\boldsymbol{\sigma_e}))\,(\boldsymbol{\sigma_e} - E(\boldsymbol{\sigma_e}))^T\right] = \sum_{i=1}^{N}\sum_{j=1}^{N} \boldsymbol{\sigma_{ei}^I}(\boldsymbol{\sigma_{ej}^I})^{\boldsymbol{T}}\left\{E\,[\alpha_i\alpha_j] - \alpha_i{}^0\alpha_j{}^0\right\}$$

(4.38)

$$Var\,[\boldsymbol{\sigma_e}, \boldsymbol{\sigma_e}] = \sum_{i=1}^{N}\sum_{j=1}^{N} diag\left[\boldsymbol{\sigma_{ei}^I}(\boldsymbol{\sigma_{ej}^I})^{\boldsymbol{T}}\left\{E\,[\alpha_i\alpha_j] - \alpha_i{}^0\alpha_j{}^0\right\}\right]$$

(4.39)

4.3 Ramberg-Osgood relationship.

Walter Ramberg and William Osgood in 1943 published an article entitled "Description of stress-strain curves by three parameters" where they describe a relationship between elastic and plastic stresses and deformations [101]. The elastic and plastic deformations, ε_e and ε_p, are considered separately and added together. An exponential relationship is used that is applied to plastic deformation [16].

$$\sigma = K\varepsilon_p^n$$

(4.40)

Where n is called the strain hardening exponent. The elastic deformation is proportional to the stress according to Hooke's law, $\varepsilon_e = \sigma/E$, and the plastic deformation ε_p is the deviation of the slope E, as shown in figure 4.2.

Solving equation (4.40) for plastic deformation and adding the elastic and plastic deformations we obtain an equation for the total deformation:

$$\varepsilon = \varepsilon_e + \varepsilon_p$$

(4.41)

$$\varepsilon = \frac{\sigma}{E} + \left(\frac{\sigma}{K}\right)^{1/n}$$

(4.42)
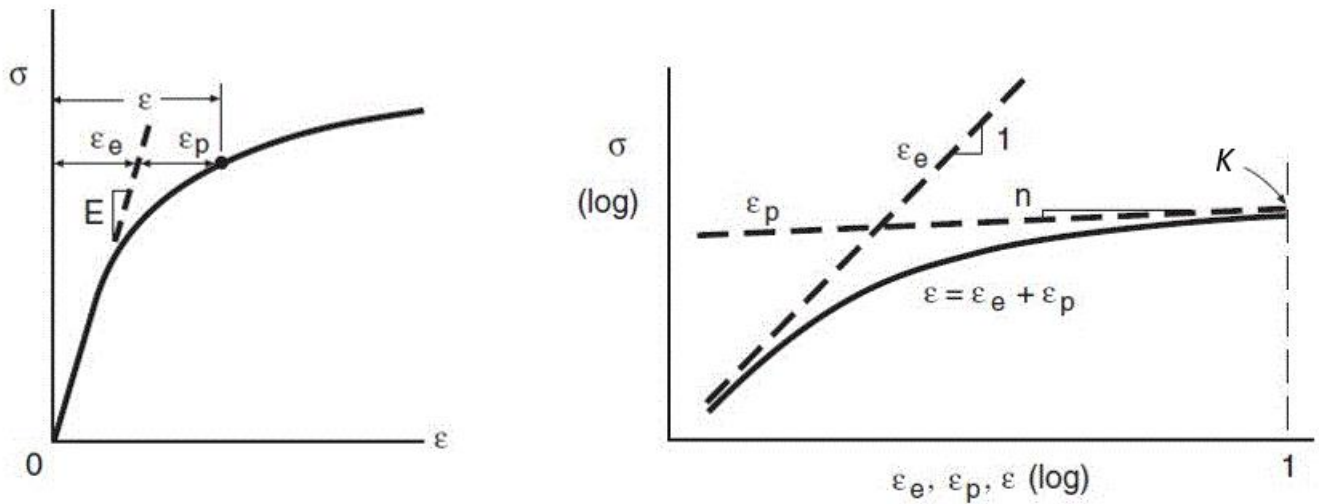
Fig. 4.2: Ramberg Osgood model [16].

An elastic limit can be defined as the stress corresponding to a given plastic deformation displacement, substituting $\varepsilon_p 0 = 0.002$ in equation (4.40) we get

$$\sigma_0 = K(0.002)^n \tag{4.43}$$

Where σ_0 is the yield stress of the material. The constants in equation (4.42) for a particular stress-strain data set are obtained by making a log-log plot of stress versus plastic strain (σ versus ε_p), as illustrated on the right in Figure 4.2. The constant K is the value of σ at $\varepsilon_p = 1$, and n is the slope on the log-log graph. In small deformations, this curve approximates the unit slope line corresponding to elastic deformations; in large deformations, it approaches the plastic deformation line of slope n. In accordance with all the above for the calculation of n we will use the following expression

$$n = \frac{\log(\sigma_2/\sigma_1)}{\log(\varepsilon_2/\varepsilon_1)} \tag{4.44}$$

where σ_2 is the ultimate stress of the material and σ_1 is the yield stress, likewise ε_2 is the ultimate strain of the material and ε_1 is the yield strain of the material. Likewise, the calculation of K is given by

$$K = \frac{\sigma_y}{\varepsilon_y^{\,n}} = \frac{\sigma_u}{\varepsilon_u^{\,n}} \tag{4.45}$$

Using the references [16], [102] for the Cr-Co with the following data we have; $E = 210,000 MPa$, $\sigma_y = 589 MPa$, $\sigma_u = 772 MPa$ and $\varepsilon_u = 0.098$, with which we obtain the stress-strain curve that appears in figure 4.3 where the values of the constants of the Ramberg-Osgood model are shown.

4.4 Plastic stress and plastic strain using Neuber's rule.

The elastic stress intensity factor K_t is defined as the ratio of the stress in the crack tip vs. the far field stress, thus having the expression

$$K_t = \frac{\sigma}{\sigma_n} = \frac{E\varepsilon}{E\varepsilon_n} = \frac{\varepsilon}{\varepsilon_n} \tag{4.46}$$
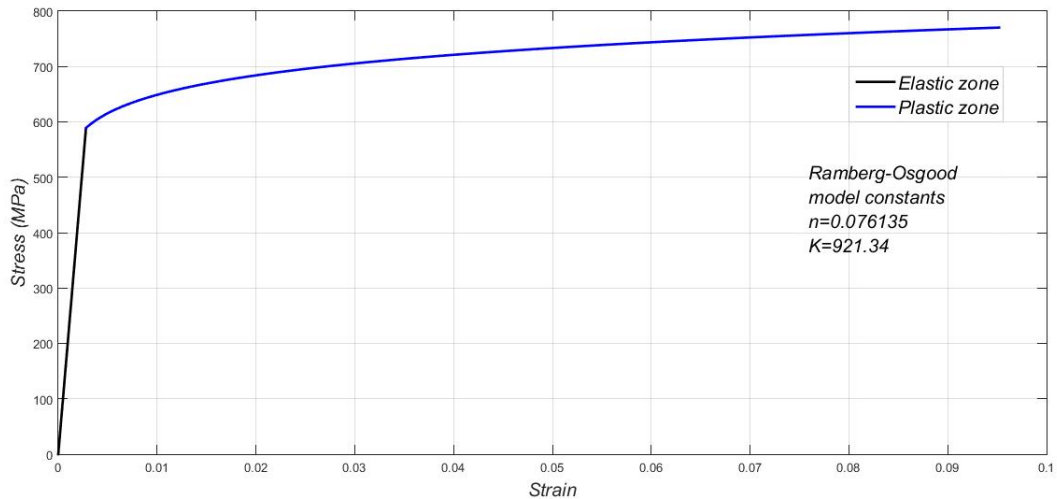
Fig. 4.3: Ramberg-Osgood model for CoCr.

Likewise, for the plastic behavior, the plastic stress concentration factor and the elastic strain concentration factor are defined as

$$K_\sigma = \frac{\sigma}{\sigma_n} \tag{4.47}$$

$$K_\varepsilon = \frac{\varepsilon}{\varepsilon_n} \tag{4.48}$$

By definition we have that $K_t \neq K_\sigma \neq K_\varepsilon$. Neuber's rule states that for the elastic behavior and for the uniaxial case

$$K_t{}^2 = K_\sigma K_\varepsilon \tag{4.49}$$

Substituting the factors defined in (4.46) to (4.48) and substituting them in (4.49) and using the condition of proportionality between the stresses and strains of elastic and plastic regime, we have [16]

$$\varepsilon\sigma = \varepsilon_e \sigma_e \tag{4.50}$$

Being ε and σ the strain and stress in the crack initiation zone and ε_e and σ_e the assumed linear strain and stresses. In Neuber's rule it is stated that the strain energy in a plastic behavior of the material is equal to the strain energy of the same material if it behaves elastically. Neuber's rule appears graphically in Figure 4.4 where the red shaded area is equal to the blue shaded area.

Applying Neuber's rule to the Ramberg-Osgood elastoplastic behavior equation, the formulated expression that relates elastic strains and stresses with elastoplastic strains and stresses remains as

$$\frac{\sigma_{ep}}{E} + \left(\frac{\sigma_{ep}}{K}\right)^{1/n} - \frac{\varepsilon_{el}^2 E}{\sigma_{ep}} = 0 \tag{4.51}$$

Where ε_{el} comes from linear elastic analysis. The coefficients n and K are the constants of the Ramberg-Osgood expression. Solving the value of σ_{ep} with the help of the iterative Newton-Raphson method we have
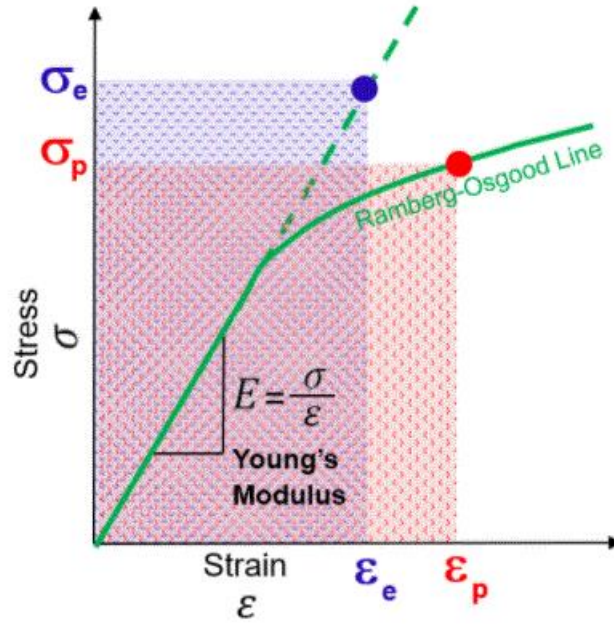
Fig. 4.4: Graphical explanation of Neuber's rule through the equality in elastic strain energy and elastoplastic strain energy [17].

$$\sigma_{n+1} = \sigma_n - \left.\frac{f(\sigma)}{f'(\sigma)}\right|_{\sigma_n} \tag{4.52}$$

where

$$f(\sigma) = \frac{\sigma}{E} + \left(\frac{\sigma}{K}\right)^{1/n} - \frac{\varepsilon_{el}^2 E}{\sigma} \tag{4.53}$$

$$f'(\sigma) = \frac{1}{E} + \frac{1}{nK}\left(\frac{\sigma}{K}\right)^{\frac{1}{n}-1} + \frac{\varepsilon_{el}^2 E}{\sigma^2} \tag{4.54}$$

until $\sigma_{n+1} - \sigma_n < tol$. Once the plastic stress is obtained, $\varepsilon_{el}\sigma_{el} = \varepsilon_{ep}\sigma_{ep}$ is applied to obtain the plastic strain [97].

4.5 *Variance of stress and plastic deformation.*

As mentioned, the $\varepsilon - N_f$ curves are obtained using a non-deterministic approach where the results of the finite element models conduct to the mean values of the problem. Applying again the Neuber rule $\varepsilon_{el}\sigma_{el} = \varepsilon_{ep}\sigma_{ep}$ to the Ramberg-Osgood equation, the expression (4.55) is obtained, which can be approximated by a first order Taylor series with respect to the elastoplastic stress random variable at the mean value of elastic strain, thus having

$$\varepsilon_{el} = \left[\frac{\sigma_{ep}^2}{E^2} + \frac{\sigma_{ep}}{E}\left(\frac{\sigma_{ep}}{K}\right)^{1/n}\right]^{1/2} \tag{4.55}$$

$$\varepsilon_{el} = \varepsilon_{el}{}^0 + \frac{\partial \varepsilon_{el}}{\partial \sigma_{ep}}\left(\sigma_{ep} - \sigma_{ep}{}^0\right) \tag{4.56}$$

where the zero superscript indicates the mean value of the elastoplastic stresses and strains. The partial derivative of the elastic strain with respect to the elastoplastic stress is defined as

$$\frac{\partial \varepsilon_{el}}{\partial \sigma_{ep}} = C|^0 = \frac{1}{2}\left[\frac{\sigma_{ep}^2}{E^2} + \frac{\sigma_{ep}}{E}\left(\frac{\sigma_{ep}}{K}\right)^{1/n}\right]^{-1/2}\left[\frac{2\sigma_{ep}}{E^2} + \frac{1}{E}\left(\frac{1}{K}\right)^{\frac{1}{n}}\left(\frac{1+n}{n}\right)(\sigma_{ep})^{\frac{1}{n}}\right] \tag{4.57}$$

Rewriting the expression (4.56) we have

$$\varepsilon_{el} = \varepsilon_{el}^0 + C|^0\left(\sigma_{ep} - \sigma_{ep}^0\right) \tag{4.58}$$

and solving for σ_{ep} from the expression (4.58) it remains

$$\sigma_{ep} = \sigma_{ep}^0 + \frac{1}{C|^0}(\varepsilon_{el} - \varepsilon_{el}^0) \tag{4.59}$$

writing in this way the variance of the elastoplastic stress

$$Var\left(\sigma_{ep}\right) = \left(\frac{1}{C|^0}\right)^2 Var\left(\varepsilon_{el}\right) \tag{4.60}$$

Now we rewrite the Ramberg-Osgood expression where the elastoplastic deformation is a function of the elastoplastic stress

$$\varepsilon_{ep} = \frac{\sigma_{ep}}{E} + \left(\frac{\sigma_{ep}}{K}\right)^{1/n} \tag{4.61}$$

Approximating the expression (4.61) with a first order Taylor series with respect to the random variable of the elastoplastic stress in the mean value of the elastoplastic strain we have

$$\varepsilon_{ep} = \varepsilon_{ep}^0 + \frac{\partial \varepsilon_{ep}}{\partial \sigma_{ep}}\left(\sigma_{ep} - \sigma_{ep}^0\right) \tag{4.62}$$

where the partial of the elastoplastic strain with respect to the elastoplastic stress is

$$\frac{\partial \varepsilon_{ep}}{\partial \sigma_{ep}} = M = \frac{1}{E} + \frac{1}{n}\left(\frac{\sigma_{ep}^0}{K}\right)^{\frac{1}{n}-1}\frac{1}{K} \tag{4.63}$$

rewriting the expression (4.62) we have

$$\varepsilon_{ep} = \varepsilon_{ep}^0 + M\left(\sigma_{ep} - \sigma_{ep}^0\right) \tag{4.64}$$

thus leaving the variance of the elastoplastic strain as

$$Var\left(\varepsilon_{ep}\right) = M^2 Var\left(\sigma_{ep}\right) \tag{4.65}$$

With what has been stated so far, it is possible to obtain the means and variances of the elastoplastic stresses and strains from the statistics of the elastic stresses and strains computed using the Probabilistic Finite Element Method [97].

4.6 *Coffin and Basquin-Manson expressions.*

Next, the random formulation of the Coffin-Basquin-Manson expressions is carried out in order to make a non-explicit relationship between the fatigue life cycles in the crack nucleation stage of a component and the strain amplitudes at which it is finds subdued.

$$\frac{\Delta\varepsilon_{ep}}{2} = \frac{\sigma_f'}{E}(2N_f)^b + \varepsilon_f'(2N_f)^c \tag{4.66}$$

where $\Delta\varepsilon_{ep}$ is the range of elastoplastic strain applied to the component in the crack initiation zone, $\sigma_f{}'$ is the fatigue strength coefficient, b is the fatigue strength exponent, $\varepsilon_f{}'$ is the fatigue ductility coefficient, c is the fatigue ductility exponent, E is the modulus of elasticity and N_f is the number of fatigue life cycles. The values of $\sigma_f{}'$, b, $\varepsilon_f{}'$ and c are properties of the material. The exponents b and c are the slopes shown in Figure 4.1. If an axial stress test is interpreted as a fatigue test where failure occurs at $N_f = 0.5$ cycles, then the intersections of the constants $\sigma_f{}'$ and $\varepsilon_f{}'$ with $N_f = 0.5$ can be approximated with the true fracture stress and strain as shown in expressions (4.67) and (4.68)

$$\sigma_f{}' \approx \tilde{\sigma}_f = \sigma_f \left(\frac{A_i}{A_f} \right) \tag{4.67}$$

$$\varepsilon_f{}' \approx \tilde{\varepsilon}_f = \ln \left(\frac{A_i}{A_f} \right) = 2\ln \left(\frac{d_i}{d_f} \right) \tag{4.68}$$

where σ_f is the fracture stress, A_i is the cross-sectional area at the start of the test and A_f is the cross-sectional area at the time of fracture [16]. There are several methods for estimating the fatigue parameters b and c [103]. For this work the Morrow estimate will be used [104], [105].

4.7 *Calculation of the fatigue life N_f.*

Starting from the Coffin-Basquín-Manson expression, we again propose an explicit relationship between the number of fatigue life cycles and the elastoplastic strain, carrying out a first-order Taylor series expansion with respect to the random variables on which $\Delta\varepsilon_{ep}$ depends, around its mean value

$$\frac{\Delta\varepsilon_{ep}}{2} = \frac{\Delta\varepsilon_{ep}}{2}\bigg|^0 + \frac{\partial\Delta\varepsilon_{ep}/2}{\partial N_f}\left(N_f - N_f{}^0\right) + \frac{\partial\Delta\varepsilon_{ep}/2}{\partial\sigma_f{}'}\left(\sigma_f{}' - \sigma_f{}'^0\right) + \frac{\partial\Delta\varepsilon_{ep}/2}{\partial\varepsilon_f{}'}\left(\varepsilon_f{}' - \varepsilon_f{}'^0\right) + \frac{\partial\Delta\varepsilon_{ep}/2}{\partial b}\left(b - b^0\right) + \frac{\partial\Delta\varepsilon_{ep}/2}{\partial c}\left(c - c^0\right) \tag{4.69}$$

In order to obtain the variance of the fatigue life we will write the expression (4.69) of the form

$$\frac{\Delta\varepsilon_{ep}}{2} = \frac{\Delta\varepsilon_{ep}}{2}\bigg|^0 + l(N_f - N_f^0) + m(\sigma_f{}' - \sigma_f{}'^0) + n(\varepsilon_f{}' - \varepsilon_f{}'^0) + s(b - b^0) + v(c - c^0) \tag{4.70}$$

where

$$l = \frac{\partial\Delta\varepsilon_{ep}/2}{\partial N_f} = \frac{2b\sigma_f{}'}{E}(2N_f)^{b-1} + 2c\varepsilon_f{}'(2N_f)^{c-1}\bigg|^0 \tag{4.71}$$

$$m = \frac{\partial\Delta\varepsilon_{ep}/2}{\partial\sigma_f{}'} = \frac{1}{E}(2N_f)^b\bigg|^0 \tag{4.72}$$

$$n = \frac{\partial\Delta\varepsilon_{ep}/2}{\partial\varepsilon_f{}'} = (2N_f)^c\big|^0 \tag{4.73}$$

$$s = \frac{\partial\Delta\varepsilon_{ep}/2}{b} = \frac{\sigma_f{}'}{E}(2N_f)^b \cdot (\log 2 + \log N_f)\bigg|^0 \tag{4.74}$$

$$v = \frac{\partial\Delta\varepsilon_{ep}/2}{c} = \varepsilon_f{}'(2N_f)^c \cdot (\log 2 + \log N_f)\bigg|^0 \tag{4.75}$$

Solving for the value of N_f we have

$$N_f = N_f{}^0 + \frac{1}{l}\left(\frac{\Delta\varepsilon_{ep}}{2} - \frac{\Delta\varepsilon_{ep}{}^0}{2}\right) - \frac{m}{l}\left(\sigma_f{}' - \sigma_f{}'^0\right) - \frac{n}{l}\left(\varepsilon_f{}' - \varepsilon_f{}'^0\right) - \frac{s}{l}\left(b - b^0\right) - \frac{v}{l}\left(c - c^0\right)$$

(4.76)

Thus having the variance of the number of fatigue life cycles

$$Var\ (N_f) = \left(\frac{1}{l}\right)^2 Var\left(\frac{\Delta\varepsilon_{ep}}{2}\right) + \left(\frac{m}{l}\right)^2 Var\left(\sigma_f{}'\right) + \left(\frac{n}{l}\right)^2 Var\left(\varepsilon_f{}'\right) + \left(\frac{s}{l}\right)^2 Var\left(b\right) + \left(\frac{v}{l}\right)^2 Var\left(c\right)$$

(4.77)

in this way [97], we can obtain the mean value of the random variable of the number of fatigue life cycles $N_f{}^0$ by solving the expression (4.74) by Newton Raphson's method, then solving

$$N_{f_{n+1}} = N_{f_n} - \frac{f\left(N_f\right)}{f'\left(N_f\right)}\bigg|$$

(4.78)

where

$$f\left(N_f\right) = -\frac{\Delta\varepsilon_{ep}}{2} + \frac{\sigma_f{}'}{E}(2N_f)^b + \varepsilon_f{}'(2N_f)^c$$

(4.79)

$$f'\left(N_f\right) = \frac{b\sigma_f{}'}{E}\frac{1}{N_f}(2N_f)^b + c\varepsilon_f{}'\frac{1}{N_f}(2N_f)^c$$

(4.80)

until $N_{f_{n+1}} - N_{f_n} < tol$.

4.8 *One-step B model.*

In 1985, Bogdanoff and Kozin [106] proposed a series of probabilistic cumulative damage models based on ideas extracted from the Markoff chains and that, through a simple mathematical structure, contemplate the largest sources of common variability in degradation processes or cumulative damage. This type of probabilistic cumulative damage model is known as the one-step B model.

The hypotheses for the development of the one-step B model are:

- There are repetitive "damage cycles" of constant severity. Hereinafter they will be denoted as DC.

- The damage levels are discrete $(1, 2, ...B)$, the latter being the failure state. This hypothesis does nothing but discretize the total life of the component in B levels.

- The cumulative damage on a DC depends only on the DC itself and the damage level at the start of the DC.

- The damage level on each DC can only be increased from the level occupied at the start of that DC to the next higher level. Hence the name of the model as "one-step B model".

This process can be considered as a Markoff chain because there are discrete damage levels and discrete load cycles in addition to having independence between non-correlative results. It is further defined that the probability of jumping from one damage level to another remains constant throughout the material degradation process, so it is a stationary Markoff process.

The proposed hypotheses define that the failure of the component is when damage level B is reached, so that state B is an absorption state and the remaining states $(1, 2, ..., B - 1)$ are called transition states. The damage is considered irreversible: once a higher damage level is reached, it cannot be returned to previous levels. The random variable D_0 is defined as the level of damage occupied at time $t = 0$. The initial distribution of the damage levels for $t = 0$ can be indicated with the vector $\boldsymbol{p_0}$:

$$\boldsymbol{P_0} = \{\pi_1, \pi_2, \ldots, \pi_{B-1}, 0\} \tag{4.81}$$

where $P\{D_0 = j\} = \pi_j \geq 0$, and it must also be satisfied that $\sum_{j=1}^{B-1} \pi$ It does not make sense that some component begins its life in state B, so $\pi_j = 0$ has been taken.

Because the damage cycles are of constant severity, there is a single matrix, called the Transition Probability Matrix, which expresses the probability that exists in each DC, given the level of damage in which the component is found in said DC, the component jumps to the next higher damage level or remains at the damage level it is currently in. This transition probability matrix is shown in (4.82) and in it p_j is the probability that the component will remain at damage level j during the CD and q_j is the probability that it will jump to the next higher level. Also the sum of p_j and q_j must be 1.

$$\boldsymbol{P} = \begin{pmatrix} p_1 & q_1 & 0 & 0 & & 0 & 0 \\ 0 & p_2 & q_2 & 0 & \cdots & 0 & 0 \\ 0 & 0 & p_3 & q_3 & & 0 & 0 \\ & & \vdots & & \ddots & & \vdots \\ 0 & 0 & 0 & 0 & & p_{B-1} & q_{B-1} \\ 0 & 0 & 0 & 0 & \cdots & 0 & 1 \end{pmatrix} \tag{4.82}$$

We define the random variable D_x as the level of damage occupied at discrete time $t = x$, it is possible to define, in a similar way to what was done for $\boldsymbol{p_0}$, the new vector $\boldsymbol{p_x}$, a vector that shows the distribution of damage levels for time $t = x$. Expressing this mathematically we have

$$\boldsymbol{P_x} = \{p_x(1), p_x(2), \ldots, p_x(B)\} \tag{4.83}$$

where

$$P(D_x = j) = p_x(j) \geq 0 \tag{4.84}$$

fulfilling itself

$$\sum_{j=1}^{B-1} p_x(j) = 1 \tag{4.85}$$

Using the results of the Markoff chains [107], it is possible to obtain the vector $\boldsymbol{p_x}$ as

$$\boldsymbol{p_x} = \boldsymbol{p_{x-1}}\boldsymbol{P} = \boldsymbol{p_0}\boldsymbol{P^x}, \; with \; x = 0, \; 1, \; 2 \ldots \tag{4.86}$$

In this way, a family of B-component vectors is obtained, a vector for each discrete time x considered. If we construct a matrix with the successive $\boldsymbol{p_x}$ vectors obtained, each of the columns of that matrix is the probability distribution function of each of the damage levels. In particular, the distribution function (F_w) of the time (W_B) to reach the failure state (level B) can be defined as $p_x(B)$

$$F_w(x; B) = P\{W_B \leq x\} = p_x(B) \; con \; x = 0, \; 1, \; 2 \ldots \tag{4.87}$$

If we assume that the cumulative damage process starts at damage level 1 for the time value $x = 0(\pi_1 = 1)$, the new random variable time to reach the failure state, starting from the initial damage level, is $W_{1,B}$, which in the case of fatigue failure can be defined as the number of load cycles until fatigue failure, N_f, identifying time with duty cycles.

In order to obtain a relationship between the statistical estimators of the random variable N_f (or $W_{1,B}$) and the main parameters of the proposed cumulative damage model (p, q and B), the geometric transformation of the cumulative distribution function of $F_{Nf}(x; 1, B)$ of random variable N_f as indicated in [108]. The result of this transformation is obtaining the expectation and variance of N_f, as shown in (4.88) and (4.89).

$$E\{N_f\} = \sum_{j=1}^{B-1} (1 + r_j) \tag{4.88}$$

$$Var\{N_f\} = \sum_{j=1}^{B-1} r_j (1 + r_j) \tag{4.89}$$

where

$$r_j = \frac{p_j}{q_j} \tag{4.90}$$

$$p_j = \frac{r_j}{1 + r_j} \tag{4.91}$$

The mean and variance statistical estimators of the random variable N_f have been determined in the previous section. From these, the one-step B model is built.

4.9 Determination of $\varepsilon - N_f$ curves and one-step B models for the implants researched.

To obtain the $\varepsilon - N_f$ curves and one-step B models for the implants of the first metatarsophalangeal joint, a code has been developed in MATLAB R2013b that receives the results of the deterministic finite element analysis as input data. The analysis is carried out on a group of elements in the crack nucleation zone. This group of probabilistic elements has been located in the area where Von Mises's greatest stress occurs in each implant. Figure 4.4 shows the groups of elements analyzed for each implant. For the hemi implant AnaToemics®Phalangeal Prosthesis the group to be analyzed consists of 70 elements, for the HemiCAP®Toe DF and ToeMotion® Modular Restoration System implants the analysis groups are 61 elements each.

The first sensitivity to consider is the modulus of elasticity. Therefore applying equation (4.21) we have

$$\frac{\partial \boldsymbol{u}}{\partial E} = \boldsymbol{K}^{-1} \left[\frac{\partial \boldsymbol{q}}{\partial E} - \frac{\partial \boldsymbol{K}}{\partial E} \boldsymbol{u} \right] \tag{4.92}$$

We will name the sensitivity of the displacements with respect to the variation of the elastic modulus as $\boldsymbol{u_1}$ and we will name the displacements obtained in the deterministic analysis (mean values) as $\boldsymbol{u_0}$ having then

$$\boldsymbol{u_1} = \frac{1}{E} \boldsymbol{u_0} \tag{4.93}$$

To calculate the sensitivities of the deformation with respect to the elastic modulus, the displacements $\boldsymbol{u_1}$ were applied to the group of elements of each implant in the two analysis steps. This was done directly in the .inp file using programming in MATLAB R2013b.
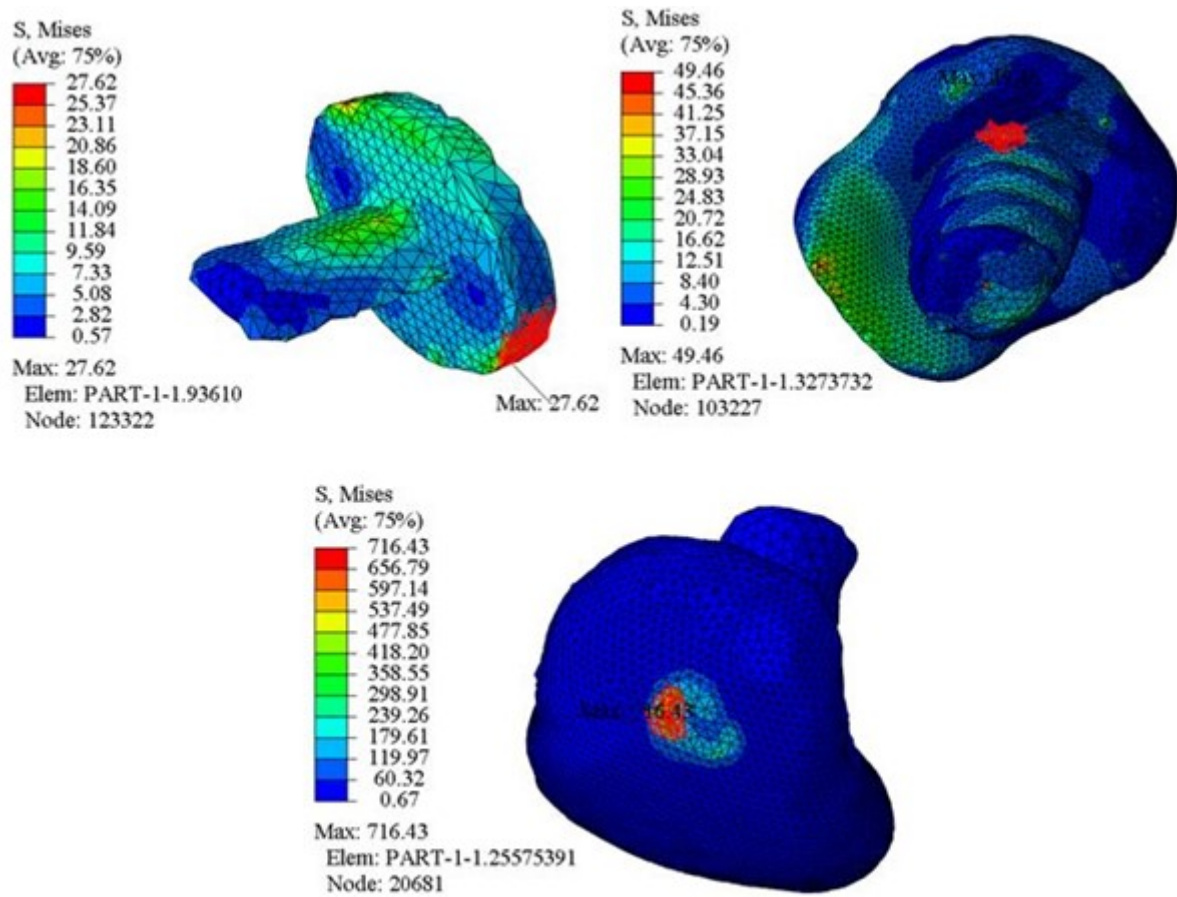
Fig. 4.5: Crack nucleation zones in implants.

The second sensitivity to consider in the analysis is the force modulus. Having then

$$\frac{\partial \boldsymbol{u}}{\partial |q|} = \boldsymbol{K}^{-1} \left[\frac{\partial \boldsymbol{q}}{\partial |q|} - \frac{\partial \boldsymbol{K}}{\partial |q|} \boldsymbol{u} \right] \tag{4.94}$$

We will name the sensitivity of the displacements with respect to the variation of the force module as $\boldsymbol{u_2}$. The derivative of the loads vector with respect to the force module is the unit loads vector which we will call $\boldsymbol{q_2}$. Remaining the sensitivity calculation as

$$\boldsymbol{u_2} = -\boldsymbol{K}^{-1} \boldsymbol{q_2} \tag{4.95}$$

Solving this equation is solving the model with a unit loads vector that is declared in the .inp file. The pretension forces in the muscles do not affect the sensitivities with respect to the force module, so only one step is used for this calculation of sensitivities.

To calculate the other two sensitivities it is necessary to first define the variables of the directions of the applied force. We consider the following unit force applied to a point of origin with the following coordinate axes as shown in figure 4.6.

The loads vector in terms of its three spatial components is given by

$$|\boldsymbol{q}| = |q|_x \boldsymbol{i} + |q|_y \boldsymbol{j} + |q|_z \boldsymbol{k} \tag{4.96}$$

where

$$|q|_x = |q| \sin(\alpha) cos(\beta) \tag{4.97}$$
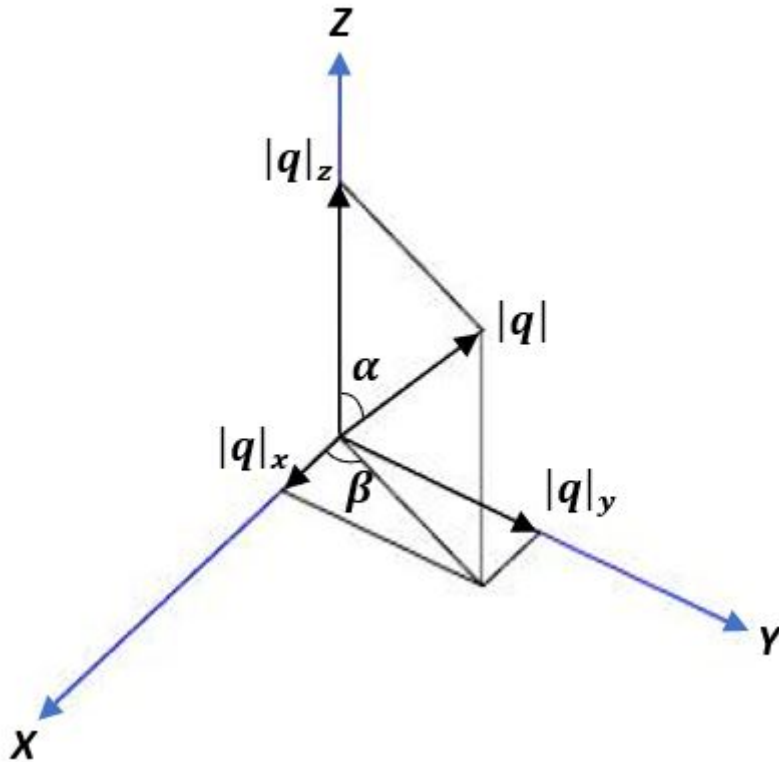
Fig. 4.6: Nodal force directions for sensitivities calculation.

$$|q|_y = |q| \sin{(\alpha)} sin(\beta) \tag{4.98}$$

$$|q|_z = |q| \cos{(\alpha)} \tag{4.99}$$

We will calculate the sensitivity of the displacements with respect to the variation of the angle α, For this we apply again the expression (4.21) having then

$$\frac{\partial u}{\partial \alpha} = K^{-1} \left[\frac{\partial q}{\partial \alpha} - \frac{\partial K}{\partial \alpha} u \right] \tag{4.100}$$

We will name the sensitivity of the displacements with respect to the variation of the direction α of the force as u_3. The derivative of the loads vector with respect to the variation of the direction α of the force will be called q_3. Remaining the sensitivity calculation as

$$u_3 = -K^{-1} q_3 \tag{4.101}$$

where

$$q_3 = \begin{bmatrix} |q| \cos{(\alpha)} \cos{(\beta)} \\ |q| \cos{(\alpha)} \sin{(\beta)} \\ -|q| \sin{(\alpha)} \end{bmatrix} \tag{4.102}$$

The angles α and β are given by

$$\alpha = \arccos \left[\frac{|q|_z}{\sqrt{|q|_x^2 + |q|_y^2 + |q|_z^2}} \right] \tag{4.103}$$

$$\beta = \arctan \left[\frac{|q|_y}{|q|_x} \right] \tag{4.104}$$

As a last sensitivity analysis, we calculate the sensitivity of the displacements with respect to the β direction of the force. Following the same order that has been described we have

$$\boldsymbol{u_4} = -\boldsymbol{K^{-1}q_4} \tag{4.105}$$

where $\boldsymbol{q_4} = \frac{\partial \boldsymbol{q}}{\partial \beta}$ and $\boldsymbol{u_4} = \frac{\partial \boldsymbol{u}}{\partial \beta}$, leaving the nodal component of the loads vector is given by

$$\boldsymbol{q_4} = \begin{bmatrix} -|q|\sin(\alpha)\sin(\beta) \\ |q|\sin(\alpha)\cos(\beta) \\ 0 \end{bmatrix} \tag{4.106}$$

Once the sensitivities of the problem are obtained, we apply equation (4.36) to each of them, thus obtaining 4 square 6x6 matrices. The sum of the traces of these matrices is the variance vector of the elastic strains. Then the coefficients of the Ramberg-Osgood expression are obtained and the Newton-Raphson method is used applying equations (4.52) to (4.54) to obtain the mean value of the plastic stresses of the problem. Using Neuber's rule, expression (4.50), the plastic strains of the problem are obtained. The variance of the plastic stresses is calculated with the expression (4.60) and for the variance of the plastic strains we apply the expression (4.65). The coefficients of the Coffin-Basquin-Manson expressions are calculated according to the references [102], [105] considering the values shown in table 4.1. The mean

Tab. 4.1: Main statistics of the coefficients of the Coffin-Basquin-Manson expressions.

$\boldsymbol{Variable}$	$\boldsymbol{Mean\ value}$	$\boldsymbol{Standard\ deviation}$
$\sigma_f{'}$	$817.82 MPa$	$4.09 MPa$
$\varepsilon_f{'}$	0.05766295	$2.88E-04$

value of the number of fatigue life cycles, N_f is calculated using again the Newton-Raphson method but now with expressions (4.78) to (4.80). It is worth to note that the term $\frac{\Delta\varepsilon_{ep}}{2}$ must always be positive. Then equation (4.77) is applied to obtain the variance of the mean value of the number of fatigue life cycles. Many methods for estimating the exponents of the Coffin-Basquin-Manson expressions use a null variance [103], so for the calculation of the expression (4.77) the variance of the fatigue strength exponent and the variance of the fatigue ductility exponent have been considered equal to zero. The mean value of the number of fatigue life cycles and its variance are subsequently used in equations (4.88) to (4.91) for construct the transition probability matrix, expression (4.82). Finally, expressions (4.83) to (4.87) are used to construct the one step B model. Table 4.2 shows the computed elastoplastic strain amplitudes, the mean value of the number of fatigue life cycles and their coefficient of variation according to a Monte Carlo simulation and the first-order Taylor approximation developed in this chapter. Since the elastic strain and stress obtained by finite element analysis for the ToeMotion® Modular Restoration System implant are very close to the ultimate strain and stress, the results of the mean value of the number of life cycles have been omitted. Figures 4.7 and 4.8 show the curve of probability of failure versus number of life cycles for the implants, in the two cases $B = 123$ in the one step B model.

4.10   *Discussion of non-deterministic results.*

In this chapter, a methodology has been developed to perform non-deterministic analyzes with a strain-based approach. The results of stresses, deformations and displacements in the simulations of the implants researched in this thesis have been used to obtain the mean value of

Tab. 4.2: Fatigue life for implants.

	$\frac{\Delta\varepsilon_{ep}}{2}$	0.000370465		$\frac{\Delta\varepsilon_{ep}}{2}$	0.000493618
	Montecarlo	Taylor		Montecarlo	Taylor
N_f	$1.68934E+18$	$1.68609E+18$	N_f	$9.26409E+15$	$9.25806E+15$
$C_v(\%)$	6.4	9.1	$C_v(\%)$	3.7	9.1
AnaToemics® Phalangeal Prosthesis			HemiCAP® Toe DF		
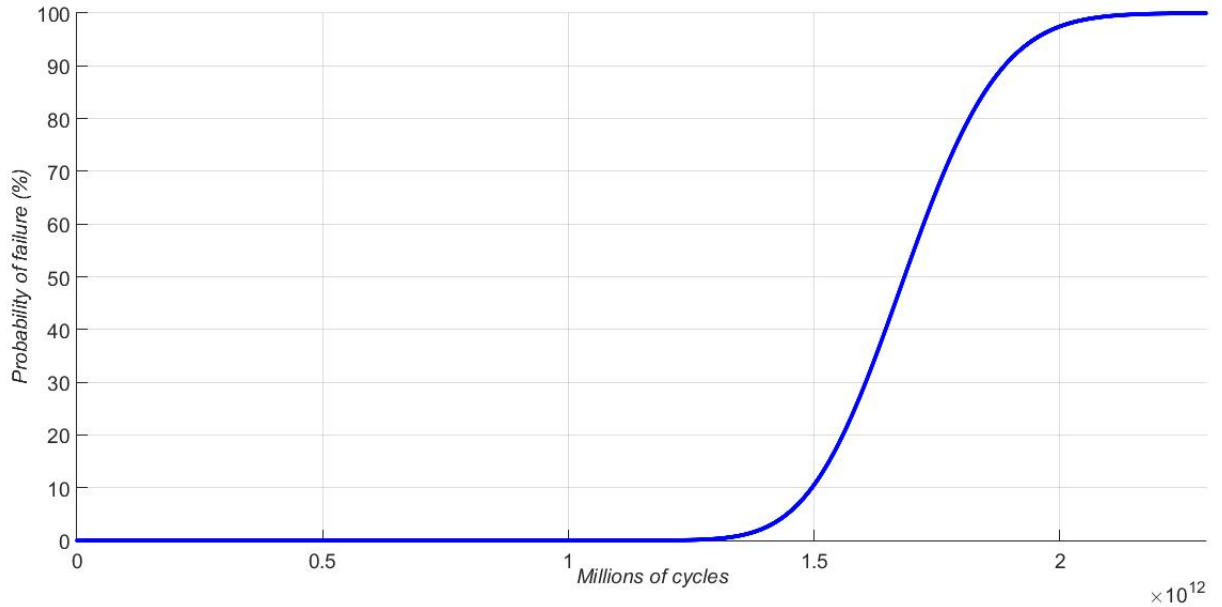
Fig. 4.7: Probability of failure versus cycles for hemi implant AnaToemics® Phalangeal Prosthesis.

the fatigue life and its variance. With these last two values, a one step B model has been constructed that allows us to obtain the curve of probability of failure versus fatigue life in the implants. It can be seen in Figures 4.7 and 4.8 that for these B models, the calculation of the damage level B leads a curve where the mean value of the number of fatigue cycles corresponds to a failure probability of 50 %.

According to the results obtained after 1.68e12 million cycles, a crack nucleation is made in the AnaToemics®Phalangeal Prosthesis and after 9.25e9 million cycles, a crack nucleation in the HemiCAP®Toe DF implant is developed.

According to figures 4.7 and 4.8 and based on the idea that an active person can walk 10,000 steps per day, these implants can last the entire life of the patient without causing any damage. It is worth to note that for this analysis only walking has been taken into account and jumping or running has not been considered. On the other hand, the ToeMotion® Modular Restoration System implant has shown poor fatigue performance.
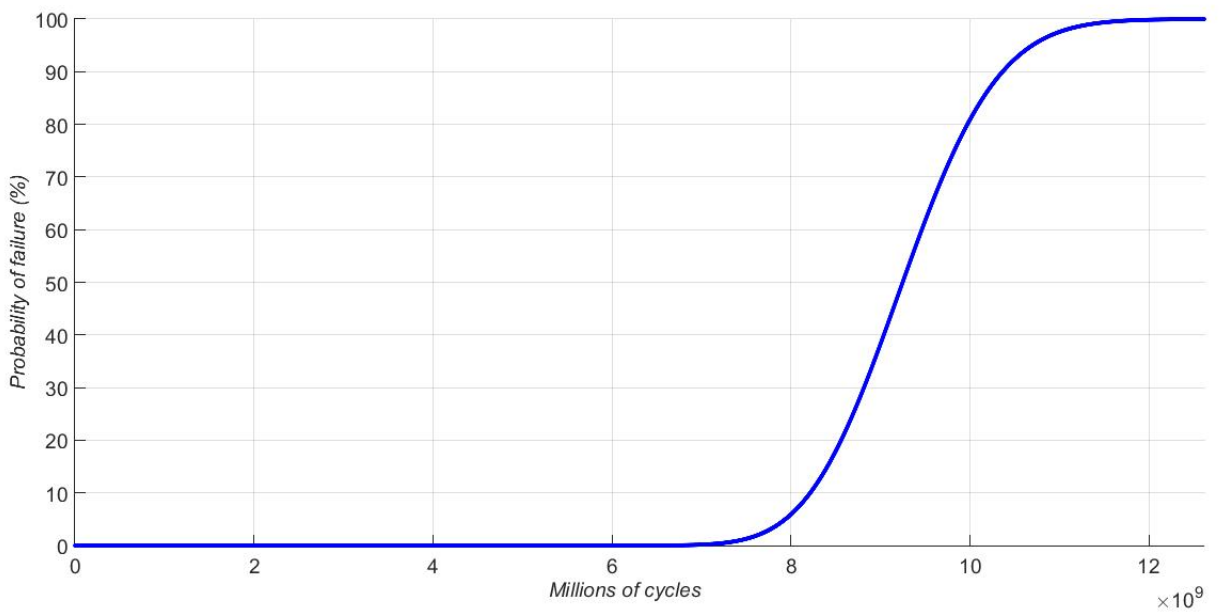
Fig. 4.8: Probability of failure versus cycles for hemi implant HemiCAP® Toe DF.

5. CONCLUSIONS AND FUTURE DEVELOPMENTS.

5.1 *Conclusions.*

In the present work, a biomechanical evaluation of the four types of arthroplasty in the first metatarsophalangeal joint has been carried out. These surgical procedures are well known as; Hemiarthroplasty in the first proximal phalanx, hemiarthroplasty in the first metatarsal, total arthroplasty and Keller resection arthroplasty, the latter is the oldest of the four techniques and is performed without an implant. The simulations of 4 types of arthroplasty, developed through finite element analysis, have been compared with the simulation of a foot model free of pathologies. For the three implants investigated, a non-deterministic analysis has been carried out using the probabilistic finite element method where the sensitivities of elastic strains with respect to random variables have been studied. This random variables are the modulus of elasticity, modulus of forces applied to the model (the person's own weight) as well as the directions α and β of the forces applied to the model, which are shown in figure 4.6. Taking as mean values of the displacements, strains and forces those calculated with the finite element simulations. Neuber's rule has been applied to obtain elastoplastic stresses and deformations in implants. Using a strain-based approach, the Ramberg-Osgood, Coffin-Basquin-Manson expressions and the B models have been applied to obtain a curve of probability of failure versus millions of cycles in each implant. The conclusions of the present work are shown below.

- According to finite element models, a consequence of the surgical procedure of arthroplasty in the first metatarsophalangeal joint is the loss of the passive Windlass mechanism. Despite the fact that arthroplasty is a procedure that relieves pain caused by the pathologies of hallux valgus and hallux rigidus, it is possible that people who undergo this procedure have a lower efficiency in the human gait cycle than a person free of pathologies.

- Physicians are recommended to evaluate the active Windlass mechanism during post-operative follow-up.

- The arthroplasty procedure, according to the simulations carried out, causes an increase in the stresses and displacements of the lesser toes, which can lead to post-operative consequences.

- For the pathology-free model, as the weight of the person increases, the displacements of the lesser toes increase without the displacements of the hallux having variation. For the arthroplasty models, the hallux displacements are nulls and the displacements of the lesser toes increase as the weight of the person increases, presenting values greater than those of the pathology-free model.

- The articular components of the implants develop Von Mises stresses greater than those developed in the components of conical post or skewer. The HemiCAP®Toe DF implant is inserted into the metatarsal in first metatarsal hemiarthroplasty and in total arthroplasty. When the hemiarthroplasty procedure is carried out, the maximum stresses are generated in the area of union with the conical post component, while when a total arthroplasty is performed, the maximum stresses increase considerably and occur on the surface that contacts the component made of ultra-high polyethylene molecular weight.

- The scan of the foot in the toe-off stage was performed with a foot free of pathologies where maximum dorsiflexion is reached, later in the models the implants were inserted in that position, it is possible that a person who undergoes a total arthroplasty do not reach this maximum dorsiflexion and the stresses and strains of the implant decrease considerably.

- The articular component of the researched hemi implants contacts the articular cartilage that have a very low modulus of elasticity, while when the total arthroplasty is performed the two articular components have a high modulus of elasticity and contact each other, adding to this the bad implant congruence upon reaching maximum dorsiflexion, the stresses and strains obtained in the model are too close to the ultimate stress and strain of the material.

- To build the one step B model, it is necessary to calculate the mean value of the number of life cycles and its variance. the value of N_f depends on the elastic and plastic strain amplitudes, which can be computed by applying; Nueber, Ramgerg-Osgood, and Coffin-Basquin-Manson. The variance of the fatigue life, $Var(N_f)$, can be approximated by means of first order Taylor series obtaining an acceptable coefficient of variation. This coefficient of variation becomes smaller when the amplitudes of the elastic and plastic deformations are increased. All this procedure can be an alternative with a lower computational cost than a Montecarlo simulation.

- The results obtained in the non-deterministic analysis show good fatigue performance in the metallic components of the AnaToemics®Phalangeal and HemiCAP®Toe DF implants.

- This thesis does not try to show that one implant is better than another, it only tries to show the behavior of implants in a person who has undergone some arthroplasty process in the first metatarsophalangeal joint. When the choice of the implant is made, it is made based on the joint damage that the patient presents.

5.2   *Original contributions.*

The original contributions of this thesis in the study of finite elements and fatigue studies with a strain-based approach can be summarized in the following points.

- Four finite element models of the foot were made. One for each type of arthroplasty; Hemiarthroplasty in the first proximal phalanx using the AnaToemics®Phalangeal Prosthesis hemi implant, hemiarthroplasty in the first metatarsal using the HemiCAP®Toe DF hemi implant, total atroplasty using the ToeMotion® Modular Restoration System implant and Keller resection arthroplasty

- Comparison of stresses and displacements in the 5 rays of the foot before and after each surgical procedure.

- Construction of one-step B models fed from the results of numerical simulations to study the useful life of each implant.

Original contributions also include publications made during the development of this thesis:

International congresses.

- M.A. Madrid Pérez, R. Becerro de Bengoa Vallejo, J. Bayod López (2019). Biomechanical Evaluation of Hemiarthroplasty in First Metatarsal Bone. *VI Latin American Conference on Biomedical Engineering.* Cancún.

- M.A. Madrid Pérez, M. A. Martínez Bocanegra, R. Becerro de Bengoa Vallejo, J. Bayod López (2021). Biomechanical Evaluation of Arthroplasty in the First Ray of the Foot. *International Foot and Ankle Biomechanics Meeting.* Sao Paulo (Virtual Meeting).

National congresses.

- M.A. Madrid Pérez, J. Bayod López (2018). Comparison between Hemiarthroplasty in the First Proximal Phalanx and Keller's Arthroplasty. A Finite Element Study. *VII Jornada de Jóvenes Investigadores del I3A.* Zaragoza.

- M.A. Madrid Pérez, J. Bayod López (2018). Mechanical evaluation for two implants for the first ray of the foot. *V Jornadas doctorales del Campus Iberus.* Jaca.

Indexed journals.

- M.A. Madrid Pérez, R. Becerro de Bengoa Vallejo, J. Bayod López (2019). Biomechanical Evaluation of Hemiarthroplasty in First Metatarsal Bone. *IFMBE Proceedings Volume 75 VIII Latin American Conference on Biomedical Engineering and XLII National Conference on Biomedical Engineering.* Vol. 75 pp 831 a 840.

- M.A. Madrid Pérez, R. Becerro de Bengoa Vallejo, J. Bayod López (2021). Biomechanical Evaluation of Hemiarthroplasty in First Proximal Phalanx. A Finite Element Study. *Revista Mexicana de Ingeniería Biomédica*, Vol. 42. No. 2. MAY – AUGUST. pp 58-66.

5.3 Future developments.

Future developments as a continuation of this work are listed below:

- With the content of this thesis, a research article can be written that reports the results of the ToeMotion® Modular Restoration System implant and also makes a comparison between the 4 types of arthroplasty. A research article has already been published for each of the other two implants investigated.

- The results of the non-deterministic analysis of the present work can be used for the development of a publication of a research article.

- One consequence of the arthroplasty procedure in finite element models is the loss of the passive Windlass mechanism. It is possible to investigate which part of the procedure is the cause of this consequence. The effects of disinserting the muscles and ligaments lost in the surgical procedure can be studied one by one or in their combinations, and the effect of joint remodeling can be studied.

- Research on these implants can be improved by performing a biomechanical evaluation based on a scan of a foot that has undergone the surgical procedure.

- Starting from the healthy model, the biomechanical effects of performing various surgical procedures such as different types of osteotomies, arthrodesis or other types of arthroplasty can be investigated.

- When using a mesh of tetrahedra it is easy to obtain the sensitivity analysis with respect to the elastic modulus and when using a mesh of plate elements it is easy to obtain the sensitivities with respect to the elastic modulus and Poisson's ratio. It is possible to use different types of meshes to study their effect on the results of a non-deterministic analysis such as the one presented in this thesis.

- The methodology set out in this thesis shows how to calculate the life cycles of a structural element, as well as its variance through the development of first-order Taylor series, for the construction of a step B model. This can be used for the planning, comparison and validation of various experimental fatigue studies.

- With the results of the simulations of the ToeMotion® Modular Restoration System implant, the wear of the UHMWPE joint component can be researched and a fatigue study of this component can be carried out.

- To perform the probabilistic analysis, programming in MATLAB R2013b was used. This code can be used as an engine code for the development of free probabilistic analysis software. It is possible to use a UEL subroutine for writing sensitivities and to create a graphical interface for software development.

5. CONCLUSIONES Y DESARROLLOS FUTUROS.

5.1 *Conclusiones.*

En el presente trabajo se ha realizado una evaluación biomecánica de los cuatro tipos de artroplastia en la primera articulación metatarsofalángica. Estos procedimientos quirúrgicos son bien conocidos como; hemiartroplastia en la primera falange proximal, hemiartroplastia en el primer metatarsiano, artroplastia total y artroplastia de resección de Keller, esta última es la técnica más antigua de las cuatro y se realiza sin implante. Las simulaciones de 4 tipos de artroplastia, desarrolladas mediante análisis de elementos finitos han sido comparadas con la simulación de un modelo de pie libre de patologías. Para los tres implantes investigados se ha realizado un análisis no determinista utilizando el método de los elementos finitos probabilistas donde se han estudiado las sensibilidades de las deformaciones elásticas respecto de las variables aleatorias; módulo de elasticidad, módulo de fuerzas aplicadas al modelo (peso propio de la persona) así como las direcciones α y β de las fuerzas aplicadas al modelo las cuales son mostradas en la figura 4.6. Tomando como valores medios de los desplazamientos, deformaciones y esfuerzos los calculados con las simulaciones por elementos finitos. Se ha aplicado la regla de Neuber para obtener esfuerzos y deformaciones elastoplásticas en los implantes. Usando un enfoque basado en deformaciones se han aplicado las expresiones de Ramberg-Osgood, Coffin-Basquin-Manson y los modelos b para obtener una curva de probabilidad de fallo versus millones de ciclos en cada implante. Las conclusiones del presente trabajo se muestran a continuación.

- De acuerdo con los modelos de elementos finitos, una consecuencia del procedimiento quirúrgico de artroplastia en la primera articulación metatarsofalángica es la pérdida del mecanismo pasivo de Windlass. A pesar de que la artroplastia es un procedimiento que alivia el dolor ocasionado por las patologías de hallux valgus y hallux rigidus, es posible que las personas que se someten a este procedimiento tengan una eficiencia menor en el ciclo de la marcha humana que una persona libre de patologías.

- Se hace la recomendación a los médicos de evaluar el mecanismo activo de Windlass durante el seguimiento post operatorio.

- El procedimiento de artroplastia, de acuerdo con las simulaciones realizadas, ocasiona un aumento en los esfuerzos y desplazamientos de los dedos menores, lo que puede conducir a consecuencias post operatorias.

- Para el modelo libre de patologías, al aumentar el peso de la persona aumentan los desplazamientos de los dedos menores sin tener variación los desplazamientos del hallux. Para los modelos de artroplastia los desplazamientos del hallux son nulos y los desplazamientos de los dedos menores aumentan al aumentar el peso de la persona, presentando valores mayores a los del modelo libre de patología.

- Las componentes articulares de los implantes desarrollan esfuerzos de Von Mises mayores a los desarrollados en las componentes de poste cónico o pincho. El implante HemiCAP®Toe DF es insertado en el metatarsiano en la hemiartroplastia de primer

metatarsiano y en la artroplastia total. Cuando se desarrolla el procedimiento de hemi-artroplastia los esfuerzos máximos se generan en la zona de unión con la componente de poste cónico mientras que cuando se desarrolla una artroplastia total los esfuerzos máximos aumentan considerablemente y ocurren en la superficie que contacta con la componente de polietileno de ultra peso molecular.

- El escaneo del pie en la posición de toe-off se realizó con un pie libre de patologías donde se alcanza una dorsiflexión máxima, posteriormente en los modelos se insertaron los implantes en esa posición, es posible que una persona que se somete a una artroplastia total no alcance esa dorsiflexión máxima y los esfuerzos y deformaciones del implante disminuyan considerablemente.

- La componente articular de los hemi implantes investigados contactan con el cartílago articular que tienen un módulo de elasticidad muy bajo, mientras que cuando se desarrolla la artroplastia total las dos componentes articulares tienen un alto módulo de elasticidad y contactan entre sí, sumando a esto la mala congruencia del implante al alcanzar una dorsiflexión máxima los esfuerzos y deformaciones obtenidas en el modelo son demasiado cercanas a la deformación y esfuerzo último del material.

- Para construir el modelo B de salto de unidad es necesario calcular el valor medio del número de ciclos de vida y su varianza. el valor de N_f depende de las amplitudes de deformación elástica y plástica, lo cual se puede computar aplicando; Nueber, Ramgerg-Osgood y Coffin-Basquin-Manson. La varianza de la vida a fatiga, $Var(N_f)$, se puede aproximar mediante series de Taylor de primer orden obteniendo un coeficiente de variación aceptable. Este coeficiente de variación se vuelve más pequeño cuando las amplitudes de las deformaciones elásticas y plásticas se incrementan. Todo este procedimiento puede ser una alternativa con un costo computacional menor al de una simulación de Montecarlo.

- Los resultados obtenidos en el análisis no determinista muestran un buen desempeño a fatiga en las componentes metálicas de los de los implantes AnaToemics®Phalangeal y HemiCAP®Toe DF.

- Esta tesis no intenta demostrar que un implante sea mejor a otro, solo intenta mostrar el comportamiento de los implantes en una persona que se ha sometido a algún proceso de artroplastia en la primera articulación metatarsofalángica. Cuando se realiza la elección del implante se hace en base al daño articular que presenta el paciente.

5.2 *Aportaciones originales.*

Las aportaciones originales de esta tesis en el estudio de los elementos finitos y los estudios a fatiga con enfoque basado en deformaciones pueden resumirse en los siguientes puntos.

- Se realizaron 4 modelos de elementos finitos del pie. Uno para cada tipo de artroplastia; Hemiartroplastia usando el hemi implante AnaToemics®Phalangeal Prosthesis en la primera falange proximal, hemiartroplastia en el primer metatarsiano usando el hemi implante HemiCAP®Toe DF, artroplastia total usando el implante ToeMotion® Modular Restoration System y artroplastia de resección de Keller

- Comparación de esfuerzos y desplazamientos en los 5 radios del pie antes y después de cada procedimiento quirúrgico.

- Construcción de modelos B de salto de unidad alimentados de resultados de simulaciones numéricas para estudiar la vida útil de los implantes.

Como aportaciones originales también se incluyen las publicaciones realizadas durante el desarrollo de esta tesis:

Congresos internacionales.

- M.A. Madrid Pérez, R. Becerro de Bengoa Vallejo, J. Bayod López (2019). Biomechanical Evaluation of Hemiarthroplasty in First Metatarsal Bone. *VI Latin American Conference on Biomedical Engineering.* Cancún.

- M.A. Madrid Pérez, M. A. Martínez Bocanegra, R. Becerro de Bengoa Vallejo, J. Bayod López (2021). Biomechanical Evaluation of Arthroplasty in the First Ray of the Foot. *International Foot and Ankle Biomechanics Meeting.* Sao Paulo (Virtual Meeting).

Congresos nacionales.

- M.A. Madrid Pérez, J. Bayod López (2018). Comparison between Hemiarthroplasty in the First Proximal Phalanx and Keller's Arthroplasty. A Finite Element Study. *VII Jornada de Jóvenes Investigadores del I3A.* Zaragoza.

- M.A. Madrid Pérez, J. Bayod López (2018). Mechanical evaluation for two implants for the first ray of the foot. *V Jornadas doctorales del Campus Iberus.* Jaca.

Revistas indexadas.

- M.A. Madrid Pérez, R. Becerro de Bengoa Vallejo, J. Bayod López (2019). Biomechanical Evaluation of Hemiarthroplasty in First Metatarsal Bone. *IFMBE Proceedings Volume 75 VIII Latin American Conference on Biomedical Engineering and XLII National Conference on Biomedical Engineering.* Vol. 75 pp 831 a 840.

- M.A. Madrid Pérez, R. Becerro de Bengoa Vallejo, J. Bayod López (2021). Biomechanical Evaluation of Hemiarthroplasty in First Proximal Phalanx. A Finite Element Study. *Revista Mexicana de Ingeniería Biomédica*, Vol. 42. No. 2. MAY – AUGUST. pp 58-66.

5.3   Desarrollos futuros.

Los desarrollos futuros como continuación del presente trabajo se listan a continuación:

- Con el contenido de esta tesis se puede redactar un artículo de investigación que reporte los resultados del implante ToeMotion® Modular Restoration System y además realice una comparación entre los 4 tipos de artroplastia. Ya se ha publicado un artículo de investigación por cada uno de los otros dos implantes investigados.

- Los resultados del análisis no determinista del presente trabajo pueden ser usados para el desarrollo de una publicación de un artículo de investigación.

- Una consecuencia del procedimiento de artroplastia en los modelos de elementos finitos es la pérdida del mecanismo pasivo de Windlass. Es posible investigar qué parte del procedimiento es la causante de dicha consecuencia. Se puede estudiar uno a uno o en sus combinaciones los efectos de desinsertar los músculos y ligamentos perdidos en el procedimiento quirúrgico y se puede estudiar el efecto de la remodelación articular.

- La investigación acerca de estos implantes puede mejorar al realizar una evaluación biomecánica partiendo del escaneo de un pie que haya sido sometido al procedimiento quirúrgico.

- Partiendo del modelo sano se pueden investigar los efectos biomecánicos de desarrollar diversos procedimientos quirúrgicos como diferentes tipos de osteotomías, artrodesis u otros tipos de artroplastia.

- Cuando se usa un mallado de tetraedros es fácil obtener el análisis de sensibilidades respecto del módulo elástico y cuando se usa un mallado de elementos placa es sencillo obtener las sensibilidades respecto del módulo elástico y la relación de Poisson. Es posible usar diferentes tipos de mallas para estudiar el efecto de éstas en los resultados de un análisis no determinista como el presentado en esta tesis.

- La metología expuesta en esta tesis muestra como calcular los ciclos de vida de un elemento estructural, así como su varianza mediante el desarrolo de series de Taylor de primer orden, para la construcción de un modelo B de salto de unidad. Esto puede ser usado para la planeación, comparación y validación de diversos estudios experimentales a fatiga.

- Con los resultados de las simulaciones del implante ToeMotion® Modular Restoration System se puede estudiar el desgaste de la componente articular de UHMWPE y realizar un estudio a fatiga de esta componente.

- Para realizar el análisis probabilista se utilizó programación en MATLAB R2013b. Este código puede ser usado como un código motor para el desarrollo de un software gratuito de análisis probabilistas. Es posible ayudarse de una subrutina UEL para la escritura de las sensibilidades y elaborar una interfaz gráfica para el desarrollo de software.

BIBLIOGRAPHY

[1] A. G. Nerlich, A. Zink, U. Szeimies, and H. G. Hagedorn, "Ancient Egyptian prosthesis of the big toe," *Lancet*, vol. 356, no. SUPPL., pp. 2176–2179, 2000.

[2] M. DE PRADO SERRANO and R. L. RIPOL PÉREZ DE LOS COBOS, "Cirugía percutánea del antepié," in *Manual de cirugía ortopédica y traumatología II.* (Panamericana, ed.), ch. 20, pp. 2541–9., Madrid: Sociedad Española de Ortopedia y Traumatología., 2da ed., 2010.

[3] A. Carranza Bencano, E. Maceira Suárez, R. Viladot Pericé, and M. De Prado Serrano, "Estado actual de la cirugía del hallux valgus," *37 Congreso Nacional SECOT*, no. 1, 2000.

[4] Instituto Mexicano del Seguro Social, "Diagnóstico y Tratamiento del Hallux Valgus. Guía de Práctica Clínica," tech. rep., IMSS, México, 2013.

[5] V. Uroz Alonso, *Influencia De La Cirugía Percutánea En Hallux Valgus Sobre Las Presiones Plantares En Dinámica.* PhD thesis, Universidad de Granada, 2008.

[6] J. Asunción Márquez and X. Martín Oliva, "Hallux rígidus: Etiología, diagnóstico, clasificación y tratamiento," *Revista Espanola de Cirugia Ortopedica y Traumatologia*, vol. 54, no. 5, pp. 321–328, 2010.

[7] A. D. Perler, V. Nwosu, D. Christie, and K. Higgins, "End-Stage Osteoarthritis of the Great Toe/Hallux Rigidus. A review of the alternatives to Arthrodesis: Implant versus Osteotomies and Arthroplasty techniques.," *Clinics in Podiatric Medicine and Surgery*, vol. 30, no. 3, pp. 351–395, 2013.

[8] H. Polzer, S. Polzer, M. Brumann, W. Mutschler, and M. Regauer, "Hallux rigidus: Joint preserving alternatives to arthrodesis - a review of the literature.," *World journal of orthopedics*, vol. 5, no. 1, pp. 6–13, 2014.

[9] C. Delman, C. Kreulen, M. Sullivan, and E. Giza, "Proximal Phalanx Hemiarthroplasty for the Treatment of Advanced Hallux Rigidus," *Foot and Ankle Clinics*, vol. 20, no. 3, pp. 503–512, 2015.

[10] A. J. Kline and C. T. Hasselman, "Resurfacing of the Metatarsal Head to Treat Advanced Hallux Rigidus," *Foot and Ankle Clinics*, vol. 20, no. 3, pp. 451–463, 2015.

[11] S. V. Corey, "THE KELLER PROCEDURE : The Good , The Bad , and The Not So Ugly," *podiatryinstitute.com*, pp. 139–142, 2009.

[12] S. Nakamura, R. D. Crowninshield, and R. R. Cooper, "An analysis of soft tissue loading in the Foot — A preliminary report," *Bulletin of Prosthetics Research*, vol. 18, no. 1, pp. 27–34, 1981.

[13] K. M. Patil, L. H. Braak, and A. Huson, "Analysis of stresses in two-dimensional models of normal and neuropathic feet," *Medical and Biological Engineering and Computing*, vol. 34, no. 4, pp. 280–284, 1996.

[14] W. M. Chen, T. Lee, P. V. S. Lee, J. W. Lee, and S. J. Lee, "Effects of internal stress concentrations in plantar soft-tissue-A preliminary three-dimensional finite element analysis," *Medical Engineering and Physics*, vol. 32, no. 4, pp. 324–331, 2010.

[15] C. Cifuentes-De la Portilla, R. Larrainzar-Garijo, and J. Bayod, "Analysis of biomechanical stresses caused by hindfoot joint arthrodesis in the treatment of adult acquired flatfoot deformity: A finite element study," *Foot and Ankle Surgery*, vol. 26, no. 4, pp. 412–420, 2020.

[16] R. N. Norman E. Dowling, Katakam Silva Prasad, *Mechanical Behavior of Materials. Engineering Methods for Deformation, Fracture, and Fatigue.* 2013.

[17] Siemens Digital Industries Software, "Neuber's Rule," 2020.

[18] E. Madenci, *The Finite Element Method and Applications in Engineering Using ANSYS.* Springer, 2015.

[19] J. M. Soto Castaño, "Ingeniería biomédica. Historia en construcción," *Ingeniería biomédica*, vol. 3, no. 5, pp. 28–30, 2009.

[20] G. G. Glave, "Ingeniería biomédica," *Revista Ciencia y Cultura*, vol. 24, pp. 99–118, 2010.

[21] J. BAYOD LÓPEZ, *Evaluación biomecánica de componentes protésicos de rodilla y estudio del desgaste en el polietileno.* PhD thesis, Universidad de Zaragoza, 2006.

[22] EMB, "Designing a Career in Biomedical Engineering," tech. rep., 2015.

[23] E. Arus, *Biomechanics of Human Motion Applications in the Martial Arts.* Group, CRC Press Taylor and Francis, 2012.

[24] J. M. Rincon López and F. Martínez Rúiz, "Los Vidrios y Materiales Vitrocerámicos como Implantes Quirúrgicos," *Revista Española de Cirugía Osteoarticular*, vol. 19, pp. 77–95, 1984.

[25] R. Calvo Gonçalves, "Clasificación del Hallux valgus. The manchester scale," *el peu. Revista de podología*, vol. 35, no. 2, pp. 24–27, 2014.

[26] A. M. Perera, L. Mason, and M. M. Stephens, "The pathogenesis of hallux valgus.," *The Journal of bone and joint surgery. American volume*, vol. 93, no. 17, pp. 1650–61, 2011.

[27] M. Núñez-Samper and L. F. Llanos Alcázar, *Biomecánica, medicina y cirugía del pie.* Barcelona: Masson, S. A, primera ed., 2000.

[28] U. Koller, M. Willegger, R. Windhager, A. Wanivenhaus, H.-J. Trnka, and R. Schuh, "Plantar pressure characteristics in hallux valgus feet.," *Journal of orthopaedic research : official publication of the Orthopaedic Research Society*, vol. 32, no. 12, pp. 1688–93, 2014.

[29] S. Chopra, K. Moerenhout, and X. Crevoisier, "Characterization of gait in female patients with moderate to severe hallux valgus deformity," *Clinical Biomechanics*, vol. 30, no. 6, pp. 629–635, 2015.

[30] D. Wai-Chi Wong, Y. Wang, M. Zhang, and A. Kam-Lun Leung, "Functional restoration and risk of non-union of the first metatarsocuneiform arthrodesis for hallux valgus: A finite element approach," *Journal of Biomechanics*, vol. 48, no. 12, pp. 3142–3148, 2015.

[31] B. Mafart, "Hallux valgus in a historical French population: Paleopathological study of 605 first metatarsal bones," *Joint Bone Spine*, vol. 74, no. 2, pp. 166–170, 2007.

[32] T. E. Kilmartin and W. A. Wallace, "The aetiology of hallux valgus: a critical review of the literature," *The Foot*, vol. 3, pp. 157–167, 1993.

[33] D. Y. Wu and K. F. Lam, "Osteodesis for hallux valgus correction: is it effective?," *Clinical orthopaedics and related research*, vol. 473, pp. 328–36, jan 2015.

[34] N. Gutteck, D. Wohlrab, A. Zeh, F. Radetzki, K.-S. Delank, and S. Lebek, "Immediate fullweightbearing after tarsometatarsal arthrodesis for hallux valgus correction—Does it increase the complication rate?," *Foot and Ankle Surgery*, vol. 21, no. 3, pp. 198–201, 2015.

[35] M. A. Marínez Bocanegra, J. Bayod López, A. Vidal-Lesso, R. Becerro de Bengoa Vallejo, R. Lesso Arroyo, and H. Corro Hernández, "Biomechanics Aspects for Silastic Implant Arthroplasty Simulation of the First Metatarsophalangeal Joint," *Proceedings of ASME 2015 International Mechanical Engineering Congress and Exposition IMECE2015*, pp. 1–7, 2015.

[36] J. Asunción, D. Poggio, M. J. Pellegrini, R. Melo, and J. Ríos, "Evaluation of first metatarsal head declination through a modified distal osteotomy in hallux rigidus surgery. A cadaveric model," *Foot and Ankle Surgery*, vol. 21, pp. 187–192, 2014.

[37] R. A. Mann and T. O. Clanton, "Hallux Rigidus: Treatment by Cheilectomy," *The Journal of Bone and Joint Surgery*, pp. 400–406, 1988.

[38] M. J. Coughlin and P. S. Shurnas, "Hallux Rigidus. Grading and long-term results of operative treatment," *Journal of Bone and Joint Surgery*, vol. 85-A, no. 11, pp. 2072–2088, 2003.

[39] W. Beertema, W. F. Draijer, J. J. van Os, and P. Pilot, "A retrospective analysis of surgical treatment in patients with symptomatic hallux rigidus: long-term follow-up," *The journal of foot and ankle surgery*, vol. 45, no. 4, pp. 244–251, 2006.

[40] R. Kakwani and M. Siddique, "Clinical rating systems for the ankle-hindfoot, midfoot, hallux, and lesser toes," *Foot and Ankle International*, vol. 15, no. 7, pp. 349–353, 1994.

[41] G. Bonney and I. Macnab, "Hallux Valgus and Hallux Rigidus," *The Journal of Bone and Joint Surgery*, vol. 34-B, no. 3, pp. 366–385, 1952.

[42] TsinghuaX, "Finite Element Analysis and Applications."

[43] A. Ramos Rosas, *Estudio por elementos finitos del comportamiento del pie.* Bachelor's degree thesis, Universidad de Zaragoza, 2006.

[44] Enrique Morales Orcajo, *Computational foot modeling for clinical assessment.* PhD thesis, 2014.

[45] Enrique Morales Orcajo, *Influencia de la geometría de la falange proximal en la formación de juanetes.* Master's degree thesis, Universidad de Zaragoza, 2012.

[46] A. Coutts, T. E. Kilmartin, and M. J. H. Ellis, "The long-term patient focused outcomes of the Keller's arthroplasty for the treatment of hallux rigidus," *Foot*, vol. 22, no. 3, pp. 167–171, 2012.

[47] F. Endler, "Development of a prosthetic arthroplasty of the head of the first metatarsal bone, with a review of present indications.," *Zeitschrift fur Orthopadie und ihre Grenzgebiete*, vol. 80, no. 3, p. 480, 1951.

[48] C. O. Townley and W. S. Taranow, "A Metallic Hemiarthroplasty Resurfacing Prosthesis for the Hallux Metatarsophalangeal Joint," *Foot and Ankle International*, vol. 15, no. 11, pp. 575–580, 1994.

[49] A. B. Swanson, "Implant Arthroplasty of the Great Toe," *Clinical Orthopaedics and Related Research*, vol. 85, 1972.

[50] R. H. Seeburger, "SURGICAL IMPLANTS OF ALLOYED METAL IN JOINTS OF THE FEET.," *Journal of the American Podiatry Association*, vol. 54, p. 391, 1964.

[51] N. S. Shankar, "Silastic single-stem implants in the treatment of hallux rigidus.," *Foot and ankle international*, vol. 16, no. 8, pp. 487–491, 1995.

[52] H. S. Granberry, W. M., Noble, P. C., Bishop, J. O., and Tullos, "Use of a hinged silicone prosthesis for replacement arthroplasty of the first metatarsophalangeal joint," *JBJS*, vol. 73, no. 10, pp. 1453–1459, 1991.

[53] J. Jarvis, B. D. et al, "Lawrence design first metatarsophalangeal joint prosthesis.," *Journal of the American Podiatric Medical Association*, vol. 76, no. 11, pp. 617–624, 1986.

[54] C. F. DeCarbo, W. T. et al, "Modern techniques in hallux rigidus surgery," *Clinics in Podiatric Medicine and Surgery*, vol. 28, no. 2, pp. 361–83, 2011.

[55] S. L. Kampner, "Long-term experience with total joint prosthetic replacement for the arthritic great toe," *Bulletin of the Hospital for Joint Diseases Orthopaedic Institute*, vol. 47, no. 2, pp. 153–177, 1987.

[56] M. Kim, P. J. et al, "A multicenter retrospective review of outcomes for arthrodesis, hemi-metallic joint implant, and resectional arthroplasty in the surgical treatment of end-stage hallux rigidus.," *The Journal of foot and ankle surgery*, vol. 51, no. 1, pp. 50–56, 2012.

[57] M. A. Martínez Bocanegra, *Análisis Biomecánico de una Artroplastia Restitutiva en la Primer Articulación Metatarsofalángica*. Master's degree tehsis, Universidad de Guanajuato, 2016.

[58] E. Giza, M. Sullivan, D. Ocel, G. Lundeen, M. Mitchell, and L. Frizzell, "First metatarsophalangeal hemiarthroplasty for hallux rigidus," *International Orthopaedics*, vol. 34, no. 8, pp. 1193–1198, 2010.

[59] K. F. Konkel, A. G. Menger, and S. A. Retzlaff, "Results of Metallic Hemi-Great Toe Implant for Grade III and Early Grade IV Hallux Rigidus," *Foot & Ankle International*, vol. 30, no. 7, pp. 653–660, 2009.

[60] M. L. Butterworth and M. Ugrinich, "First Metatarsophalangeal Joint Implant Options," *Clinics in Podiatric Medicine and Surgery*, vol. 36, no. 4, pp. 577–596, 2019.

[61] A. E. Ulusal and D. Akseki, "The Journal of Foot & Ankle Surgery Short-Term Clinical Outcomes After First Metatarsal Head Resurfacing Hemiarthroplasty for Late Stage Hallux Rigidus G o," vol. 54, pp. 173–178, 2015.

[62] W. Sung, L. Weil, L. S. Weil, and T. Stark, "Total First Metatarsophalangeal Joint Implant Arthroplasty: A 30-year Retrospective," *Clinics in Podiatric Medicine and Surgery*, vol. 28, no. 4, pp. 755–761, 2011.

[63] A. B. Putti, S. Pande, R. F. Adam, and R. J. Abboud, "Keller's arthroplasty in adults with hallux valgus and hallux rigidus," *Foot and Ankle Surgery*, vol. 18, no. 1, pp. 34–38, 2012.

[64] R. B. Mackey, "The Modified Oblique Keller Capsular Interpositional Arthroplasty for Hallux Rigidus," *The Journal of Bone and Joint Surgery*, vol. 92, no. 10, p. 1938, 2010.

[65] M. R. Mankovecky, M. A. Prissel, and T. S. Roukis, "Incidence of Nonunion of First Metatarsal-Phalangeal Joint Arthrodesis with Autogenous Iliac Crest Bone Graft after Failed Keller-Brandes Arthroplasty: A Systematic Review," *Journal of Foot and Ankle Surgery*, vol. 52, no. 1, pp. 53–55, 2013.

[66] M. J. TURNER, R. W. CLOUGH, H. C. MARTIN, and L. J. TOPP, "Stiffness and Deflection Analysis of Complex Structures," *Journal of the Aeronautical Sciences*, vol. 23, no. 9, pp. 805–823, 1956.

[67] J. Fish and T. Belytschko, *A First Course in Finite Elements*. 2007.

[68] A. Khennane, *Introduction to FEA using Matlab and ABAQUS*. 2013.

[69] K. M. Patil, L. H. Braak, and A. Huson, "Stresses in a simplified two dimensional model of a normal foot - A preliminary analysis," *Mechanics Research Communications*, vol. 20, no. 1, pp. 1–7, 1993.

[70] D. Lemmon, T. Y. Shiang, A. Hashmi, J. S. Ulbrecht, and P. R. Cavanagh, "The effect of insoles in therapeutic footwear - A finite element approach," *Journal of Biomechanics*, vol. 30, no. 6, pp. 615–620, 1997.

[71] A. Gefen, M. Megido-Ravid, Y. Itzchak, and M. Arcan, "Biomechanical analysis of the three-dimensional foot structure during gait: A basic tool for clinical applications," *Journal of Biomechanical Engineering*, vol. 122, no. 6, pp. 630–639, 2000.

[72] F. A. Bandak, R. E. Tannous, and T. Toridis, "On the development of an osseo-ligamentous finite element model of the human ankle joint," *International Journal of Solids and Structures*, vol. 38, no. 10-13, pp. 1681–1697, 2001.

[73] J. Guo, L. Wang, Z. Mo, W. Chen, and Y. Fan, "Biomechanical behavior of valgus foot in children with cerebral palsy: A comparative study," *Journal of Biomechanics*, vol. 48, no. 12, pp. 1–8, 2015.

[74] J. T. M. Cheung, M. Zhang, A. K. L. Leung, and Y. B. Fan, "Three-dimensional finite element analysis of the foot during standing - A material sensitivity study," *Journal of Biomechanics*, vol. 38, no. 5, pp. 1045–1054, 2005.

[75] X. Q. Dai, Y. Li, M. Zhang, and J. T. M. Cheung, "Effect of sock on biomechanical responses of foot during walking," *Clinical Biomechanics*, vol. 21, no. 3, pp. 314–321, 2006.

[76] G. d. V. J.T-MCheung and B. Nigg, "Biomechanical Effects of Midfoot Fusion. A finite element study," *XXI ISB Congress, Podium Sessions*, vol. 40, no. July, p. 2007, 2007.

[77] J. Yu, J. T. M. Cheung, Y. Fan, Y. Zhang, A. K. L. Leung, and M. Zhang, "Development of a finite element model of female foot for high-heeled shoe design," *Clinical Biomechanics*, vol. 23, no. SUPLL.1, pp. 31–38, 2008.

[78] A. García-González, J. Bayod, J. C. Prados-Frutos, M. Losa-Iglesias, K. T. Jules, R. B. de Bengoa-Vallejo, and M. Doblaré, "Finite-element simulation of flexor digitorum longus or flexor digitorum brevis tendon transfer for the treatment of claw toe deformity," *Journal of Biomechanics*, vol. 42, no. 11, pp. 1697–1704, 2009.

[79] T.-x. Qiu, E.-c. Teo, Y.-b. Yan, and W. Lei, "Medical Engineering and Physics Finite element modeling of a 3D coupled foot – boot model," *Medical Engineering and Physics*, vol. 33, no. 10, pp. 1228–1233, 2011.

[80] E. Brilakis, E. Kaselouris, F. Xypnitos, C. G. Provatidis, and N. Efstathopoulos, "Effects of Foot Posture on Fifth Metatarsal Fracture Healing: A Finite Element Study," *Journal of Foot and Ankle Surgery*, vol. 51, no. 6, pp. 720–728, 2012.

[81] J. Yu, J. T.-m. Cheung, D. W.-c. Wong, Y. Cong, and M. Zhang, "Biomechanical simulation of high-heeled shoe donning and walking," *Journal of Biomechanics*, vol. 46, no. 12, pp. 2067–2074, 2013.

[82] D. W. C. Wong, M. Zhang, J. Yu, and A. K. L. Leung, "Biomechanics of first ray hypermobility: An investigation on joint force during walking using finite element analysis," *Medical Engineering and Physics*, vol. 36, no. 11, pp. 1388–1393, 2014.

[83] Z. Taha, M. S. Norman, S. F. S. Omar, and E. Suwarganda, "A Finite Element Analysis of a Human Foot Model to Simulate Neutral Standing on Ground," *Procedia Engineering*, vol. 147, pp. 240–245, 2016.

[84] M. A. Martinez Bocanegra, J. Bayod Lopez, A. Vidal-Lesso, R. Becerro de Bengoa Vallejo, and R. Lesso-Arroyo, "Structural interaction between bone and implants due to arthroplasty of the first metatarsophalangeal joint," *Foot and Ankle Surgery*, 2017.

[85] J. Guo, L. Wang, R. Mao, C. Chang, J. Wen, and Y. Fan, "Biomechanical evaluation of the first ray in pre-/post-operative hallux valgus: A comparative study," *Clinical Biomechanics*, vol. 60, no. 2017, pp. 1–8, 2018.

[86] T. L.-w. Chen, D. W.-c. Wong, Y. Wang, J. Lin, and M. Zhang, "Foot arch deformation and plantar fascia loading during running with rearfoot strike and forefoot strike : A dynamic finite element analysis," *Journal of Biomechanics*, vol. 83, pp. 260–272, 2019.

[87] E. Morales-Orcajo, J. Bayod, R. Becerro-de Bengoa-Vallejo, M. Losa-Iglesias, and M. Doblare, "Influence of first proximal phalanx geometry on hallux valgus deformity: a finite element analysis," *Medical and Biological Engineering and Computing*, vol. 53, no. 7, pp. 645–653, 2015.

[88] J. Bayod, M. Losa-Iglesias, R. Becerro de Bengoa-Vallejo, J. C. Prados-Frutos, K. T. Jules, and M. Doblare, "Advantages and Drawbacks of Proximal Interphalangeal Joint Fusion Versus Flexor Tendon Transfer in the Correction of Hammer and Claw Toe Deformity. A Finite-Element Study," *Journal of Biomechanical Engineering*, vol. 132 (5), no. May 2010, pp. 51002–51007, 2010.

[89] J. Bayod, R. Becerro de Bengoa Vallejo, M. E. Losa Iglesias, and M. Doblaré, "Stress at the second metatarsal bone after correction of hammertoe and claw toe deformity: a finite element analysis using an anatomical model.," *Journal of the American Podiatric Medical Association*, vol. 103, no. 4, pp. 260–73, 2013.

[90] J. M. García-Aznar, "Load Transfer Mechanism for Different Metatarsal Geometries: A Finite Element Study," *Journal of Biomechanical Engineering*, vol. 131, no. 2, p. 021011, 2008.

[91] R. Becerro de Bengoa Vallejo, M. E. Losa Iglesias, and K. T. Jules, "Tendon Insertion at the Base of the Proximal Phalanx of the Hallux: Surgical Implications," *Journal of Foot and Ankle Surgery*, vol. 51, no. 6, pp. 729–733, 2012.

[92] N. Moharrami, D. J. Langton, O. Sayginer, and S. J. Bull, "Why does titanium alloy wear cobalt chrome alloy despite lower bulk hardness: A nanoindentation study?," *Thin Solid Films*, vol. 549, pp. 79–86, 2013.

[93] I. Çelik, "Influence of CrN Coating on Electrochemical Behavior of Plasma Nitrided Pure Titanium in Bio-simulated Environment," *Journal of Bionic Engineering*, vol. 13, no. 1, pp. 150–155, 2016.

[94] D. M. Brunette, P. Tengvall, M. Textor, and P. Thomsen, *Titanium in Medicine. Material Science, Surface Science, Engineering, Biological Responses and Medical Applications.* 2001.

[95] J. E. L. Buddy D. Ratner, Allan S. Hoffman, Frederick J. Schoen, *Biomaterials Science. An Introduction to Materials in Medicine.* 2004.

[96] C. Sanz, "Cinesiologia de la marcha humana normal," *Universidad de Zaragoza*, pp. 1–14, 2011.

[97] J. L. NÚÑEZ BRUIS, *Análisis del fenómeno de fatiga en metales en etapa de nucleación mediante la utilización de modelos estadísticos de daño acumulado y elementos finitos probabilistas.* PhD thesis, Universidad de Zaragoza, 2003.

[98] J. A. Bea, *Simulación del crecimiento de grietas por fatiga aleatoria mediante elementos finitos probabilistas.* PhD thesis, Universidad de Zaragoza, 1997.

[99] O. C. Zienkiewicz and R. Taylor, "Zienkiewicz, Olgierd Cecil-El método de los elementos finitos, vol 1.pdf," 1994.

[100] M. A. Madrid, *Apuntes de Análisis Estrucural II.* Universidad Autónoma de Chihuahua, 2019.

[101] W. Ramberg and W. R. Osgood, "Description of stress-strain curves by three parameters," *Technical Notes National Advisory Committe for Aeronautics*, vol. 902, 1943.

[102] Y. Okazaki, E. Gotoh, H. Nakada, and K. Kobayashi, "Mechanical property, fatigue strength and clinical trial of dental cast Ti-15Zr-4Nb-4Ta alloy," *Materials Transactions*, vol. 46, no. 7, pp. 1545–1550, 2005.

[103] M. F. Harun and R. Mohammad, "Fatigue properties of JIS H3300 C1220 copper for strain life prediction," *AIP Conference Proceedings*, vol. 1958, no. May, 2018.

[104] C. R. Yesid Aguilar, Ramiro Catacolí, Daniel Atehortua, "Determinación de los exponentes b y c en la ecuación Coffin and Manson – Basquin – C and M – B," *Revista Colombiana de Materiales*, vol. 5, no. Edición Especial Artículos Cortos, pp. 283–291, 2012.

[105] J. Shit F, S. Dhar, and S. Acharyya, "Characterization of Cyclic Plastic Behavior of SS 316 Stainless Steel," *International Journal of Engineering Science and Innovative Technology (IJESIT)*, vol. 2, no. 5, pp. 524–538, 2013.

[106] F. Bogdanoff, J.L., Kozin, "Probabilistic Models of Cumulative Damage.," *Wiley, New York*, 1985.

[107] J. A. Bea, M. Doblaré, and L. Gracia, "Evaluation of the probability distribution of crack propagation life in metal fatigue by means of probabilistic finite element method and B-models," *Engineering Fracture Mechanics*, vol. 63, no. 6, pp. 675–711, 1999.

[108] L. Bea, J.A., Doblaré, M., Gracia, "Fiabilidad de Elementos Metálicos en Crecimiento de Grieta por Fatiga Aleatoria mediante Elementos Finitos Probabilistas y Modelos B,," *Rev. Int. Métodos Numéricos para Cálculo y Diseño en Ing.*, vol. 15, pp. 85–112, 1999.

APPENDIX

A. MODEL VALIDATION.

Let be a round bar on which is applied an axial stress in tension as shown in the figure A.1. The elastic strain is given by $\varepsilon_0 = \sigma_0/E$. The sensitivity of elastic strains with respect to
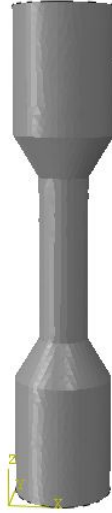

Fig. A.1: bar subjected to axial stress.

Young's modulus is given by $\varepsilon_1 = \varepsilon_0/E$. The sensitivity of the elastic deformation with respect to the applied force module is $\varepsilon_2 = 1/AE$, where A is the area corresponded by the lesser diameter in the test. Since the resultant force applied to the test is parallel to a global axis, we have to $\varepsilon_3 = \varepsilon_4 = 0$. The variance of the elastic deformation is calculated as the sum of the square of the sensitivities of the elastic strain with respect to the random variables. Using the Ramberg-Osgood expression for plastic strain and applying Neuber's rule we can solve the value of the plastic stress, equations (4.51) to (4.54), and then reapply Neuber's rule and calculate the plastic strain. The mean value of the number of fatigue life cycles can be obtained with the elastic and plastic deformations calculated by applying the Coffin-Basquin-Manson expression. Applying first-order Taylor series developments as described in chapter four, the variances of the plastic strain and the number of fatigue life cycles of the test can be obtained. Knowing the mean value of the number of fatigue life cycles and their variance, one step B model is constructed. Figure A.2 shows the probability of failure versus the number of cycles obtained with the one step B model where time in the horizontal axis is in billions of cycles (Thousands of millions). A cobalt chromium specimen with a lesser diameter of 3 mm and a normal stress of 120 MPa has been considered. The calculated value of N_f is equal to $2.26311e + 09$ and its coefficient of variation is 0.09. The number of damage cycles calculated was 120. The figure also shows the results of a Monte Carlo simulation where the modulus of elasticity, the magnitude of the applied force and the coefficients of the Coffin-Basquin Manson expressions have been varied by 2%. 1604 data have been used for the Monte Carlo simulation. Table A.1 shows the value of the number of life cycles and its coefficient of variation computed when changing the normal stress applied to the specimen.

Tab. A.1: Number of life cycles under test when normal stress is varied.

Stress (MPa)	N_f (Cycles)	$C_v(\%)$
60	6.51169e+14	9.56
120	2.26311e+09	9.19
180	1.4683e+06	9.04
240	10954.2	7.33
300	826.117	3.86
360	239.629	2.26
420	114.208	1.59
480	66.766	1.24
540	43.0767	1.05
600	29.8566	0.93
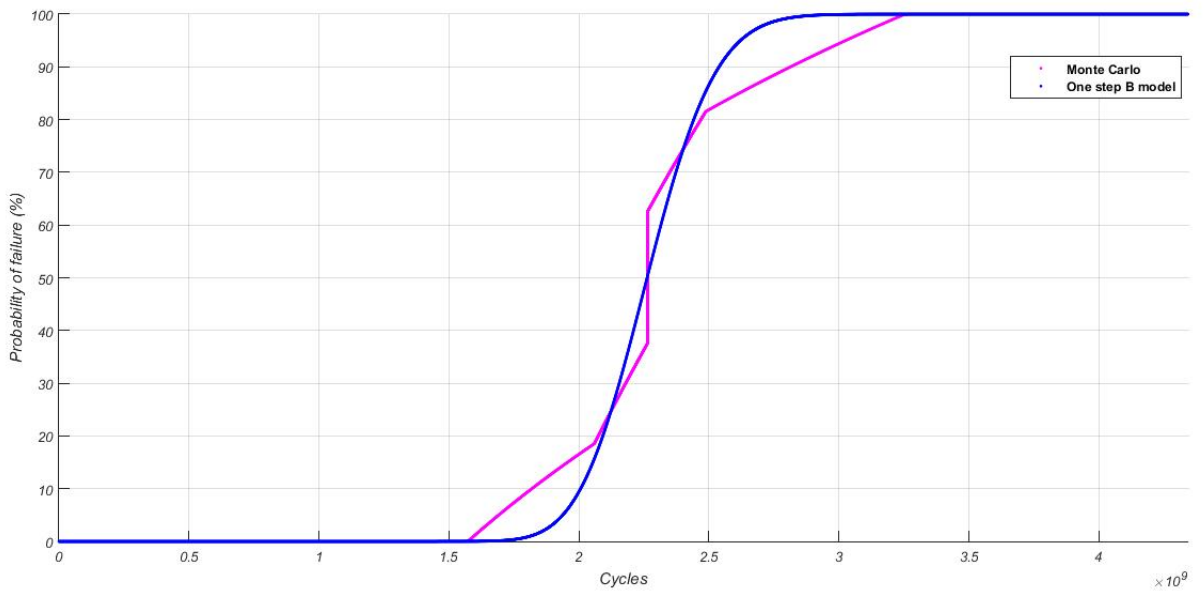
Fig. A.2: Comparison of one step B model and Monte Carlo simulation for specimen subjected to normal stress.